SCOUR AND FILL IN EPHEMERAL STREAMS

by
Michael G. Foley

W. M. Keck Laboratory of Hydraulics and Water Resources
Division of Engineering and Applied Science
CALIFORNIA INSTITUTE OF TECHNOLOGY
Pasadena, California
91125

Report No. KH-R-33

November 1975

SCOUR AND FILL IN EPHEMERAL STREAMS

by

Michael G. Foley

Project Supervisors:

Robert P. Sharp
Professor of Geology

and

Vito A. Vanoni
Professor of Hydraulics

Technical Report to:

U. S. Army Research Office, Research Triangle Park, N. C.
(under Grant No. DAHCO4-74-G-0189)

and

National Science Foundation
(under Grant No. GK31802)

Contribution No. 2695 of the Division of Geological and Planetary Sciences, California Institute of Technology

W. M. Keck Laboratory of Hydraulics and Water Resources
Division of Engineering and Applied Science
California Institute of Technology
Pasadena, California
91125

Report No. KH-R-33

November 1975

ACKNOWLEDGMENTS

The writer would like to express his deep appreciation to his advisor, Dr. Robert P. Sharp, for suggesting this project and providing patient guidance, encouragement, support, and kind criticism during its execution. Similar appreciation is due Dr. Vito A. Vanoni for his guidance and suggestions, and for generously sharing his great experience with sediment transport problems and laboratory experiments.

Drs. Norman H. Brooks and C. Hewitt Dix read the first draft of this report, and their helpful comments are appreciated. Mr. Elton F. Daly was instrumental in the design of the laboratory apparatus and the success of the laboratory experiments. Valuable assistance in the field was given by Mrs. Katherine E. Foley and Mr. Charles D. Wasserburg. Laboratory experiments were conducted with the assistance of Ms. Carol E. Lyons, Mr. Eduardo S. Espiritu, Miss Jill E. Bechtold, Mr. David C. Crocker, Miss Judith S. Greengard, Mr. Craig S. MacInnes, Mr. Randall B. Page, and Mr. Dennis W. New. Thesis preparation was greatly aided by the participation of Mrs. Joan L. Mathews and Mrs. Patricia A. Rankin.

Permission to pursue the field study in the Los Padres National Forest was kindly granted by the U. S. Forest Service. Field work for this project was supported by Geological Society of America Penrose Grant 1716-73. Laboratory support was by National Science Foundation Grant GK 31802, U. S. Army Research Office Grant DAHC04-74-G-0189, and research funds generously made available by Dr. Robert P. Sharp and by the Division of Geological and Planetary Sciences, California Institute of Technology.

This report was submitted by the writer on 28 October 1975 as a thesis with the same title to the California Institute of Technology in partial fulfillment of the requirements for the degree of Doctor of Philosophy in Geology. Since the experimental work was conducted in the Keck Laboratory of Hydraulics and Water Resources, this report is being issued in the Keck Lab KH-R series.

ABSTRACT

The classical concept that mean bed elevation over an entire stream reach is lowered by scour during flood-wave passage and is restored by deposition in the waning flood phase (mean-bed scour and fill) can be challenged. The alternative that both scour and fill occur concurrently at different migrating loci within a reach (local scour and fill) is more consistent with published field data. The field and laboratory investigations reported herein suggest that mean-bed scour and fill in a uniform channel is minor compared to local scour and fill caused by bedform migration, and that maximum local scour and fill may occur on the waning flood in some instances.

The field experiment, utilizing a rectilinear array of buried maximum-scour indicators (scour-cords), produced data for contouring of maximum scour and fill in an ephemeral streambed during two floods. In the first flood, 24 cm of scour and fill was measured for a bankfull flow depth of 23 cm. In the second, maximum scour and fill was at least 66 cm for a bankfull flow depth of 34 cm.

Estimates of antidune amplitudes for the two floods, based on theoretical models and laboratory and field observations, are 28 to 64 cm and 48 to 97 cm, respectively. This indicates that all scour and fill measured by the scour-cord array could have been caused by antidune migration.

Laboratory experiments were conducted in an 18 m-long open-circuit flume with automated sediment and water input-rate controls. A series of experiments in a 26.7 cm-wide sand-bed channel with rigid walls,

at grade for a simulated flood patterned after those typical of ephemeral streams, showed that mean-bed scour and fill was less than 3 percent of local scour and fill. For these experiments, mean sand size was 0.3 mm, channel slope was .009, maximum water depth was 40 mm, maximum local scour and fill was 22 mm, and maximum mean-bed scour and fill was 0.6 mm. Maximum mean bed elevation variation was thus only two sand-grain diameters. Fill occurred at peak flow followed by scour to the pre-flood mean bed elevation on the waning flood. Maximum local scour and fill took place near the end of the simulated floods, when bedform amplitudes were the greatest.

A series of simulated-flood experiments in a sand-bed channel with erodible sand banks showed scour and fill behavior qualitatively similar to that of the rigid-wall channel. Bank erosion, channel meandering, and braiding prevented quantitative scour and fill measurements in these alluvial-bank experiments. Measured flow and bedform parameters and scour and fill data derived from small laboratory scour-chains were compatible with those estimated from the theoretical model used in the field experiment.

TABLE OF CONTENTS

LIST OF FIGURES

LIST OF FIGURES (Cont'd)

LIST OF FIGURES (Cont'd)

LIST OF TABLES

LIST OF TABLES (Cont'd)

CHAPTER 1. INTRODUCTION

Scour and Fill

Bed behavior of steep, sand-bed streams during floods is poorly understood because large amounts of suspended sediment make direct bed observations impossible. Bed-elevation measurements of streams in flood have usually been made by sounding from bridges or cable-crossings at gaging stations. Figure 1-1 shows bed behavior so recorded at gaging stations on the Colorado and San Juan rivers during passage of major floods. Average bed elevation of these streams at the cross-sections measured was lowered approximately the same amount as the water surface rose during flood passage. On the Colorado bed and water surface elevations are about the same before and after the flood.

This behavior of the bed during flood passage is called scour and fill. In discussions to follow, reference is made to scour and fill, mean-bed scour and fill, and local scour and fill. Mean-bed scour and fill is defined as a lowering of mean bed elevation by scour during flood crest passage followed by a return to approximately the initial mean bed elevation by deposition on the waning flood. As defined, this scour occurs simultaneously over a reach of stream comparable in length to the flood crest and the subsequent filling does likewise. Local scour and fill is limited to a reach whose length is comparable to or less than stream width. Local scour and fill can be caused by flow disturbances in narrow gorges or near bridge abutments and other engineering structures, or by normal bedform development and migration. Local scour and fill does not necessarily occur simultaneously over a

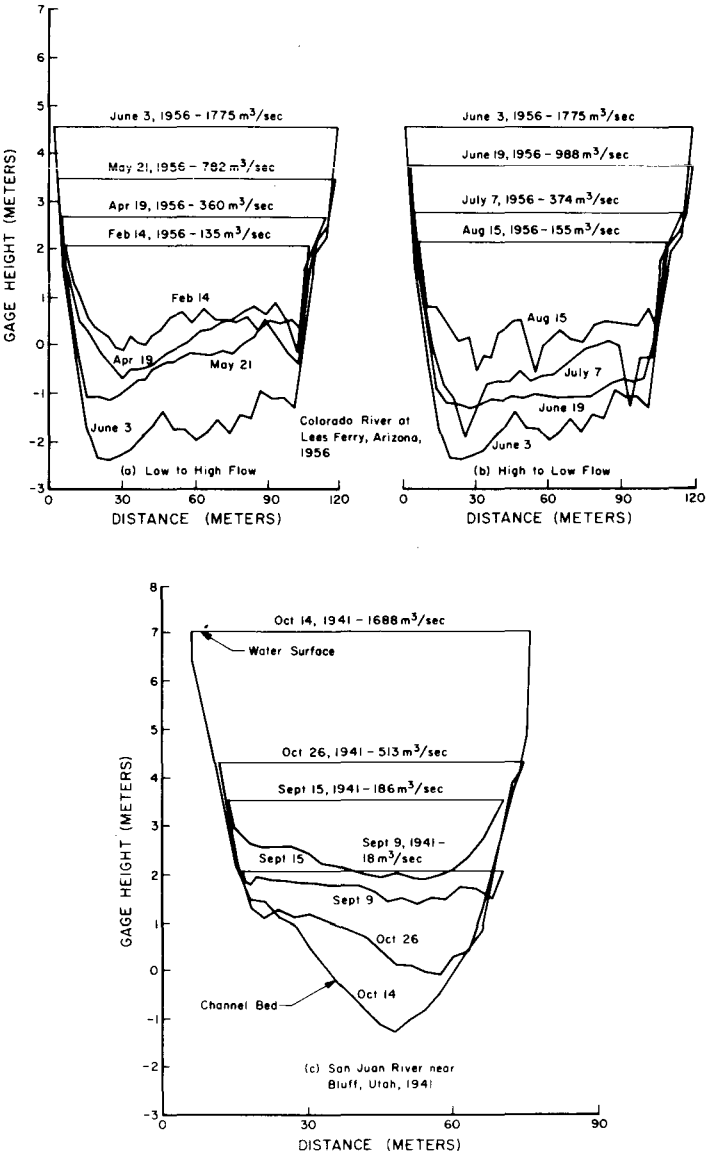

Figure 1-1. Gaging station measurements of scour and fill (after Leopold, Wolman, and Miller, 1964).

single transverse section across the stream channel, and it may occur several times at the same location during a single flood. "Scour and fill" may refer to either mean-bed or local scour and fill, and will be used interchangeably with "bed reworking" where the specific cause is unknown.

Difficulties and costs associated with gaging station siting and operation, particularly during floods, have limited the data on flood changes. For the U. S. Geological Survey gaging station on the San Juan River below Bluff, Utah, Pierce (1916) reported:

> "One of the difficulties connected with the work at the station on the San Juan ... was found to be due to high velocities. The trouble was accentuated by the fact that at the only available site for the cable the vertical rock walls on each side made it necessary to put the cable nearly 50 feet above the bed of the stream." (p.43)

Pierce was using a 60-pound torpedo weight for soundings and for steadying a current meter. At higher stages and velocities he was unable to use the current meter but continued soundings until further rises in stage made them impractical:

> "Measurements at the San Juan station were made very difficult by the large amount of trash carried in suspension in the water and the driftwood carried on the surface. The trash carried in suspension consists of weeds, water-soaked sticks and roots, and fine fibrous roots ... Soundings were not made for any stage above 9 feet because of trash and drift and of the inability of the engineer to tell when the weight touched bottom." (p.44)

As an example of practical difficulties encountered while sounding a torrential flow, Pierce suggested:

> "A small ax should be kept close at hand, so that the meter cable can be cut if absolutely necessary." (p.44)

Difficulties with soundings and the relatively small number of gaging stations, resulted in controversy concerning mean-bed scour and fill. This involved the general applicability of gaging station data to the rest of the stream: Was the gaging station measuring local or mean-bed scour and fill? The only direct sediment-transport measurements made at gaging stations were of suspended load, so the scour and fill at these stations was the best indicator of bedload transport rate. At least some early stream gagers supposed that the effect was general, not local (Pierce 1916):

> "The probability [is] that under certain conditions the bed of the stream is in a state so mobile that soundings can not be made ... This difficulty in making high-water soundings is unfortunate, for it is certain that the measuring section is enlarged at high stages ... It would seem that at the high velocities of the higher stages a large part of this loose bed of sand and gravel would be picked up and carried partly in suspension and partly by traction, thus giving considerably greater areas." (p.45)

Historical Background of Mean-Bed Scour and Fill Investigations

Mean-bed scour and fill was investigated during a U. S. Bureau of Reclamation project begun in 1948 to protect and rehabilitate the middle Rio Grande Valley in New Mexico (Lane and Borland, 1954). Leopold and Maddock (1952) based the following statement on extensive gaging station data on the Rio Grande and other arid-region rivers:

> "It is known that during the passage of a flood the channel of an alluvial stream scours and fills with considerable rapidity." (p.159)

Leopold and Wolman (1956) reiterated:

> "Channels in the semi-arid areas scour at high discharges so that the bed lowers nearly as much as the water surface rises." (p.85)

However, in a discussion of Leopold and Maddock (1952), W. Mitchell stated:

> "These [gaging] stations are intentionally located at points where the change in the width-depth-velocity relationship with discharge is as nearly regular as possible, since this reduces the cost of station operation. The width is usually well fixed and careful consideration is given to the degree of 'control' which exists to regularize the change of depth with discharge ... It is probable that Mr. Leopold has selected ... the most simple case (at constricted [gaging] sections) ... and that there are few other locations in rivers where this average relationship is applicable." (Leopold and Maddock, 1952, p.173)

That location of gaging stations in narrow reaches of streams gives scour and fill results applicable only to narrow reaches was supported by Lane and Borland (1954). They found from sediment deposition measurements in Elephant Butte Reservoir on the Rio Grande in New Mexico that maximum yearly mean-bed scour and fill of the 160-mile reach upstream was approximately 0.08 ft. Since gaging station data showed over a foot of scour at flood crest in narrow reaches of the river, Lane and Borland hypothesized simultaneous fill in wide reaches of the river farther downstream, followed by scour as the flood waned. As supporting evidence, they cited the severe scour and fill that has occurred in the narrow 12-mile reach of the Colorado River below Yuma while no appreciable change occurred in the presumably wider reach of the Colorado River at the site of Imperial Dam. Culbertson and Dawdy (1964) also supported Lane and Borland's hypothesis.

Emmett and Leopold (1963) tested Lane and Borland's hypothesis by placing scour-chains along a six-mile reach of the Arroyo de los Frijoles, an ephemeral stream in New Mexico. These were chains buried

vertically in the dry streambed with the top link approximately even with the surface. Scour at the chain location during a flood caused the exposed part of the chain to fall over, and the length of chain lying horizontal after the flood measured the amount of scour at that location. Scour-chain data over a five-year period showed no correspondence between channel width and local depth of scour, seemingly demolishing Lane and Borland's (1954) hypothesis. Emmett and Leopold (1963) also reported sounding data on two perennial streams with similar results. They could not dispute Lane and Borland's reservoir sedimentation data, so suggested that mean-bed scour and fill did occur, but bedload transport was very slow compared to water velocity. This slow movement of a significant portion of the bed, possibly as a dense slurry, was reiterated in Leopold, Wolman, and Miller (1964) and echoes a discussion by Pierce (1916, p.45).

In his discussion of Leopold and Maddock (1952), A. J. Harrison suggested:

> "Whether or not a reach of river aggrades, degrades, or remains in equilibrium depends on the balance between the bed-material load transported into the reach and that transported out of the reach. An increase in discharge can bring about an increase in the bed material load supplied to the reach, but, at the same time, it also increases the transporting capacity of the reach itself. If the increase in capacity equals the increase in supply, no net change in the bed elevation will result even though sediment concentration increases." (Leopold and Maddock, 1952, p.176)

This continuity principle was used by Colby (1964a) in an extensive discussion of scour and fill. Using bedload transport-rate curves derived from field and laboratory data, Colby (1964b) determined the

behavior of mean-bed elevation in a straight channel with uniform slope, roughness, and cross-section. For a 5000 ft reach of trapezoidal channel 84 ft wide at the bottom, Colby (1964a, p.D12) found a maximum of less than 0.01 ft net change in mean-bed elevation under assumed flash flood conditions.

Colby's (1964a, pp.D31-D32) general conclusions were: 1) Point records of scour and fill, such as made by scour-chains, represent minimum bed elevation at some unknown time during a flood. This may have been when dunes were largest but flow was much less than at flood peak, and it may have occurred when the bed was at maximum elevation nearby. 2) Mean bed elevation changes in narrow reaches, where gaging stations are usually located, are "almost always greater" than changes in reaches of average width. 3) Even in a deep, swift stream the amount of sand being transported at any moment as bedload would make a deposit only a few hundredths of a foot thick over the entire bed if it could be instantaneously stopped.

Alvarez and Alfaro (1973) collected scour and fill data along with associated hydraulic parameters for eleven rivers in Mexico. Scour and fill data were obtained by means of lead rings sliding on pipes driven into the beds of these perennial streams. These authors based most of their arguments on the possibly erroneous assumption that mean-bed scour and fill was being recorded, so their analyses and conclusions are open to question.

Purpose and Scope of this Investigation

Colby's (1964a) hypothesis, that maximum scour measured at a scour-

chain location is caused by the deepest interdune trough to pass during a flood, is supported by the observations of Culbertson and Dawdy (1964) who found on the Rio Grande that scour may alternate with fill locally several times during a flood, with only a small percentage of an entire reach experiencing either scour or fill at any one time. Colby's (1964a) hypothesis, being based in part on calculations using a flash flood with a continuous depth-velocity relation (Figure 4, p.D9), needs to be reconsidered in light of the discontinuous depth-velocity behavior known to occur in some streams during waxing and waning discharges.

Brooks' (1958) flume experiments show that uniform flow over a sand bed can occur at more than one velocity and depth for a given discharge. Colby (1960) confirmed that some sand-bed streams do not have continuous depth-discharge, velocity-discharge, or depth-velocity relations, but undergo a transition between two depth-discharge relations during change in discharge. On a waning flood, this could be the result of transition from high-velocity (low bed friction) flow over antidunes or a flat bed to low-velocity (high bed friction) flow over a dune-covered bed.

A transition from flows with antidunes to flows with dunes on a waxing flood was observed by early stream gagers (e.g., Pierce, 1916), but without realization that it was accompanied by a change in depth-discharge behavior. Anomalies measured in velocity-discharge values were attributed to changes in inferred mean bed elevation at the gaging station and were thus erroneously linked to mean-bed scour and fill.

Colby (1964a) did not use a discontinuous depth-velocity relationship in his scour and fill analysis, and he further assumed that bed

roughness varied more slowly than discharge, so that equilibrium flow could be assumed to prevail during a flood. If a discontinuous depth-velocity relation had been used together with a rapidly-decaying flood, the rate of change of bed roughness required for equilibrium flow during transition could have exceeded the rate at which bedforms were developed. Since bed roughness is caused largely by bedforms, a lag of bedform development produces a corresponding lag of the bed roughness change required for equilibrium flow. The resulting nonequilibrium flow during transition might have produced mean-bed scour or fill in Colby's uniform reach. The magnitude of this mean-bed scour and fill, caused by transition effects, compared to local scour and fill, caused by bedform migration, needs to be determined experimentally.

The current investigation involved a combined field and laboratory study to determine relative magnitudes of mean-bed and local scour and fill in steep, sand-bed ephemeral streams. The field experiment was a high-density scour-chain study of a short reach of an ephemeral stream. Channel geometry, flow depth, and sediment property data permitted estimates of flow velocities and bedform amplitudes for two major runoff events. Estimates of bedform bed-reworking at the field site are compared with the magnitude and pattern of actual scour and fill obtained for runoff events from a rectilinear array of 113 scour-chains. The ephemeral stream studied was not used as a prototype for laboratory modeling experiments but as a test area of known properties where phenomena observed in laboratory could be examined in a field context.

Laboratory experiments were directed toward measuring both mean and local scour and fill directly during floods in a steep, sand-bed

channel. After relative magnitudes were established for a specific flood in a rigid-wall channel, alluvial-bank channel experiments were run. In these experiments, scour-chain behavior was observed in different flow regimes, the field flow estimation method was tested against measured parameters, and model scour-chain data were compared with bedform amplitude measurements. Some model scale-effects were observed, allowing only a qualitative application of model data to the field scale. No attempt was made to apply laboratory results quantitatively to the field study area.

CHAPTER 2. FIELD EXPERIMENTAL PROGRAM

Introductory Statement - Purpose and Scope

A field experiment on scour and fill was conducted in an ephemeral stream in northwest Ventura County, 135 km northwest of Los Angeles in the winters of 1973-74 and 1974-75. Following general inspection and pit sampling of the stream channel, a study-reach was selected, plane-table mapped, and instrumented for recording scour and fill. Scour and fill data obtained for major floods in January and December of 1974 are presented and discussed in the next two chapters.

The purpose of the field experiment was to apply a previously developed scour and fill recording technique (Miller and Leopold, 1963) more intensively to a limited reach of an ephemeral stream so the pattern and magnitude of total bed reworking by scour and fill within that reach could be determined. Mean-bed scour and fill possibly occurring simultaneously over the entire study reach should be approximated by subtracting local scour and fill caused by migrating bedforms from total scour and fill. Since theoretical techniques permit calculation of bed-form amplitude in steep alluvial streams only to within a factor of two, the calculation of mean-bed scour and fill was little more than an order-of-magnitude estimate. A further goal was to establish a field prototype of known properties in which to seek evidence of specific features developed in laboratory experiments. The field program was not designed to provide a prototype stream for laboratory modeling.

Description of Study Area

Quatal Creek, an east side tributary of the Cuyama River, heads on

the west flank of Cerro Noroeste (2526 m) (Figure 2-1) and drains approximately 111 square kilometers in the Los Padres National Forest in Kern, Ventura, and Santa Barbara counties, California. Details of the drainage basin are shown on U. S. Geological Survey, 7.5 minute series topographic quadrangles: Sawmill Mountain, Apache Canyon, and Cuyama Peak. The study-area lies in the Apache Canyon quadrangle.

Quatal Creek (Figure 2-1) is reached by paved road to either the east or west ends of Quatal Canyon Road, a secondary dirt road, except in wet or snowy weather when the western approach must be used. Quatal Creek is accessible by one of several primitive tracks leading south from Quatal Canyon Road. The study area (Figure 2-2) can be reached by driving along the streambed of Quatal Creek, but in wet weather it is accessible only by foot. Vegetation in the vicinity of the test site is predominantly brush or scanty chaparral, with piñon and juniper dominant at higher elevations.

Geology. Quatal Canyon is part of Cuyama Badlands, an area of striking localized badland development in continental Tertiary rocks within Cuyama Valley. This valley is an elongate intermontane basin, formed as a downdropped graben-like block of Tertiary rocks, bounded to the north and south by imbricate thrusts of older rocks (Schwade, 1954). Bedrock at the study site and over about 70 percent of the 61 square kilometers of the Quatal Creek drainage immediately upstream is the continental Miocene-Pliocene Caliente Formation (James, 1963), consisting of conglomerate, coarse-grained argillaceous sandstone, mudstone, and a prominent but discontinuous bentonitic clay bed

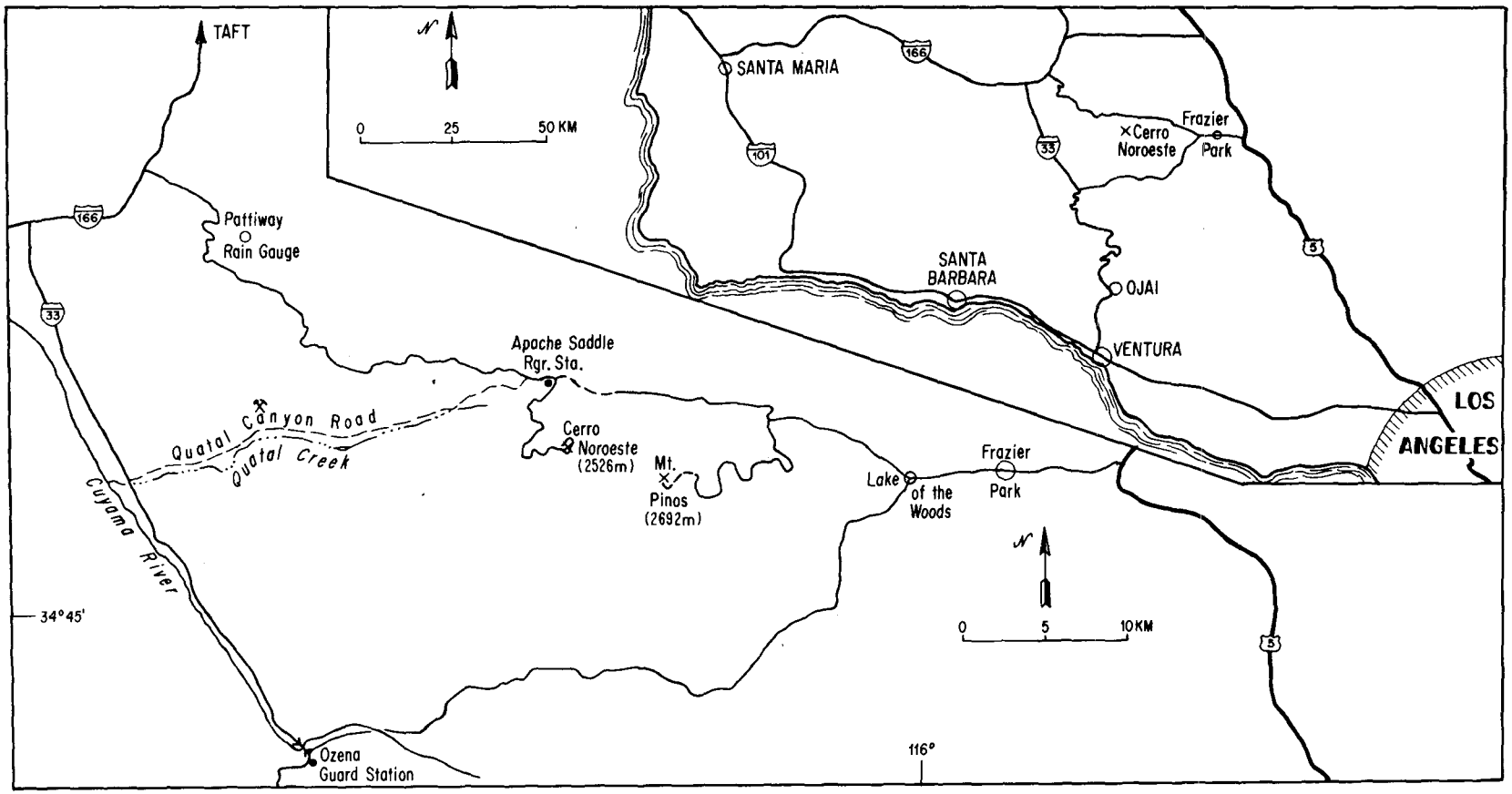

Figure 2-1. Index map showing location of field area.

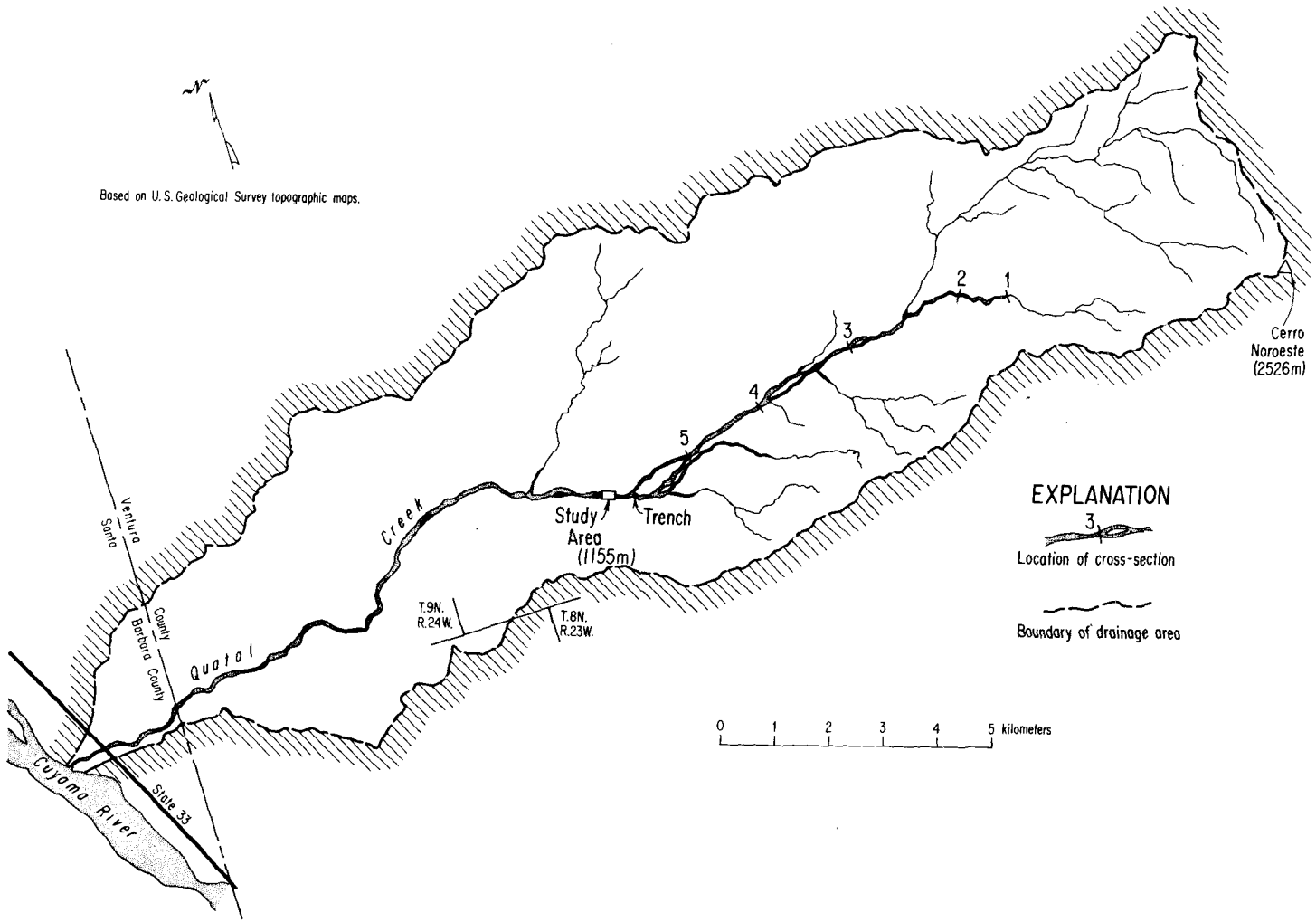

Figure 2-2. Index map showing Quatal Creek drainage basin.

(Lockwood Clay). Oligocene (?) Simmler Formation, a locally-fanglomeratic conglomerate, is thrust over the Caliente Formation north of Quatal Canyon, and composes approximately 20 percent of the bedrock exposed in the Quatal Creek drainage upstream of the study area. Small exposures of quartz diorite, quartz monzonite, and basalt lie within Quatal Canyon, and Pleistocene pediment gravels rich in crystalline clasts cap benches above the canyon floor. Fault slivers of Cretaceous and Tertiary marine beds, and Jurassic granite of the Mt. Pinos terrane compose the remainder of the bedrock in the drainage area upstream of the study area.

Outcrops upstream of the study area provide sediment from clay to cobbles, augmented with boulders from the Simmler Formation and pediment gravels. Geometric mean sediment size for the first 10 km of streambed above the study area is 1.3 mm, with a standard deviation of 5.2. As shown later, this grain size spectrum and channel cross-section geometry suggest that Quatal Creek is stable, neither actively aggrading or degrading.

Precipitation. Mean annual precipitation at Pattiway (Figure 2-1), the nearest rain-gauging station currently operating, is 9.8 inches over the 1931-1960 period, with most precipitation falling between December and April (Table 2-1).

TABLE 2-1. Monthly Precipitation Normals for Pattiway (1939-1960)
(Inches of Precipitation)

Jan	Feb	Mar	Apr	May	Jun	Jul	Aug	Sept	Oct	Nov	Dec	Total
1.87	1.70	1.64	1.10	.27	.08	0	.05	.22	.46	.82	1.57	9.78

Summer thunderstorms can cause significant runoff, but no large thunderstorms affected upper Quatal Canyon during this investigation, and all significant runoff events occurred between November and February.

Investigative Procedures

Quatal Creek was selected for this experiment on the basis of the following criteria: 1) It is primarily a sand-bed ephemeral stream, hence resembling the sand-bed laboratory flume used, and it is accessible for instrumentation when dry. 2) It is not perturbed by artificial structures or activities. 3) Relative inaccessibility minimized risk of vandalism, but the area could be reached by one-day trips from Pasadena. The experimental site (Figure 2-3) was selected to provide: 1) A downstream location so stream slope is smaller; 2) a straight reach with no significant islands or tributaries, to minimize extraneous influences and to facilitate mapping; and 3) a situation which permitted emplacement of easily accessible benchmarks and end stakes out of flood reach.

Topographic mapping. A topographic base map was prepared of the test reach at a scale of 1:1200 with a half-meter contour interval, using plane table and telescope alidade (Figure 2-4). Two primary benchmarks (BM1 and BM3, Figure 2-4) were established on adjacent high banks and two secondary benchmarks and instrument stations (BM1a and BM3a, Figure 2-4) were set in the streambed. These benchmarks were marked by truck axles driven flush with the ground surface, with BM1 and BM3 additionally located by tie distances to markers nailed to nearby trees. Relations between the benchmarks were established by transit and tape traverses, with the expectation that BM1a and BM3a

(a) Looking upstream, 4 m surveying rod (arrow) for scale.

(b) Looking downstream, car for scale.

Figure 2-3. Quatal Creek study area.

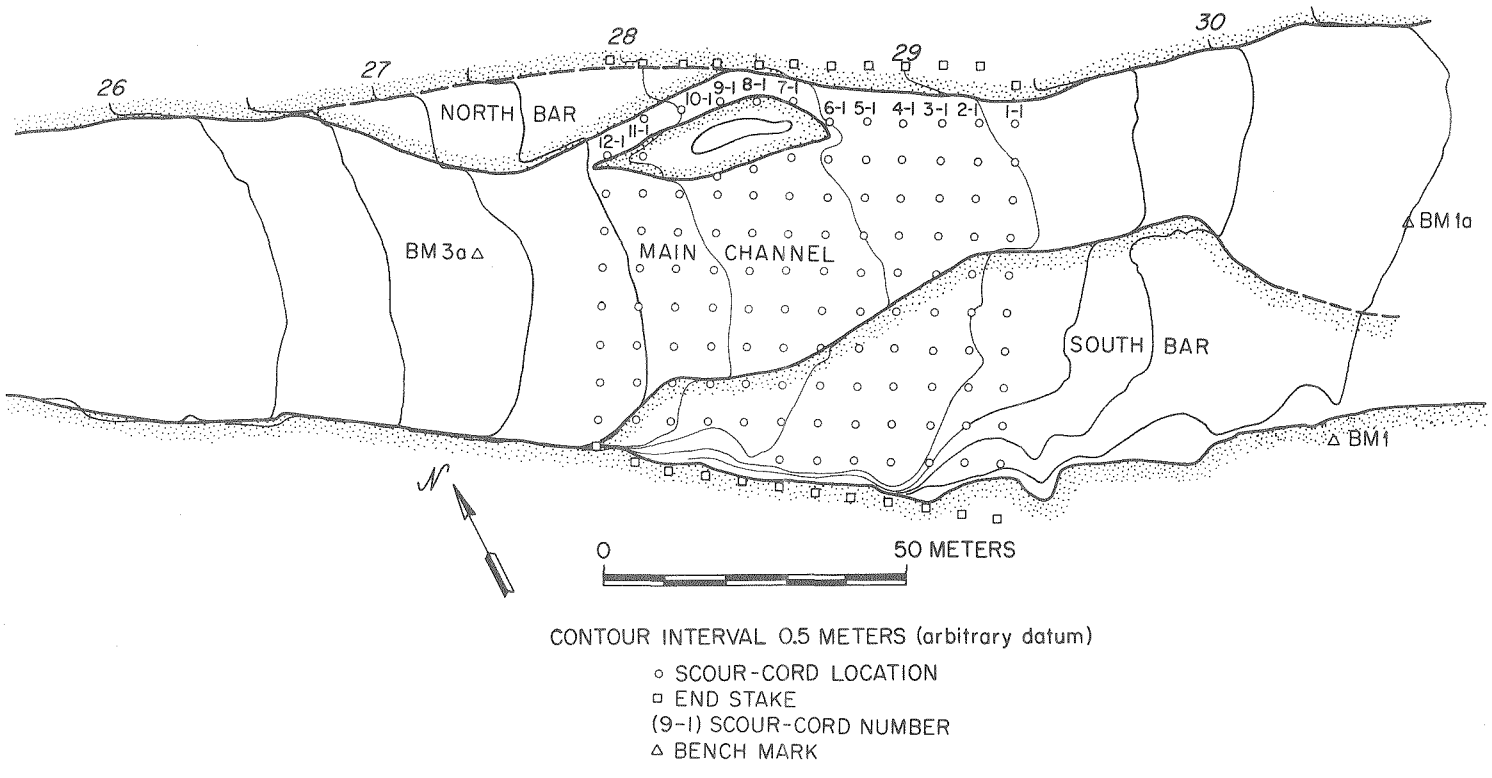

Figure 2-4. Topographic base map of Quatal Creek study area.

could be reestablished should they be swept away by floodwaters. BM1a was arbitrarily assigned an elevation of 30.5 m. Except for benchmark relations, all distances were by stadia measurements and all elevations were level-shot rod readings from instrument stations BM1a and BM3a.

Scour-cord study. The base map was necessary for proper emplacement of a scour-cord network. Previous investigators employed the technique of Miller and Leopold (1963), in which a chain of one- to two-centimeter links was emplaced vertically in an excavated hole and anchored at the bottom by a rock. The large link size allowed penetration by sand and small gravel in the hole filling, thus more securely binding the chain. This was considered desirable to counter the drag of debris caught on the exposed chain during flood flow. Chains were placed singly along the stream centerline with a 150-300 meter spacing, or at 1.5 to 3-meter intervals along more widely separated cross-sections. Recovery of chains was accomplished by taped distances from known tie points for single chains, or by distances to monuments and/or adjacent chains for cross-sections (Emmett and Leopold, 1963; Leopold, Wolman and Miller, 1964). For reasons earlier stated, interpretations of scour-chain data by Leopold and others are not considered unequivocal.

In order to gain better understanding of streambed behavior during floods, a two-dimensional array of 113 scour-cords was installed in the test reach of Quatal Creek. It was anticipated that this array would provide insight into bed reworking processes by showing the pattern of scour and fill.

To avoid bias, an equally-spaced rectilinear array was made (see

Figure 2-4). Such an array is inefficient, since some scour-cords are located where little scour or fill will occur, while areas of greater scour and fill are no more densely covered than least-affected areas. However, any attempt to predict likely areas of major scour and fill in order to design a more efficient array, introduces subjective prejudices. Array spacing was determined by cost, installation time, and desirable coverage. Budget constraints limited the total number of scour-cords to 250. Half of these were held in reserve in case investigation of another test site proved necessary. The array consisted of 12 sets of 8 to 10 scour-cords, with a 6-meter spacing. Alignment was roughly parallel/perpendicular to the highest banks of the active channel. The array was distorted only to accomodate a brushy island (see Figure 2-4), since it was felt that the brush-covered parts had not experienced appreciable scour for several years.

Endstakes for each cross-section line were established on each bank by survey, and scour-cord positions were located by taping along a cord stretched between appropriate end stakes. Even under high wind loading, deflection of the alignment cord was only about 15 centimeters and cross-stream errors were less than 3 centimeters. Recovery of cords proved relatively easy.

In this study, instead of link chain a length of orange 3-mm diameter nylon parachute cord attached to a penetrator-anchor was used (Figure 2-5). The scour-cords were driven into the streambed with a 2-meter length of Shelby tubing with an attached 15-kilogram slidehammer. The penetrator-anchor fitted into the open end of the driving tube and the attached parachute cord ran up the tube and out the top to a bulk supply.

Figure 2-5. Scour-cord with lock-screw (1), penetrator-anchor (2), and driving tube (3).

Using the slidehammer, the tube with the penetrator-anchor as a point was driven into the streambed to a depth of 1 meter. The cord was allowed to run freely and loosely through the tube to avoid dislodging the penetrator-anchor from the bottom of the hole, and the slidehammer was then used to extract the tube. The hole was back-filled and tamped using a geology pick, while the cord was held taut. When the hole was filled and the surface leveled, the cord was cut off flush with the streambed. Exclusive of location determinations, emplacement of such scour-cords averaged approximately 6 minutes.

Trenching. A single 1 x 2 meter trench 2 meters deep was dug upstream of the study area (Figure 2-2). No clear indications of layering, pebble or cobble lenses, or other primary structures were seen, even after the walls of the trench dried. Apparently, the well-graded nature of the bed material and its relatively high clay content conceals any existing sedimentary structures by smearing when a face is excavated with a shovel. Coarse layers however, indicate that armoring does occur, but pebble layers discovered during scour-cord recovery were not visible in the sides of the scour-cord search holes. Thus, no extensive trenching to investigate bed structures has been performed. The usually damp streambed prevented making peels without substantial drying, and Forest Service regulations prohibiting open fires did not permit the incendiary drying procedures used in most field peel techniques. For these reasons, knowledge of bed primary structures is limited to armoring discovered in scour-cord searches.

CHAPTER 3. FIELD EXPERIMENTAL RESULTS

Introductory Statement

Two types of data were obtained from the Quatal Creek experiment. The first is descriptive information, geometry and sediment samples, from the 10 km reach of Quatal Creek upstream of the study area. These data constitute an important context for the field experiment. The second is the actual scour and fill results from the study area. Supporting information on data collection and rainfall records is included. Discussion of scour and fill data for the two major runoff events will be deferred to the next chapter.

General Channel Characteristics

A reconnaissance of the 10 km-long, wide, sand-bedded reach of Quatal Creek above the test site was conducted in June 1973. Channel cross-sections were measured and bed and bank sediment samples were taken at numbered locations (Figure 2-2), also shown on the stream profile (Figure 3-1). This channel profile was drafted from the Apache Canyon quadrangle map.

All sample sites, for example location 1 (Figure 3-2), were in the presently-active channel which is entrenched between low vertical banks. Quatal Creek has a total channel width of 25 to 100 meters, approximately twice that of the active channel in any location, with two- to three-meter high sloping banks. The active channel is cut about one meter below this wider channel, creating brush-covered terraces which seem not to have experienced substantial flow since the floods of early 1969. Since a major flood would be a rare event within the duration of this

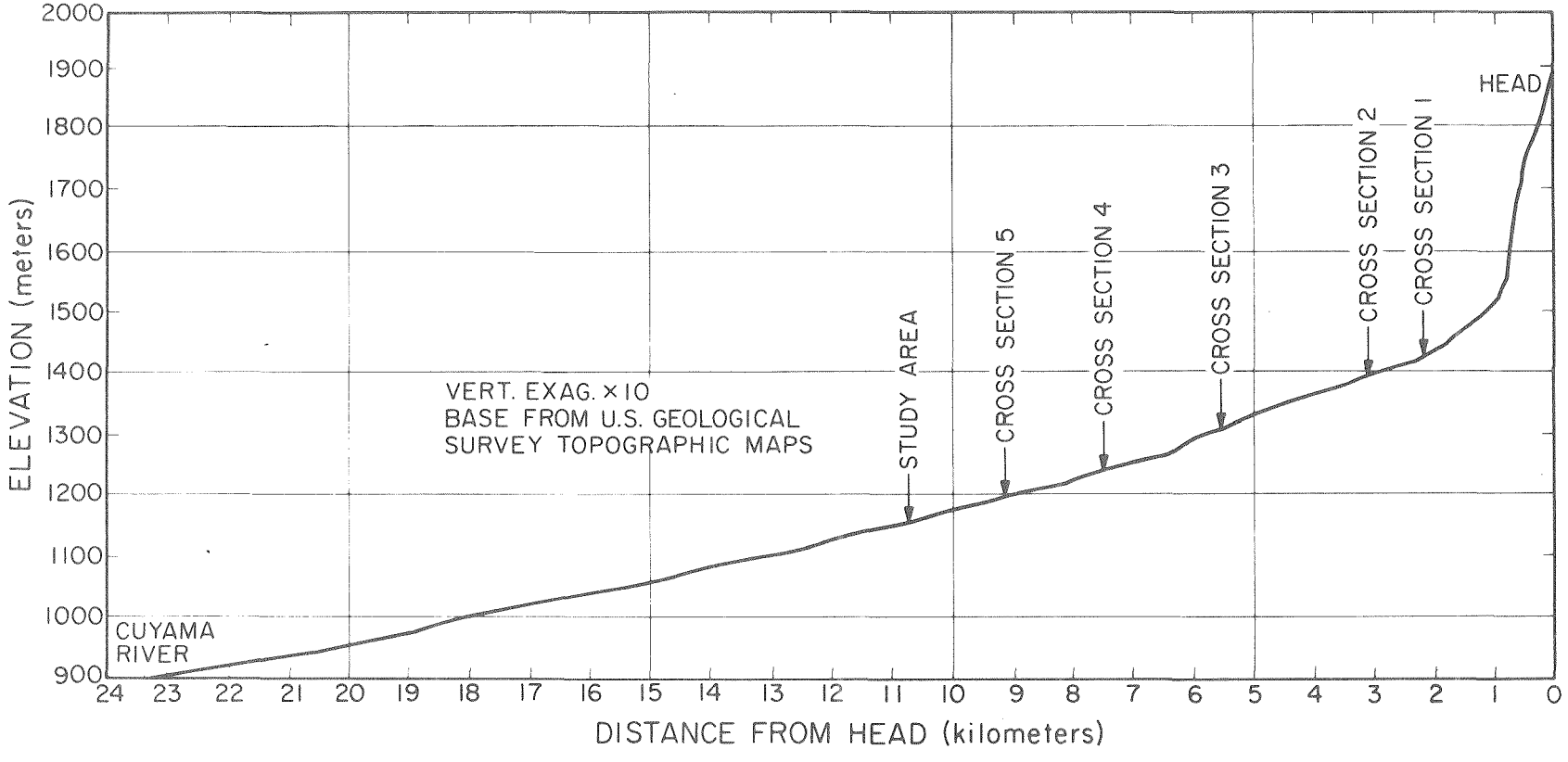

Figure 3-1. Profile of main channel of Quatal Creek.

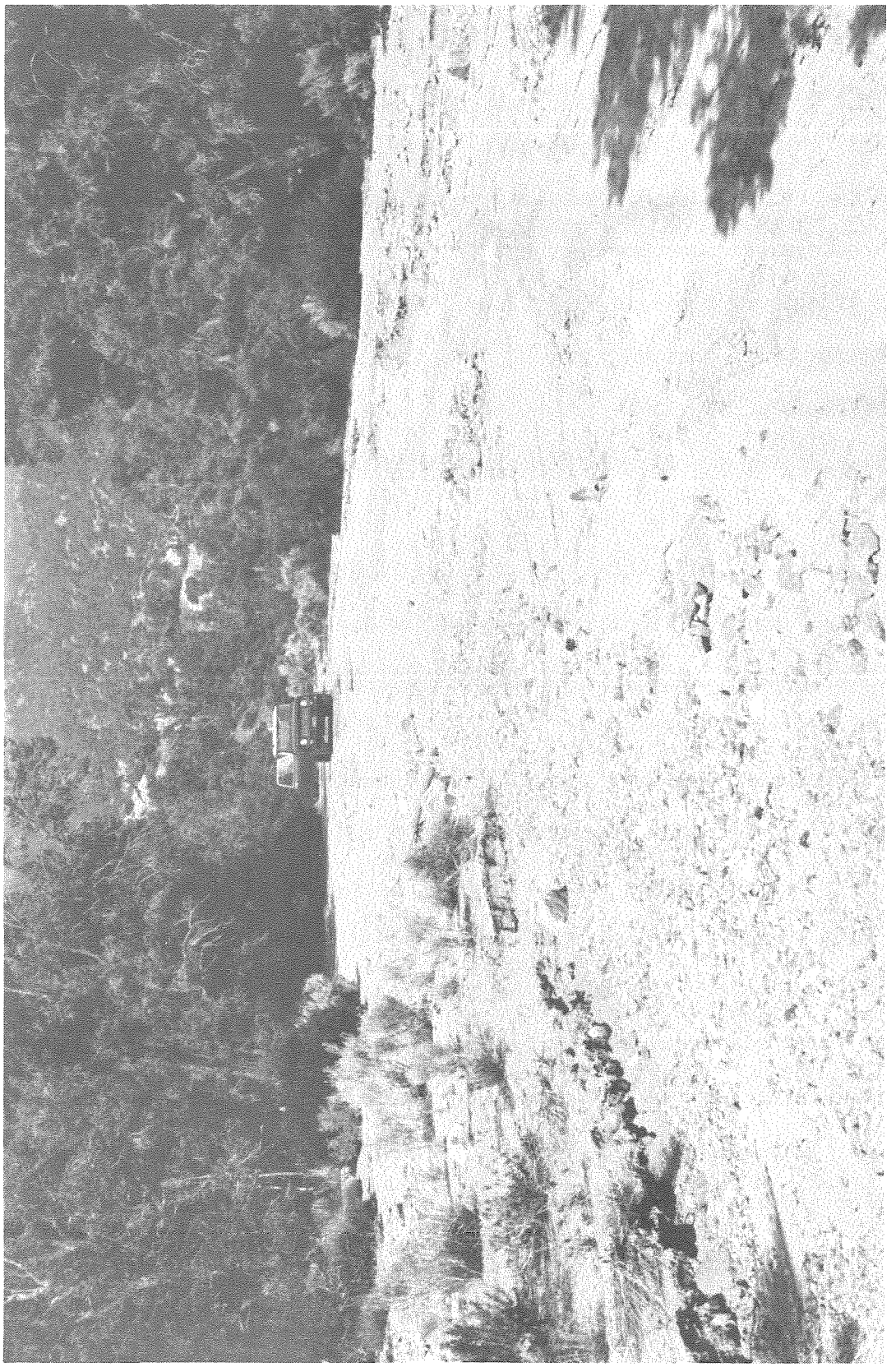

Figure 3-2. Quatal Creek, view upstream at cross section 1.

experiment, the study area was located in the active channel.

Quatal Creek may be at grade for the exceptional flows which fill the whole channel, with the narrower active channel representing a degrading regime. Such instability in the active channel, even if prolonged over decades, may not be quantitatively significant compared to the effects of a single major flood. However, the bed elevation instability would seriously affect data from a scour and fill experiment. For this reason, it was necessary to evaluate the stability of the active channel. Schumm (1960) has identified a relation between channel width-depth ratio and the silt-clay content of bed and bank sediment for stable streams, so these quantities were measured approximately every 1.5 km for the upper 10 km of the sand-bedded reach of the active channel.

Channel geometry and sediment size distribution. Channel widths were determined by pacing, and channel depths were taken as the height of the lowest active-channel bank. These measurements are presented in Table 3-2. Streambed sediment samples were taken near the center of the active channel on the surface and at 15 cm- and 30 cm-depths. Banks were channel-sampled, except that distinctly different layers were sampled separately. Because of the high silt-clay content of the samples, it was necessary to wash them in a peptizer to separate the sand for sieve analysis. After soaking 24 hours in a .01N sodium oxalate solution, as recommended by Krumbein and Pettijohn (1938), samples were washed on a Tyler number 200 sieve (.074 mm). That part of the sample passing the sieve was considered the silt-clay fraction (Schumm, 1960, p.18). The remaining sample was dried, and a sieve analysis performed using standard 10-inch Tyler sieves shaken for 10 minutes on a Tyler

Rotap Machine. Comparison of early $\sqrt{2}$ - series analyses with 2-series indicated that the 2-series was adequate, and it was used for all remaining samples. Distributions were plotted on logarithmic-probability paper. Geometric means and standard deviations for the samples are shown in Table 3-1.

Channel stability. These data were combined with channel width and depth values to derive the weighted mean percent silt-clay, designated M by Schumm (1960):

$$M = \frac{S_c \times W + S_b \times 2d}{W + 2d}$$

where S_c is percentage silt-clay in the bed, S_b is percentage silt-clay in bank material, W is channel width, and d is channel depth. Calculations of M, and tabulated values of d, W, S_c, S_b, W/d, and slope S are shown in Table 3-2 for sections shown in Figure 2-2. Figure 3-3 is Schumm's (1961) plot of W/d vs. M for stable ephemeral-stream cross-sections, with Quatal Creek data added. Quatal Creek data are within the scatter of Schumm's data, indicating that the active channel of Quatal Creek is probably stable, and therefore any scour and fill data will probably not be biased by aggradation or degradation.

Summary of Study-Area Data

Scour-cord emplacement in the study area was completed 22 November 1973. Table 3-3 is a summary of daily rain-gauge data for Pattiway for the period of this experiment, compiled from NOAA monthly Climatological Data summaries for California. The rains which occurred before all scour-cords were installed produced some runoff in Quatal Creek but no

TABLE 3-1. QUATAL CREEK SEDIMENT CHARACTERISTICS

d_g Geometric Mean Size mm	σ_g Geometric Standard Deviation of Sizes	S_c Bed Silt-Clay %	S_b Bank Silt-Clay %	Description of Sample
Cross-section 1				
.206	3.20	18.06		Streambed upper crust
1.46	7.33	6.36		Streambed 15 cm depth (incl. pebble layer)
.850	3.98	8.40		Streambed 30 cm depth
.367	2.86		10.64	North bank
.400	3.80	10.64		Streambed 0-15 cm (excl. pebble layer)
.685	4.12		8.43	South bank
Cross-section 2				
.370	5.95	19.09		Streambed upper crust
1.22	5.53	7.94		Streambed 15 cm depth
1.17	4.68	7.36		Streambed 30 cm depth
.235	3.13		16.08	North bank
.540	3.63		8.32	South bank
Cross-section 3				
.347	4.15	13.71		Streambed upper crust
1.21	4.59	6.67		Streambed 15 cm depth
1.05	4.43	8.23		Streambed 30 cm depth
.292	3.87		15.38	North bank-upper layer
.297	4.44		17.48	North bank-lower layer
Cross-section 4				
.216	3.68	20.34		Streambed upper crust
2.37	7.47	7.23		Streambed 15 cm depth
1.61	4.63	6.57		Streambed 30 cm depth
.320	3.75		14.00	North bank-upper 30 cm
.246	3.03		14.16	North bank-below 30 cm
Cross-section 5				
∿ .230	∿ 3.28	∿ 20		Streambed upper crust
2.40	8.04	6.90		Streambed 15 cm depth
1.57	4.27	5.22		Streambed 30 cm depth
.304	2.50		7.69	South bank

TABLE 3-2. QUATAL CREEK CHANNEL DATA

Cross-Section	d Depth	W Width	W/d Width-Depth Ratio	S_c Bed Silt-Clay	S_b Bank Silt-Clay	S Slope	M Weighted Mean Silt-Clay
	cm	m		%	%		%
1	30	9	30	8.5	9.5	.0344	8.56
2	45	14	30	7.7	12.2	.0333	7.98
3	60	12	20	7.5	16.4	.0333	8.31
4	60	12	20	6.9	14.1	.0239	7.55
5	60	12	20	6.1	7.7	.0239	6.54

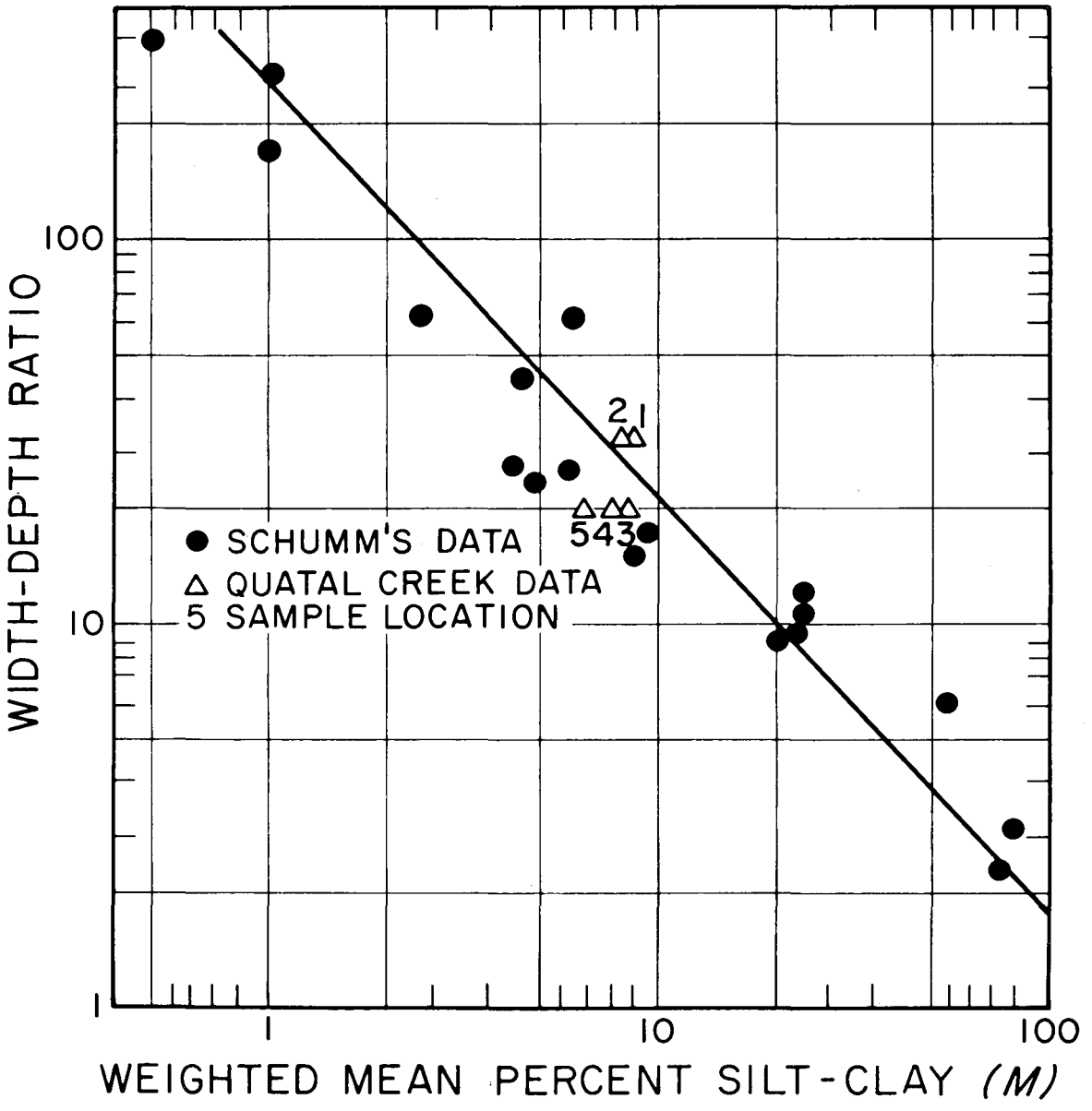

Figure 3-3. Relation between width-depth ratio and weighted mean percent silt-clay in bank and channel sediments for stable cross sections (after Schumm, 1961, Fig. 38).

TABLE 3-3. DAILY PRECIPITATION DATA - PATTIWAY, CALIF. (inches of precipitation)

		1	2	3	4	5	6	7	8	9	10	11	12	13	14	15	16	17	18	19	20	21	22	23	24	25	26	27	28	29	30	31	Total
November	1973												.06					.09	.50				F	.30		.17						1.32
December	1973	.02	.18												.20				.10				.15		T		.02				†		.67
January	1974		.04		1.10	.42			.16				.08					.43				.61										2.84
February	1974		T	*	*									T				.14		.12			T									.26
March	1974		T		.12				1.35	.05											.09			M(?)			.06	T	.01			.18	1.86
April	1974		.50								.02									.12					.01								.65
May	1974																																.00
June	1974																																.00
July	1974																								.12	.10	.03						.25
August	1974																																.00
September	1974																																.00
October	1974		.05	.17					.08											*	*								.40	.44	.02		1.16
November	1974		.26																				.21										.47
December	1974				1.64	.16							.02	*	*								.18						.11	.03		.08	2.22
January	1975							.01				*																			.01	.05	.07
February	1975			.37		.18					.08				.07						T												.70
March	1975					.08	.46		.37	.40	.02	.05	.37		.13		.12				*	*	(M .20)			.01	T						2.21

† - SCOUR - CORDS CHECKED, NO SCOUR OR FILL
* - SCOUR - CORDS RECOVERED AND MEASURED
F - SCOUR - CORD INSTALLATION COMPLETE
M(?) - MOTORCYCLE RACE, DATE UNCERTAIN, 200-400 PARTICIPANTS
M - MOTORCYCLE RACE, 400 PARTICIPANTS

measurable scour and fill of those scour-cords then in place.

Scour-cords were recovered in February, October, and December in 1974 and January and March in 1975. The October '74 recovery was made to ensure that the scour-cords were ready for the coming rainy season and not in response to a known storm. The October measurements showed a maximum of only 10 cm of scour and fill since February 1974 so these data will not be discussed in detail. Although Table 3-3 shows a 1.35-inch rainfall at Pattiway on 8 March, this event did not result in appreciable runoff in Quatal Creek. Although principal episodes of rainfall at Pattiway do not correlate one-for-one with runoff events in Quatal Creek, the two major runoff events to be discussed are probably related to storms recorded at Pattiway on 4 and 21 January 1974 and 4 December 1974. However, total runoff in Quatal Creek clearly cannot be estimated from the Pattiway data.

A storm in early March 1975 was widespread throughout southern California, and Pattiway data for that period are probably a modestly accurate indicator of precipitation in Quatal Canyon. However, peak runoff was minor and uncertainties caused by net channel fill during the event result in a 40 percent uncertainty in estimated water depth and scour and fill. Data this crude are not useful in quantitative scour and fill calculations, so they will not be discussed in detail.

January 1974 runoff event. The U. S. Forest Service reported significant rainfall and runoff in Quatal Canyon in January 1974. The study area was visited and all scour-cords recovered on 3 and 4 February 1974. Scour-cord sites were relocated using the method

described in Chapter 3. An entrenching tool was used to remove small increments of bed material until the scour-cord was seen (Figure 3-4a). The length of scour-cord turned over (Figure 3-4b) indicated the maximum scour directly, since the end of the cord had been flush with the former streambed surface. Distance from the maximum-scour elevation to the new streambed surface was measured to obtain the fill. Net scour or fill determined from scour-cord measurements was used to calculate post-runoff channel bed elevations.

This method of determining new bed elevations was not used after this event, since it is subject to error if the scour-cords sag, shrink, or stretch. Laboratory experiments have shown that a maximum of 1 percent change of scour-cord length can be expected because of wetting-drying cycles, producing an error of 1 cm or less. Very few instances of sag, where a scour-cord partly collapses down an improperly-filled emplacement hole, have been detected, and scour-cord determinations of net scour or fill in later measurements have generally agreed within 1.5 cm with transit-survey data. Post-flow bed elevations for the January 1974 runoff event were as accurate as those for later events.

Scour and fill data for the January 1974 runoff event are shown in Table 3-4. Scour-cord number designations are the scour-cord set (see Figure 2-4) followed by the position of the scour-cord south of the north-end stake. For example, scour-cord 6-6 is the sixth one south in the sixth set. A "1" in the note column indicates that fill is caused by flow from alluvial cones along the south bank. A "2" in the note column indicates that apparent fill is caused by expansion of the montmorillonite-rich surficial material of the south bar, resulting

(a) Excavating search hole.

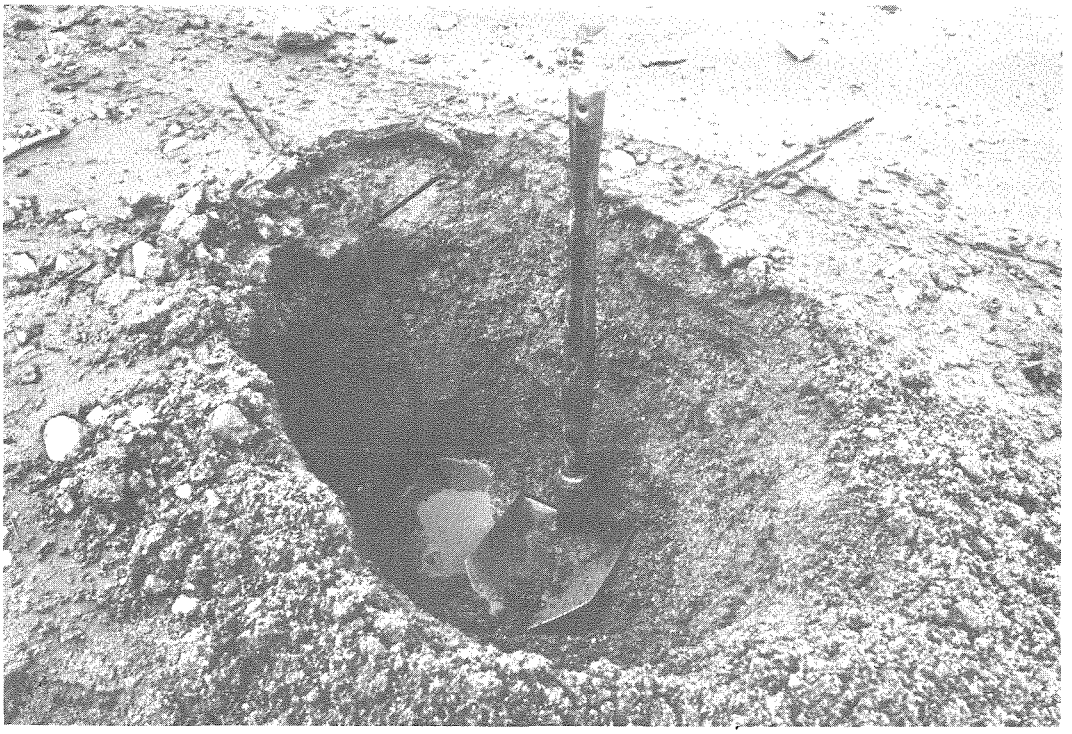

(b) Recovered scour-cord (arrow), straightened to vertical position.

Figure 3-4. Scour-cord recovery.

TABLE 3-4. QUATAL CREEK DATA - JANUARY 1974 RUNOFF EVENT

Scour Cord	Initial Bed Elev m	Scour cm	Fill cm	Final Bed Elev m	Note
1-1	29.08	10.1	10.1	29.08	---
1-2	28.94	5.5	12.8	29.01	---
1-3	28.89	11.6	11.6	28.89	---
1-4	28.88	14.3	24.1	28.98	---
1-5	29.13	0	0	29.13	---
1-6	29.02	0	0	29.04	2
1-7	29.12	0	0	29.13	2
1-8	29.13	0	4.3	29.17	1
1-9	29.39	0	0	29.39	---
1-10	29.56	0	0	29.57	2
2-1	28.93	7.6	11.6	28.97	---
2-2	28.86	0	10.1	28.96	---
2-3	28.76	7.6	12.8	28.81	---
2-4	28.67	0	11.6	28.79	---
2-5	28.93	0	0	28.93	---
2-6	28.96	0	0	28.97	2
2-7	28.90	0	0	28.90	2
2-8	29.05	0	0	29.05	---
2-9	29.13	0	1.2	29.14	1
2-10	29.20	0	1.2	29.21	1
3-1	28.84	19.8	18.6	28.83	---
3-2	28.70	10.1	15.6	28.76	---
3-3	28.63	10.7	16.2	28.68	---
3-4	28.58	11.3	14.0	28.61	---
3-5	28.50	12.5	21.0	28.59	---
3-6	28.79	0	0	28.79	---
3-7	28.79	0	0	28.80	2
3-8	28.77	0	0	28.79	2
3-9	28.92	0	0	28.92	---
3-10	28.98	0	0	28.99	2
4-1	28.71	20.7	22.6	28.73	---
4-2	28.64	6.7	4.6	28.62	---
4-3	28.52	20.1	29.6	28.61	---
4-4	28.47	8.5	8.5	28.47	---
4-5	28.40	20.4	25.3	28.45	---
4-6	28.56	0	0	28.56	---
4-7	28.62	0	0	28.61	2
4-8	28.56	0	0	28.58	2
4-9	28.73	0	0	28.73	---
4-10	28.80	0	0	28.81	2
5-1	28.60	15.2	11.0	28.56	---
5-2	28.53	17.1	14.3	28.50	---
5-3	28.39	8.5	8.5	28.39	---
5-4	28.36	18.9	18.0	28.35	---
5-5	28.25	8.5	17.7	28.35	---
5-6	28.27	15.9	19.2	28.28	---
5-7	28.47	0	0	28.47	---
5-8	28.45	0	0	28.45	---
5-9	28.63	0	1.2	28.64	2
5-10	28.78	0	0.6	28.79	2
6-1	28.36	4.3	8.5	28.40	---
6-2	28.42	13.4	16.8	28.45	---
6-3	28.32	16.5	18.9	28.35	---
6-4	28.23	11.6	11.6	28.23	---
6-5	28.17	10.7	18.3	28.24	---
6-6	28.12	23.8	29.0	28.17	---
6-7	28.08	5.2	10.7	28.13	---
6-8	28.41	0	0	28.41	---
6-9	28.50	0	1.5	28.52	2
6-10	28.65	0	1.2	28.66	2
7-1	28.23	11.0	11.0	28.23	---
7-2	28.26	13.1	13.1	28.26	---
7-3	28.18	7.9	9.1	28.19	---
7-4	28.14	17.7	17.1	28.13	---
7-5	28.02	5.5	16.2	28.13	---
7-6	27.97	10.1	20.7	28.07	---
7-7	27.95	12.8	16.5	27.99	---
7-8	28.24	0	2.7	28.26	2
7-9	28.32	0	0.6	28.33	2
7-10	28.58	0	0	28.58	---
8-1	28.14	7.9	5.2	28.11	---
8-2	28.13	15.9	14.6	28.12	---
8-3	28.06	12.2	17.1	28.11	---
8-4	28.03	21.6	17.7	27.99	---
8-5	27.91	7.9	7.6	27.91	---
8-6	27.86	10.1	16.2	27.92	---
8-7	27.82	14.6	16.2	27.83	---
8-8	28.03	0	1.2	28.04	2
8-9	28.15	0	2.1	28.17	2
9-1	27.98	8.2	7.9	27.97	---
9-2	27.97	9.1	8.8	27.97	---
9-3	27.90	3.1	11.0	27.98	---
9-4	27.86	9.8	8.5	27.86	---
9-5	27.77	17.7	17.7	27.77	---
9-6	27.72	11.3	16.8	27.77	---
9-7	27.70	14.3	18.3	27.74	---
9-8	27.88	32.9	11.6	27.67	3
9-9	28.05	0	0	28.05	---
10-1	27.79	3.4	15.8	27.91	---
10-2	27.84	12.8	12.8	27.84	---
10-3	27.70	8.5	12.2	27.74	---
10-4	27.65	7.9	13.4	27.70	---
10-5	27.57	7.0	13.1	27.63	---
10-6	27.58	10.1	11.9	27.60	---
10-7	27.78	40.5	15.2	27.53	3
10-8	27.83	0	0	27.83	---
11-1	27.69	11.9	11.9	27.69	---
11-2	27.83	0	0	27.83	---
11-3	27.72	0	4.0	27.76	---
11-4	27.55	17.4	17.1	27.55	---
11-5	27.46	6.4	15.2	27.55	---
11-6	27.44	13.1	16.5	27.48	---
11-7	27.41	22.6	18.3	27.36	---
11-8	27.37	10.1	10.7	27.41	---
11-9	27.54	0	0	27.54	---
12-1	27.50	10.1	3.0	27.43	---
12-2	27.51	0	0	27.51	---
12-3	27.39	15.2	15.2	27.39	---
12-4	27.32	8.5	19.5	27.43	---
12-5	27.32	12.2	15.2	27.35	---
12-6	27.32	22.3	22.3	27.32	---
12-7	27.23	17.4	17.4	27.23	---
12-8	27.30	11.0	4.0	27.23	---

from increased moisture content relative to the totally dry conditions of the initial survey. Two scour-cords, 9-8 and 10-7, located on the south bar were exposed to channel flow by lateral erosion of the north bank of the bar. Except for these special cases, identified by a "3" in the note column, maximum measured scour was 24 cm and maximum net bed elevation change in the main channel was 12 cm.

Figure 3-5 is an enlarged view of the scour-cord array area of Figure 2-4, with maximum-scour contours derived from data in Table 3-4 shown for flow in the main channel. The south bar was not overtopped, and is not included in the area shown. There were no signs of overbank flow on the streambanks in the study area. The scour contoured in Figure 3-5 is the difference between initial bed elevation and elevation of the bottom of the layer of reworked bed material indicated by the scour-cords. Since bed elevation changed very little during this event, as can be seen in Table 3-4 and cross-section AA' in Figure 3-5, it makes little difference if scour is measured from the initial or final bed surface. The difference was, however, important in the December 1974 runoff event.

December 1974 runoff event. The U. S. Forest Service reported heavy rain throughout the Quatal Creek area in early December 1974. All but 13 scour-cords were recovered and measured on 13 and 14 December, eight days after the storm as recorded at Pattiway (Table 3-3). The 13 unrecovered scour-cords were below the temporary water table in the streambed. All but 9-4 were recovered on 11 January 1975 under drier conditions. Scour-cord 9-4 was presumed lost since it failed to appear in an excavation deeper than the known depth of the penetrator-

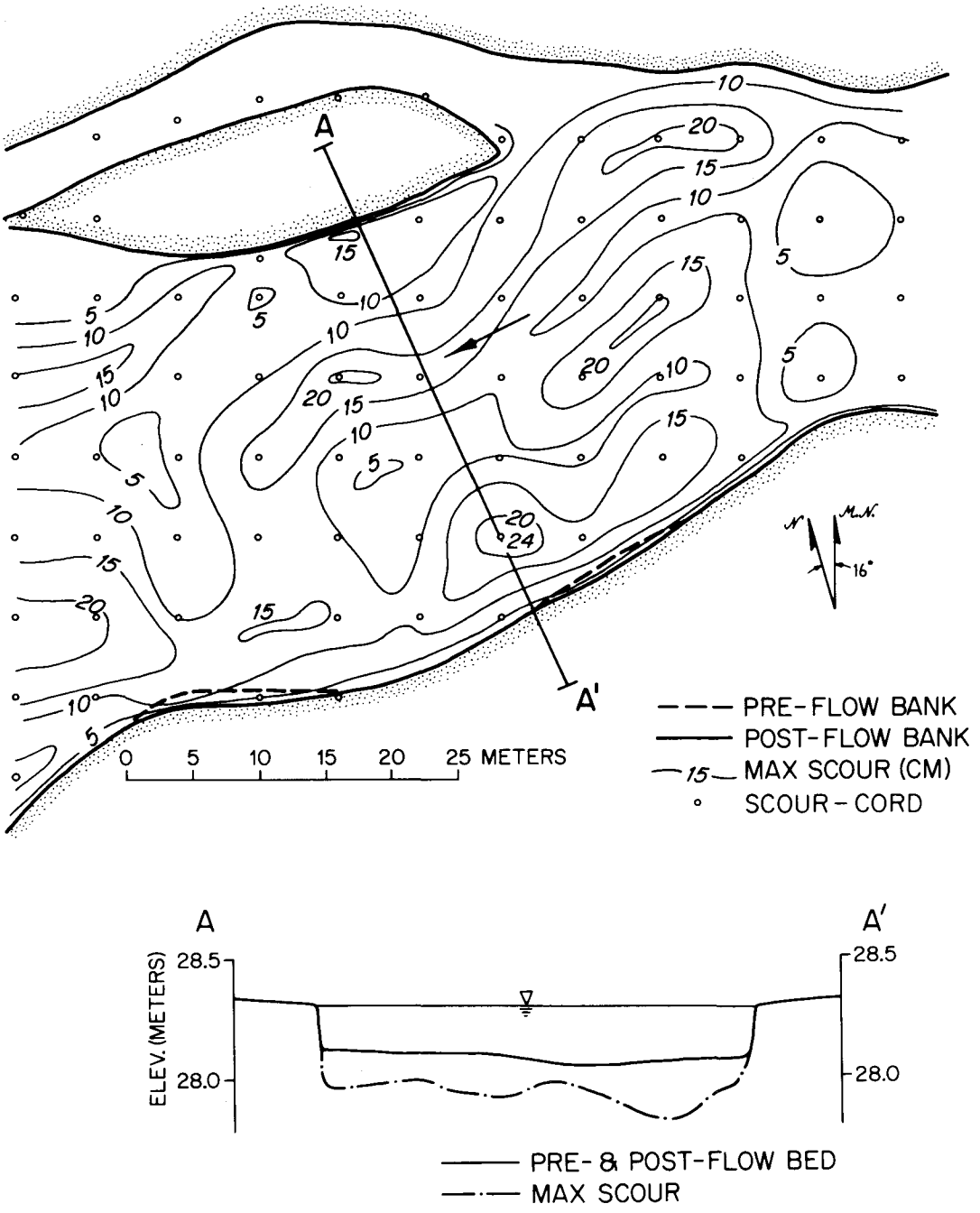

Figure 3-5. Maximum-scour map, January 1974 flood.

anchor. It was replaced.

Table 3-5 provides a summary of scour-cord data for the December 1974 event, with scour measured from the pre-flow (October '74) surface. Numbers 1-3 in the note column of Table 3-5 have the same meaning as in Table 3-4. A "4" in the note column indicates that no flow occurred at that location and any pre- and post-flow elevation difference is within the surveying error. A "5" in the note column indicates a location on the south bar where there was no apparent flow, but the ground was frozen and the scour-cord was not actually inspected.

Maximum scour from the pre-flow bed was at least 88 cm, with more possible but not probable at scour-cord location 9-4. Figure 3-6 is a contour map of maximum scour measured from the pre-flow surface. Modification of the south bar was more extensive than for the January 1974 event, but not major. Up to 21 cm of net scour from the pre-flow bed occurred in the main channel, and maximum bed reworking from the post-flow bed was 73 cm in the study reach, and 66 cm at cross-section AA' in Figure 3-6.

Net bed elevation change. Comparison of survey data from 22 November 1973 and 21 March 1975 shows a net increase in bed elevation of .033 m in the main channel. This small change encompasses at least four runoff events in which the upper .05 to .90 m of bed was reworked. The prediction of active-channel stability, made above, thus seems valid for the short period of observation.

Motorcycle races. It was discovered on 21 March 1975 that the Dirtdiggers motorcycle club was going to hold an off-road race up Quatal

TABLE 3-5. QUATAL CREEK DATA - DECEMBER 1974 RUNOFF EVENT

Scour Cord	Initial Bed Elev m	Scour cm	Fill cm	Final Bed Elev m	Note
1-1	29.08	88.4	72.5	28.92	--
1-2	28.94	17.7	23.2	28.84	--
1-3	28.89	12.2	1.5	28.78	--
1-4	28.88	10.1	5.5	28.83	--
1-5	29.11	0	0	29.10	4
1-6	29.05	20.7	5.2	28.90	3
1-7	29.12	0	0	29.13	4
1-8	29.13	0	5.8	29.15	1,4
1-9	29.39	0	4.8	29.43	1,4
1-10	29.57	0	4.1	29.58	1,4
2-1	28.93	72.5	56.4	28.76	--
2-2	28.95	44.5	23.5	28.74	--
2-3	28.75	15.8	5.5	28.65	--
2-4	28.75	20.4	13.1	28.68	--
2-5	28.93	0	0	28.92	4
2-6	28.96	0	0	28.95	4
2-7	28.90	0	0	28.93	4
2-8	29.05	0	0	29.07	4
2-9	29.15	0	1.5	29.15	1,4
2-10	29.23	0	8.1	29.27	1,4,5
3-1	28.81	44.2	31.7	28.69	--
3-2	28.75	64.3	49.1	28.60	--
3-3	28.65	29.3	18.6	28.54	--
3-4	28.61	19.5	13.7	28.55	--
3-5	28.58	0	16.5	28.70	4
3-6	28.79	0	0	28.77	4
3-7	28.79	0	0	28.80	4
3-8	28.77	0	1.3	28.76	1,4
3-9	28.93	0	0	28.91	4
3-10	29.00	0	1.3	29.00	1,4
4-1	28.72	26.5	7.6	28.45	4
4-2	28.60	69.5	56.1	28.47	--
4-3	28.52	30.5	16.2	28.37	--
4-4	28.46	24.4	12.2	28.34	--
4-5	28.46	20.7	24.1	28.49	--
4-6	28.50	0	4.1	28.49	4
4-7	28.62	0	0	28.64	4
4-8	28.59	0	1.3	28.58	4
4-9	28.73	0	0	28.75	4
4-10	28.83	0	0	28.84	4,5
5-1	28.57	0	0	28.57	--
5-2	28.51	63.1	48.2	28.36	--
5-3	28.40	41.1	35.7	28.35	--
5-4	28.36	32.9	51.2	28.54	--
5-5	28.32	13.1	24.7	28.43	--
5-6	28.29	0	0	28.30	--
5-7	28.47	0	0	28.47	--
5-8	28.45	0	0	28.47	4
5-9	28.66	0	1.3	28.68	4
5-10	28.80	0	0	28.81	4,5
6-1	28.36	0	0	28.38	4
6-2	28.44	32.9	12.5	28.24	--
6-3	28.26	63.1	60.4	28.24	--
6-4	28.22	30.5	22.3	28.14	--
6-5	28.18	16.2	4.0	28.06	--
6-6	28.13	0	11.3	28.25	--
6-7	28.08	0	5.2	28.13	--
6-8	28.41	0	0	28.40	4
6-9	28.50	0	0	28.54	4,5
6-10	28.66	0	0	28.67	4,5
7-1	28.24	0	0	28.23	4
7-2	28.25	0	9.4	28.35	--
7-3	28.17	76.5	64.0	28.04	--
7-4	28.08	32.3	23.2	27.99	--
7-5	28.06	28.0	16.5	27.94	--
7-6	28.01	0	13.7	28.15	--
7-7	27.97	0	6.1	28.04	--
7-8	28.22	0	0	28.24	4
7-9	28.29	0	0	28.32	4,5
7-10	28.55	0	0	28.56	4,5
8-1	28.09	0	1.5	28.11	--
8-2	28.11	0	7.0	28.18	--
8-3	28.09	16.5	0.6	27.93	--
8-4	27.98	67.1	58.2	27.89	--
8-5	27.92	18.0	13.4	27.88	--
8-6	27.93	13.7	18.6	27.98	--
8-7	27.86	0	6.1	27.92	--
8-8	28.05	0	0	28.04	4,5
8-9	28.16	0	0	28.15	4,5
9-1	27.92	0	3.7	27.96	--
9-2	27.95	4.6	13.1	28.04	--
9-3	27.95	4.3	7.9	27.98	--
9-4	27.85	>79.2	>76.2	27.81	--
9-5	27.81	26.5	13.1	27.68	--
9-6	27.76	30.8	23.2	27.68	--
9-7	27.72	2.7	9.8	27.79	--
9-8	27.65	12.8	12.5	27.65	--
9-9	28.07	0	0	28.09	4
10-1	27.86	16.8	15.2	27.84	--
10-2	27.81	0	0	27.84	4
10-3	27.70	41.8	42.4	27.71	--
10-4	27.72	57.6	44.2	27.58	--
10-5	27.65	20.7	14.3	27.58	--
10-6	27.57	6.7	4.6	27.55	--
10-7	27.52	19.8	21.0	27.53	--
10-8	27.83	0	8.8	27.92	1,5
11-1	27.69	0.3	0	27.68	--
11-2	27.83	0.6	0	27.82	--
11-3	27.72	1.5	0	27.70	--
11-4	27.54	17.7	23.8	27.60	--
11-5	27.55	69.8	59.4	27.45	--
11-6	27.44	15.2	7.6	27.37	--
11-7	27.41	17.7	17.7	27.41	--
11-8	27.39	16.5	21.3	27.44	--
11-9	27.55	0	0	27.58	4
12-1	27.44	4.0	7.9	27.48	--
12-2	27.51	0	1.2	27.52	--
12-3	27.39	17.1	21.0	27.43	--
12-4	27.40	67.4	66.8	27.39	--
12-5	27.38	30.8	19.2	27.26	--
12-6	27.29	8.8	4.0	27.24	--
12-7	27.23	10.1	19.2	27.32	--
12-8	27.27	10.1	16.8	27.33	--

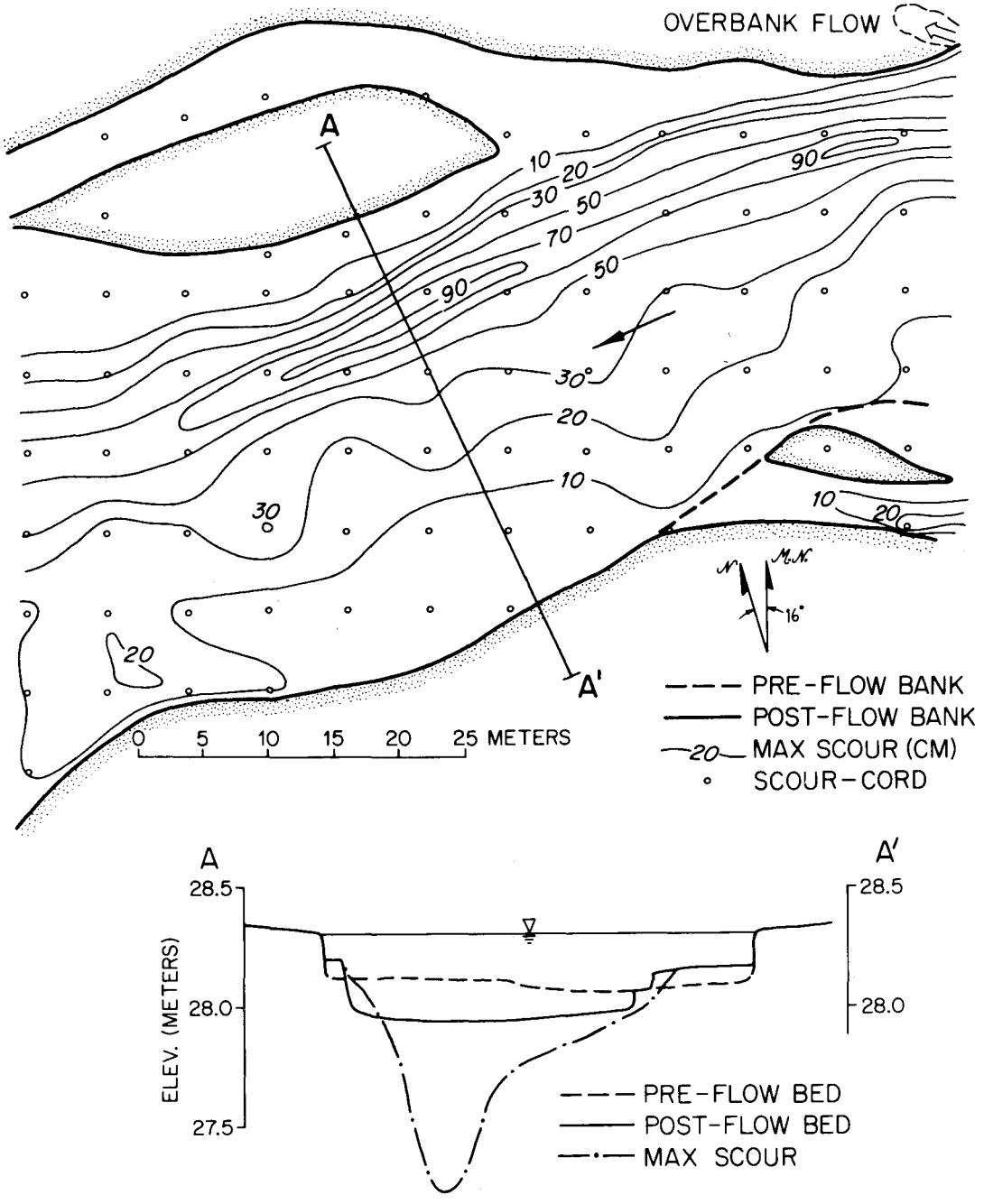

Figure 3-6. Maximum-scour map, December 1974 flood.

.Creek for 400 motorcycles on 22 March. The race course crossed through the study area approximately along the seventh row of scour-cords south of the end stakes. The motorcycles were expected to run in a line astern, so a fairly narrow trench would be plowed-up along the course. A similar race held in the spring of 1974 had no apparent effect on the south bar, except to knock down the banks on the course. It is possible that bank modification of the south bar in the December 1974 runoff event was along the course of this previous race.

Motorcycle races probably do not affect the accuracy of scour and fill data for the main channel. However, they do cast doubt on the mechanisms responsible for bank modification and the origins of some "channels" on the bars. A freshly-excavated scour-cord could be moved by a direct hit from a motorcycle tire. Also, the influx of race spectators into the area greatly increases the probability of vandalism in the study area.

CHAPTER 4. DISCUSSION OF FIELD RESULTS

Introductory Statement

Scour and fill data presented in Chapter 3 do not automatically differentiate mean-bed scour and fill and local scour and fill caused by bedform migration. However, if maximum bedform scour and fill can be estimated, an order-of-magnitude estimate of mean-bed scour and fill is possible. Since there is no gaging station on Quatal Creek and runoff events were not directly observed, it is necessary to estimate flow depth and velocity from hydraulic theory before maximum bedform amplitude can be determined.

Analysis of Flow Behavior of a Steep Sand-Bed Stream

The dune is the most common bedform in alluvial streams, but it varies greatly in amplitude for given flow parameters (Vanoni, 1971). Antidunes are less common, as they only occur in steep, sand-bed streams, but they have maximum amplitudes analytically related to flow parameters (Kennedy, 1961). For antidune regime, flow velocity can be estimated to within 50 percent, if channel geometry, bed sediment size, and water depth are known.

Flow parameter estimation. If a flow is assumed to be in equilibrium, that is, not changing its depth or velocity along a uniform channel at constant slope, the gravitational driving force is balanced by channel frictional resistance. The mean flow velocity, V, can be calculated using the definition of the Darcy-Weisbach friction factor (Kennedy, 1971, eq. 2-F.2):

$$V = \left(\frac{8grS}{f}\right)^{1/2} \qquad \text{(Equation 4-1)}$$

f = Darcy-Weisbach friction factor

where r = hydraulic radius = $\frac{Wd}{W+2d}$ (for rectangular channel)

S = channel slope << 1.

If channel geometry is known and bankfull flow is assumed, the only unknown on the right side of this equation is f. Since f is dependent both on bed-sediment grain roughness and bedform roughness, it cannot generally be determined where bedform size is unknown. However, Taylor and Brooks (1961), and Kennedy (1961) have found for antidune flow:

$1 \leq f/f' \leq 2$ where f' = equivalent pipe friction factor for bed sediment grain roughness.

Nordin (1964, Figure 7) found for antidune-regime flow in the Rio Grande that

$$0.9 \leq f/f' \leq 2 \qquad \text{(Equation 4-2)}$$

for $d_g = 0.29$ mm, $\sigma_g = 1.62$.

Apparently in such a stream the turbulence-damping effect of suspended sediment reduces the friction factor below that for grain roughness of a flat bed (Vanoni, 1944). Figure 4-1 is Moody's (1944) diagram of friction factor as a function of Reynolds number for commercial pipes, where for channel flow:

Reynolds number: $Re = \frac{4rV}{\nu}$

Pipe relative roughness: (Based on diameter) $\left(\frac{\varepsilon_s}{d}\right) = \frac{d_g}{4r}$

} Kennedy, 1971

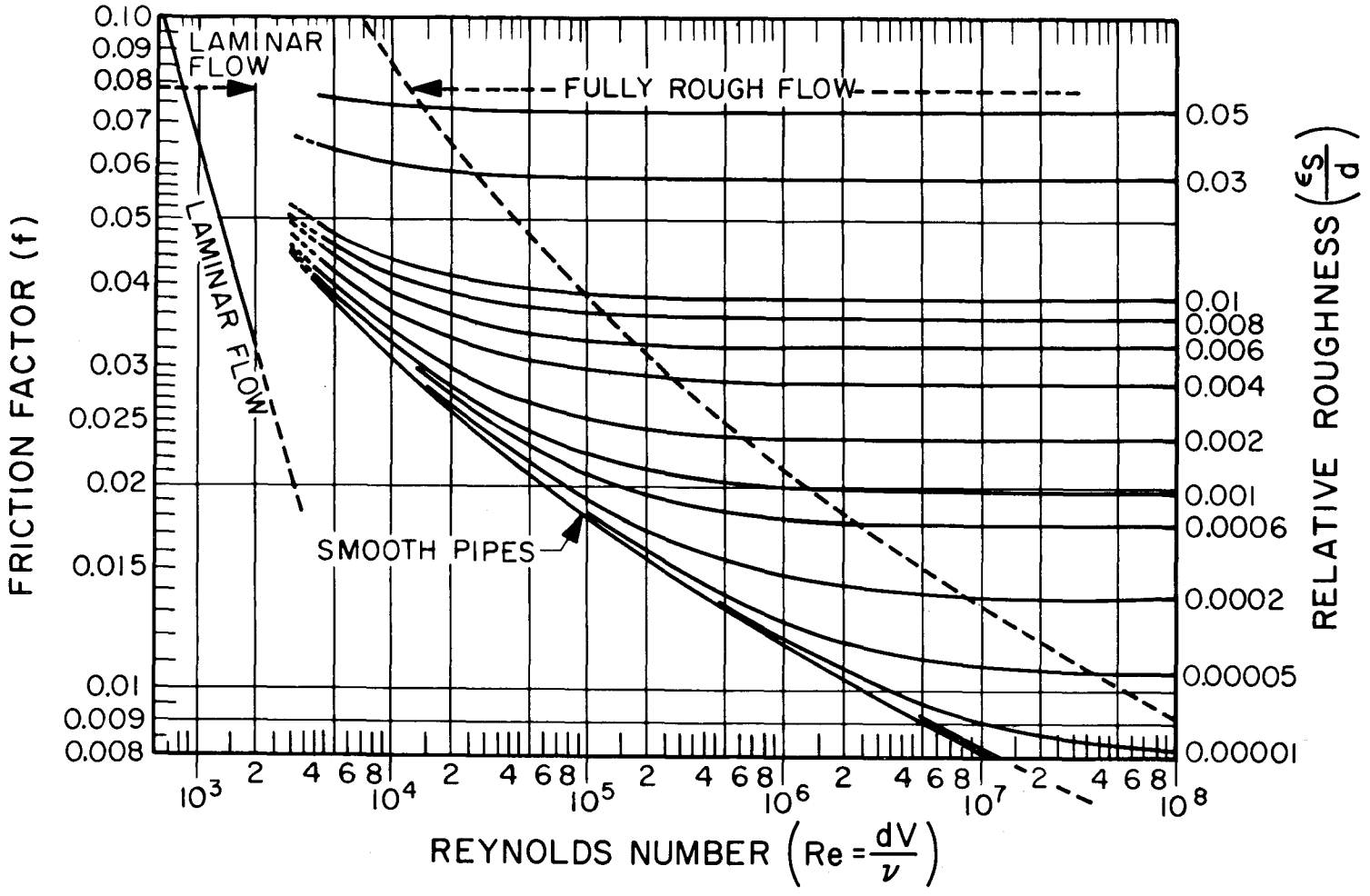

Figure 4-1. Friction factor as a function of Reynolds number for round pipes of various relative roughness ratios (Moody, 1944).

and: ν = water kinematic viscosity

Reynolds number can be calculated only after velocity of flow has been estimated, but for fully rough flow f is independent of Reynolds number. Thus, a range of flow velocity can be estimated in a channel whose slope, width, depth, and bed material size are known, by means of equation 4-1 with the range of f derived from equation 4-2. After the velocity is estimated, Reynolds number can be calculated and validity of the assumption of fully rough flow checked. If the Reynolds number is too low for fully rough flow, the f for that Reynolds number from Figure 4-1 can be used to calculate a new velocity and Reynolds number. This iterative process is continued until the friction factor and Reynolds number match for a given relative roughness.

Antidune amplitude estimation. The term "antidune" was coined by Gilbert (1914) to describe bedforms which moved upstream in his flume experiments, although the bedforms had been described by others as early as 1899 (Kennedy, 1961, p.4-5). In his experimental and analytical study of antidunes, Kennedy (1961, p.3) defined them "... as any disturbances on the bed of an alluvial channel which are periodic or nearly so, and which are strongly coupled with stationary free-surface waves. Under this definition, dunes are a type of antidune when they interact with the free surface...". Kennedy's definition of antidunes includes bedforms which move downstream. Figure 4-2 shows water-surface waves which accompany antidunes, called "stationary waves" by Kennedy (1961, p.3), on the San Juan River at Eight-Mile Rapids near Mexican Hat, Utah. Figure 4-3 shows antidune and stationary wave geometry for

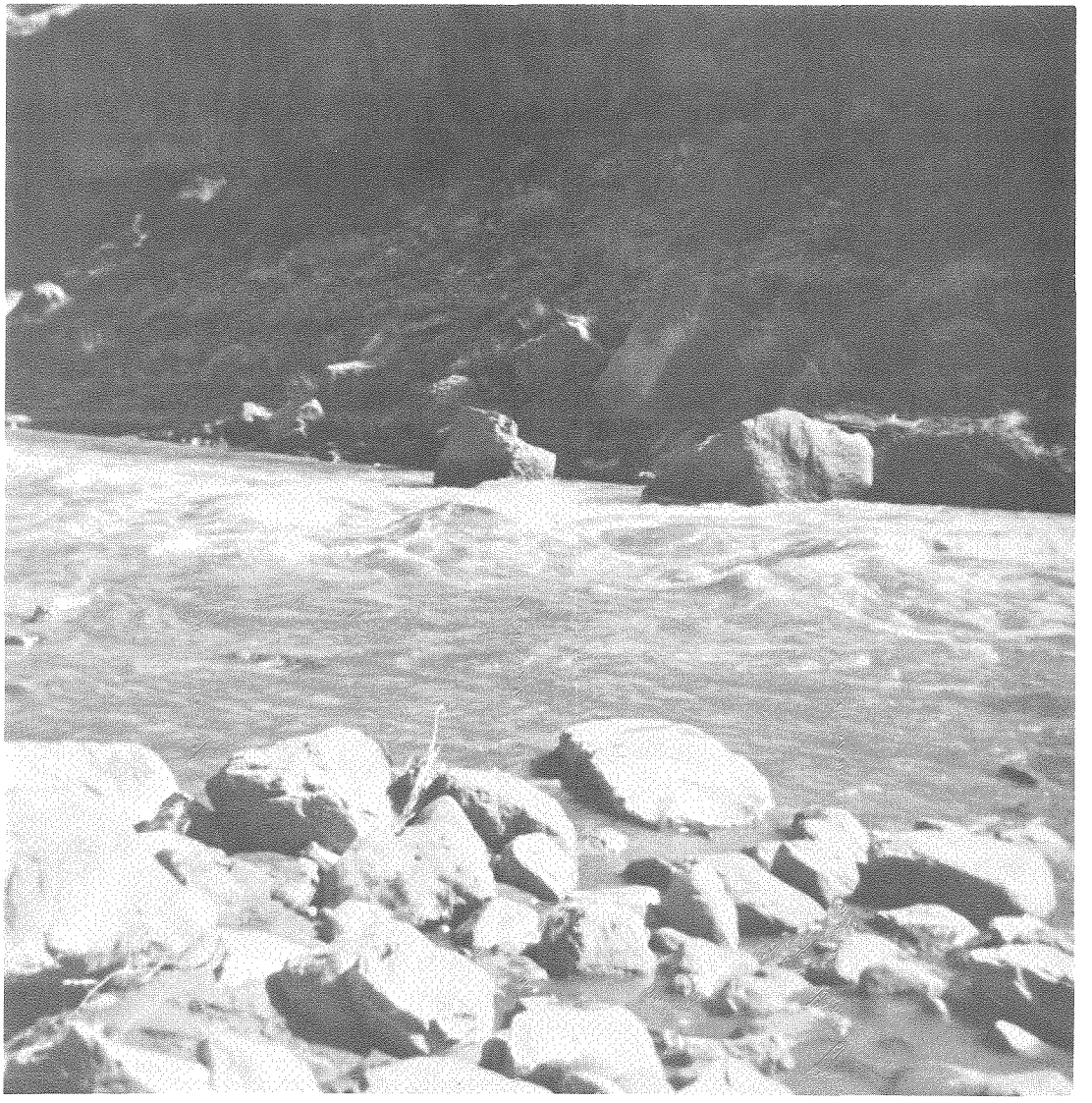

Figure 4-2. Stationary waves at Eight-Mile Rapids on San Juan River near Mexican Hat, Utah. Wavelength approximately 3 meters.

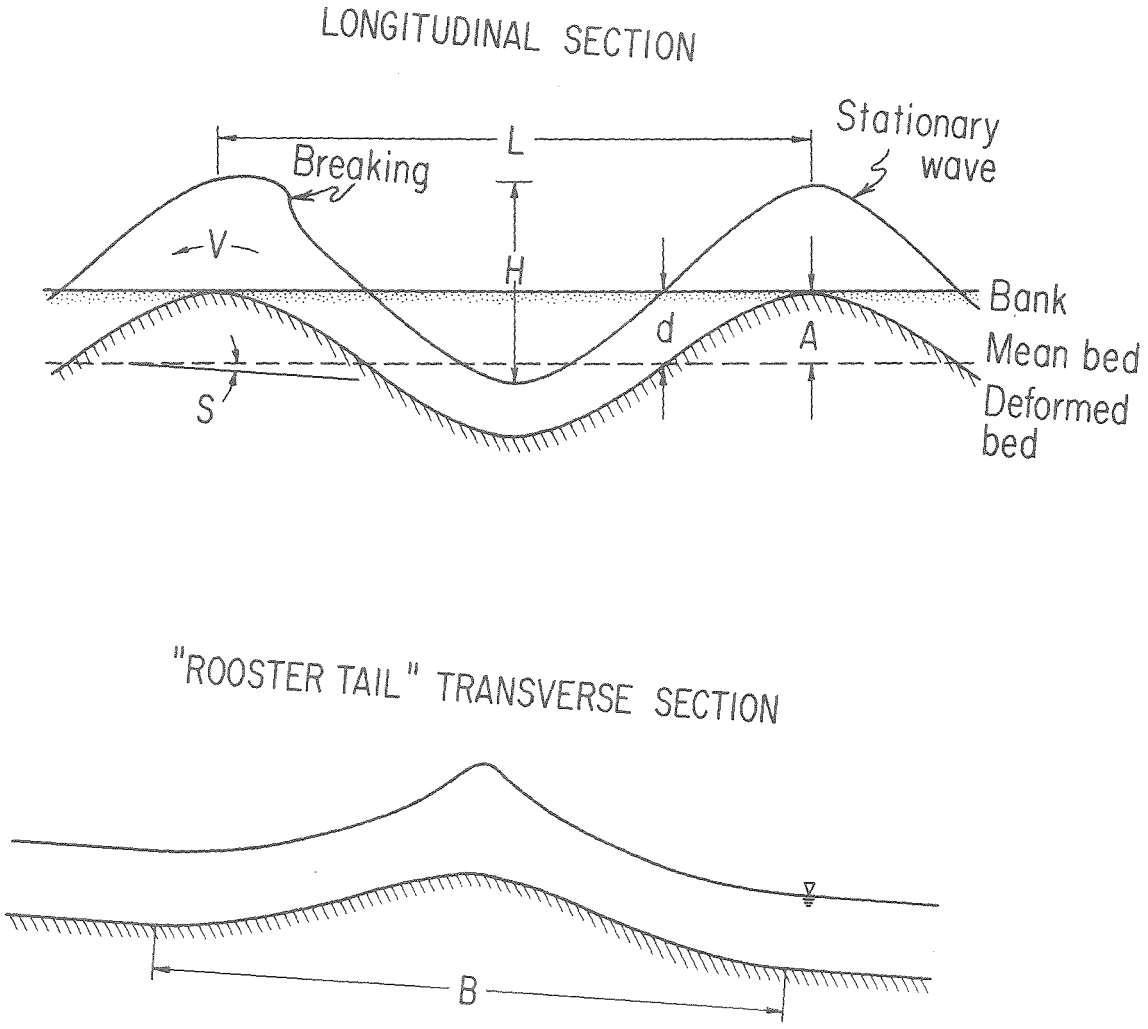

Figure 4-3. Stationary wave and antidune geometry (vertical exaggeration 2x).

along-stream (longitudinal) and across-stream (transverse) sections.

For antidunes, Kennedy (1961) has found that wavelength, L, of antidunes and stationary waves (Figure 4-3) is related to mean flow velocity by the equation:

$$V = \left(\frac{gL}{2\pi}\right)^{1/2} \qquad \text{(Equation 4-3)}$$

This relation was confirmed in field measurements by Nordin (1964). However, equation 4-3 is only applicable to stationary waves with crests that are wide relative to wavelength. Three-dimensional stationary waves, called rooster tails, are more common in streams. The velocity-wavelength relation derived using inviscid flow theory by Kennedy (1961) for this type of stationary wave and antidune is:

$$V = \left(\frac{gL}{2\pi}\right)^{1/2} \left[1 + \left(\frac{L}{B}\right)^2\right]^{1/4} \qquad \text{(Equation 4-4)}$$

where B is the transverse wavelength (see Figure 4-3). Kennedy (1961) found qualitative experimental agreement with this relation. Thus, if B can be estimated, the range of L can be determined from the flow velocities calculated using equations 4-1 and 4-2.

Kennedy (1961) found that maximum stationary wave height, H_{max} (Figure 4-3), was:

$$H_{max} = .142\ L \qquad \text{(Equation 4-5)}$$

Finally, Kennedy derived the relation between stationary wave height and antidune amplitude, A, for an inviscid flow:

$$\frac{A}{H} = \frac{1}{2}\left(1 - \frac{g}{V^2 k} \tanh kd\right) \cosh kd \qquad \text{(Equation 4-6)}$$

where $k = \frac{2\pi}{L}$ = wave number

This relation has not been verified in the laboratory or field. Pierce (1916) reported:

> "The writer was informed by Prof. H. E. Gregory, of Yale University, that in swimming down through a short section of the San Juan he found that in going over the crest of the antidunes he could touch bottom with his feet and at the same time keep his head above water, but that in the trough of a wave he had to go down more than arm's length below the surface to touch bottom." (p.43)

Gregory's experience in this case seems to be that antidune height was greater than stationary wave height and that the difference was in the direction of deeper antidune troughs, although Henderson (1966, p.410) does not support Gregory's observations on theoretical grounds. Equation 4-6 is probably accurate, since it requires that $\frac{2A}{H} < 1$, and may be conservative.

Therefore, using equations 4-1, 4-2, 4-4, 4-5, and 4-6, the range of maximum possible antidune amplitudes can be determined for the assumptions of bankfull flow and breaking stationary waves.

Estimation of Flow Behavior in Quatal Creek

Equations 4-1 through 4-6 are not applicable to Quatal Creek unless antidunes are the largest bedforms developed during runoff events. The steep slope (Figure 3-1) suggests that all Quatal Creek flow should be in the upper flow regime (flat bed or antidunes). The relatively flat bed (Figure 2-3) left after a flow shows that no dunes formed on the waning flood. If dunes had formed in some part of the waning flow, they would

not have been destroyed by subsequent lower discharges and would be preserved. All recovered scour-cords were straight and inclined downstream except where there were local effects in the lee of boulders. This behavior suggests that the deepest bed reworking occurred in the upper flow regime.

Pattern of scour and flow regime. The pattern of maximum scour (Figures 3-5 and 3-6) also supports the hypothesis that maximum bed reworking was by antidunes. In the January 1974 runoff (Figure 3-5), maximum scour occurred in three troughs subparallel to the flow. In natural streams, antidunes frequently occur in trains with widths smaller than stream width (e.g., Pierce, 1916, p.42-43). A train of slowly-moving antidunes reworks the streambed along the axis of the train. Since greatest bedform scour and fill occurs where antidunes are the largest, a scour-fill trough results. Figure 3-5 suggests that three separate trains of antidunes operated during the January 1974 runoff. Figure 3-6 indicates that the December 1974 runoff had only one such train, and further that the principal discharge lay along the outside of the bend around the south bar.

Thus, the slope, residual bed pattern, scour-cord behavior, and pattern of scour all suggest that upper-regime flows prevailed during the January and December 1974 runoff events. Scour-cord behavior and the recorded pattern of scour also suggest that the major part of bed reworking was by antidunes. This last hypothesis can be tested by calculating probable antidune amplitudes for the January and December 1974 runoff events.

January 1974 runoff event. For a given channel geometry and bed material, equations 4-1 through 4-6 show that the shallower of two flows has a higher relative roughness, hence higher friction factor. This means that the shallower flow has a lower velocity and smaller antidunes. For bankfull stage, the shallowest, hence most conservative, case occurs when there is no mean-bed scour and flow depth is the bankfull depth of the undisturbed channel (Figure 4-3). Table 4-1 lists the results of calculations using equations 4-1 through 4-6 for the undisturbed channel bed at cross-section AA' of Figure 3-5.

In the calculations in Table 4-1, flow depth is used instead of hydraulic radius because it gives maximum flow conditions in the channel, and not just average flow conditions for the cross-section. Kennedy (1961) notes the desirability of using local flow conditions for antidune calculations in natural streams, where maximum flow conditions may vary greatly from the mean because of irregular channel cross-sections. The difference between maximum depth and hydraulic radius for the January 1974 runoff event is only 1.4 percent, so the distinction is not very important. Stationary wave transverse wavelength is taken as the width of the maximum-scour trough nearest the south bar in cross-section AA', Figure 3-5. Sediment size used for relative roughness calculations in Table 4-1 is d_g = 1.99 mm, the average of the 15 cm- and 30 cm-depth samples at location 5 in Table 3-1, because most of the upper 30 cm of bed was probably being reworked during the peak of the runoff event. Minimum equivalent pipe Reynolds number calculated assuming T = 10°C is 2.04×10^6, well within the fully rough region of Figure 4-1.

TABLE 4-1. CALCULATED FLOW BEHAVIOR - JANUARY 1974 RUNOFF EVENT

d	Maximum flow depth	(m)	0.229
W	Channel width	(m)	32.8
S	Channel slope	-	.0229
$\frac{d_g}{4d}$	Relative roughness factor (d_g = 1.99 mm)	-	.0022
f'	Equivalent pipe friction factor (Figure 4-1)	-	.0241
f	Flow friction-factor range (Equation 4-2)	-	.0482-.0217
V	Maximum mean flow velocity (Equation 4-1)	(m/sec)	2.92-4.35
B	Estimated stationary wave transverse wavelength	(m)	14.63
L	Stationary wave wavelength (Equation 4-4)	(m)	5.15-10.01
H_{max}	Maximum stationary wave height (Equation 4-5)	(m)	.736-1.43
$\frac{A_{max}}{\frac{1}{2} H_{max}}$	Antidune relative amplitude (Equation 4-6)	-	.772 - .891
A_{max}	Maximum antidune amplitude	(cm)	28.4 - 63.7

Calculations in Table 4-1 suggest that a bankfull flow in Quatal Creek, with no change in mean bed elevation, will cause the upper 28 to 64 cm of the bed to be reworked by antidunes. Maximum bed reworking measured by scour-cords for the January 1974 runoff event, shown in Table 3-4, was 24 cm. The calculations used the geometry of the channel cross-section where maximum reworking was observed. These results imply that all bed reworking was by antidune migration. Validity of these calculations will be further considered later.

December 1974 runoff event. Calculated flow behavior for December is the same as for January (Table 4-1), if initial channel cross-section geometry is used. Maximum bed reworking from initial bed elevation in cross-section AA' (Figure 3-6) was 82 cm. At the maximum antidune amplitude of Table 4-1, this amount of reworking implies an additional 18 cm of mean-bed scour. Since 17 cm of net scour of the channel occurred during the December event, use of the initial geometry in maximum-flow calculations is valid only if the net scour occurred after maximum-flow conditions occurred.

If the observed net scour had occurred before or during peak flow, an antidune amplitude range of 48 to 97 cm would have resulted (Table 4-2), enough to account for all the bed reworking. Behavior of the channel as a whole supports this interpretation. Net fill, mostly fine sand, occurred at the edges of the scoured channel (Figure 3-6, cross-section AA'). Scour-cords showed no reworking of the initial bed under this fill, suggesting that filling occurred early in the runoff event and was not disturbed by subsequent antidune development near the banks at peak flow. This asymmetry of channel reworking with net scour in

TABLE 4-2. CALCULATED FLOW BEHAVIOR - DECEMBER 1974 RUNOFF EVENT

d	Maximum flow depth	(m)	.344
W	Channel width	(m)	32.8
S	Channel slope	-	.0229
$\frac{d_g}{4d}$	Relative roughness factor (d_g = 1.99 mm)	-	.0014
f'	Equivalent pipe friction factor (Figure 4-1)	-	.0210
f	Flow friction-factor range (Equation 4-2)	-	.0420-.0189
V	Maximum mean flow velocity (Equation 4-1)	(m/sec)	3.84-5.72
B	Estimated stationary wave transverse wavelength	(m)	15.54
L	Stationary wave wavelength (Equation 4-4)	(m)	8.33-15.05
H_{max}	Maximum stationary wave height (Equation 4-5)	(m)	1.19-2.14
$\frac{A_{max}}{\frac{1}{2} H_{max}}$	Antidune relative amplitude (Equation 4-6)	-	.803 - .907
A_{max}	Maximum antidune amplitude	(cm)	47.8 - 97.0

one part and fill in another contrasts with channel behavior in the January 1974 runoff event. It appears that the December flow was modifying the channel toward a smaller width-depth ratio. The smaller width-depth ratio implies that the December flow carried a larger proportion of fine material than the January flow (Schumm, 1960), and the relatively fine-grained nature of the channel-edge deposition supports this implication. It is more likely that the modification toward a smaller width-depth ratio occurred at peak flow than on the waning flow, so conditions of Table 4-2 probably prevailed.

Comparison between calculated and observed maximum scour supports this conclusion. The January flow inferred from scour-cord measurements is at the lower end of the calculated velocity range of Table 4-1 while the December flow is near the middle of the calculated range of Table 4-2. This suggests that the December flow had a lower friction factor than the January flow. This lower friction factor could have been the result of a higher proportion of fine-grained material carried as suspended load in the December flow. Localization of heavy rainfall in different tributary drainages with dissimilar sediment sizes available for transport could easily account for the difference in load calibre of the two flows. If the sediment source area for the December flow was rich in silt and clay-sized material and deficient in the sand-sizes, the effect on Quatal Creek would have been a reduction of the friction factor ratio and an accompanying trend toward net scour of the channel bed. Although it is possible to account for bed reworking in the December 1974 runoff event entirely by antidune development, under the assumption that the transported load was more fine-grained than usual,

an alternate possibility is that the December channel asymmetry developed because part of the streambed was frozen. The southern half of the streambed is shaded by a cliff, and in episodes of cold winter weather it escapes diurnal thaw. Under such conditions a midday runoff event would scour the northern part of the channel more easily than the southern part. However, the flow would probably thaw the thin (less than 5 cm thick) frozen layer on the southern part of the channel before the end of peak flow, and an initially partly-frozen bed does not explain the fine-grained fill on both the northern and southern channel edges. The assumption of fine-grained load is thus preferred.

Bed "armoring" and flow competence. Since none of the runoff events were directly observed, the validity of the calculations in Tables 4-1 and 4-2 cannot be directly checked. However, in the few instances where pebble or cobble layers were found above or below the turned-over parts of buried scour-cords, competence of the runoff events can be estimated. The pebble layers at the level of the turned-over scour-cords may represent armoring as usually defined, that is a residual accumulation or lag of coarse material as finer debris is removed. However, there is no way to prove that such an armor was formed by the runoff event which exposed it; it may have been formed by an earlier, greater flow with the scour-cord emplaced through it.

Pebble layers above the turned-over parts of buried scour-cords were definitely formed during the runoff event, provided there have been no succeeding effective runoffs. These layers may be formed by dropout from bedload as the flow wanes, or by dropout from bedload at peak flow

in the disrupted flow of a breaking stationary wave over an antidune. The latter type will be called bedload-dropout "armor". Single large clasts may have been transported a short distance by impact or lee-side scouring. These clasts will be larger than those normally transported in the bedload and are invalid as indicators of flow competence.

Table 4-3 is a list of occurrences of "armor" layers in reworked sediment above scour-cords, excluding single large clasts. Sizes tabulated are only order-of-magnitude, since they were estimated by eye. For the December 1974 runoff event, three instances of double "armor" layers were found, for scour-cords 1-1, 5-2, and 10-3 (Table 4-3). These supposed bedload-dropout "armor" layers can form at any depth between the turned-over scour-cord and the bed surface at peak flow, depending on antidune trough position when the stationary wave breaks. Thus, several layers of peak flow dropout armor over a given scour-cord, would indicate the passage of several antidunes. The fact that the upper layer contains smaller size material at scour-cord 1-1 may indicate it formed on the waning flow. However, the upper layer at scour-cord 10-3 is the coarser, suggesting a flow resurgence following deposition of the lower layer, a variety of dropout "armor" sizes possible at a given flow depending on supply, or the lower layer formed on the rising flood before peak discharge and competence.

Theoretical bedload competence of the Quatal Creek flows can be estimated using Shield's shear-stress criterion. Bed shear-stress, τ_o, of the flows is given by: $\tau_o = \rho grS \approx \rho gdS$. Figure 4-4 shows critical bed shear stress for movement of material of a given diameter (Blatt,

TABLE 4-3. OBSERVATIONS OF "ARMOR"-LAYERS ABOVE SCOUR-CORDS

Scour Cord	Armor Size mm	Comment
JANUARY 1974 RUNOFF EVENT		
2-2	100	
3-2	100	
5-1	15-30	
9-2	30-60	
10-1	15-30	
DECEMBER 1974 RUNOFF EVENT		
1-1	65	Upper "armor" layer
1-1	115-130	Lower "armor" layer
2-1	15-30	
3-1	15-30	
3-2	15-30	
5-2	15-30	Upper "armor" layer
5-2	15-30	Lower "armor" layer
5-4	15-30	
6-4	15-30	
7-3	15-30	
7-4	150	On surface
8-5	15-30	On surface
8-6	65-100	On surface
10-3	65-100	Upper "armor" layer on surface
10-3	30-60	Lower "armor" layer
11-5	30-60	
12-5	100	

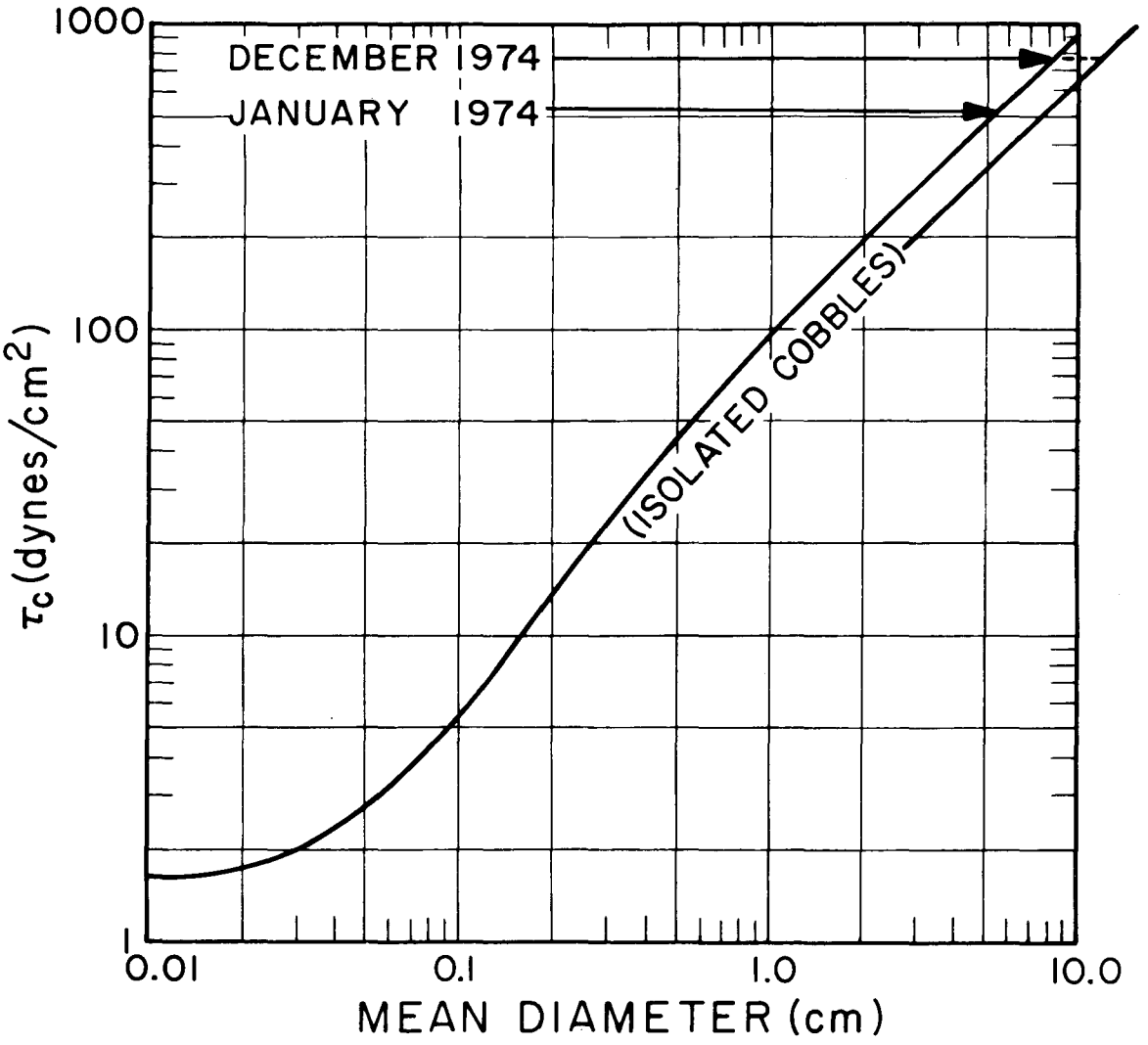

Figure 4-4. Critical bed shear-stress, τ_c, for initiation of movement of quartz debris on a plane bed (after Blatt, Middleton, and Murray, Fig. 4-6, 1972).

Middleton and Murray, 1972). This curve was calculated for quartz-density material from Shield's diagram for T = 16°C, but at grain sizes greater than 10 mm it is independent of temperature (Vanoni, 1966, Figure 2-E.3). The shear stress equation and Figure 4-4 give maximum bedload-transport particle sizes of 52 mm for the January 1974 flow and 85 mm for the December 1974 flow, as calculated for flow through the channel at section AA' in Figures 3-5 and 3-6.

These calculated sizes show reasonable agreement for the January flow with observed "armor" sizes at scour-cords near section AA', Table 4-3. Scour-cords 5-1 and 9-2 bracket section AA' and have maximum "armor" sizes of 15-60 mm. For the December flow, scour-cords 5-2 to 12-5 have observed maximum "armor" sizes of 15-100 mm, with 150 mm cobbles on the surface at scour-cord 7-4. Except for these surface cobbles, "armor" size is in agreement with competence predicted by calculation.

Scour-cord 7-4 is almost on the line of cross-section AA', so maximum flow depth for cobbles <u>on the surface</u> is that used in the calculations in Table 4-2. These competence calculations assume that bedload particles are partly sheltered from the flow in a group of similar-sized particles. A larger relatively isolated clast will have a drag contribution which decreases calculated critical shear stress by a factor of 1.4 (Gessler, 1973). From Figure 4-4, maximum size for isolated large clasts in the bedload is 120 mm. This is a good agreement with the observation at location 7-4, considering the calibre of the measurements.

This general agreement between calculated and observed stream competence suggests that the assumption of bankfull flow in the calculation of Tables 4-1 and 4-2 is reasonable. It is important to note that the observed competence sizes are meaningful only if they represent the largest clast sizes transported as bedload. If the hypothetical formation of bedload-dropout "armor" is correct, the assumption of maximum antidune amplitude in Tables 4-1 and 4-2 is also reasonable. Validity of the theoretical approach of equations 4-1 through 4-6 will be discussed in Chapter 7, as will scour-cord behavior and bedload-dropout "armoring".

CHAPTER 5. LABORATORY EXPERIMENTAL PROGRAM

Introductory Statement -- Purpose and Scope

A series of laboratory experiments on scour and fill was conducted in the W. M. Keck Laboratory of Hydraulics and Water Resources, California Institute of Technology, from April 1974 to May 1975. These open-circuit sand-bed flume experiments were run in both rigid-wall and alluvial-bank channels with constant and time-varying discharges. The purpose was to observe scour and fill caused by floods in a steep sand-bed stream in a controlled laboratory environment. Constant-discharge experiments were run initially to develop laboratory techniques for simulated flood experiments and to investigate general sediment-transport characteristics of the sand and of channel geometry. These experiments were not intended as a detailed investigation of constant-discharge sediment transport or for comparison of open-circuit and closed-circuit sediment transport behavior.

Time-varying discharge experiments, with hydrographs and sediment input-rate curves patterned upon natural ephemeral stream data, were conducted to investigate scour and fill at laboratory scale. Rigid-wall experiments were not exact models of existing ephemeral streams, since bank contribution to the erosion-deposition balance was not occurring, but they did allow observation of basic processes responsible for scour and fill. Although the scour and fill behavior of these rigid-wall laboratory streams, presented and discussed in the next two chapters, cannot be quantitatively scaled to actual field situations, it effectively demonstrated that reworking during floods in a sand-bed stream at grade for the input parameters of these experiments is predominantly by bedform

migration, with only minor mean-bed scour and fill.

Alluvial-bank channel experiments were conducted to test in the laboratory the validity of analytical techniques used in the field observational program. These laboratory channels developed features similar to field channels and aided measurably in interpretation of field data. Although results of these experiments cannot be directly scaled to a field situation, field-scale processes are similar to those observed in these experiments, as will be shown in Chapter 7.

Laboratory Apparatus

The primary laboratory component is a 60-foot tilting flume, a recirculating configuration as described most recently by Taylor (1971). The extensive modifications necessary to convert the flume to a programmable-inlet, open-circuit configuration are outlined below.

The 60-foot tilting flume. The flume (Figure 5-1) consists of two 12-inch structural steel channels bolted to a steel bottom plate, forming a trough 18.3 m-long, 85 cm wide, and 30.5 cm deep. A glass observation window 6.1 m-long is in one flume wall. An inlet stilling basin and an outlet box, formerly a pump well, are attached to the flume. The flume is supported by a structural truss, which in turn is supported by a fixed pivot and a screwjack pivot 10 m apart. A scale at the jack point allows flume slope adjustments resolvable to 2.5×10^{-6}. The flume walls are painted with an epoxy resin to produce a hydraulically smooth surface. Adjustable rails on top of the flume walls allow free movement of carriages the length of the flume. Flume stations are referenced to zero at the upstream rail stop and marked by a steel tape

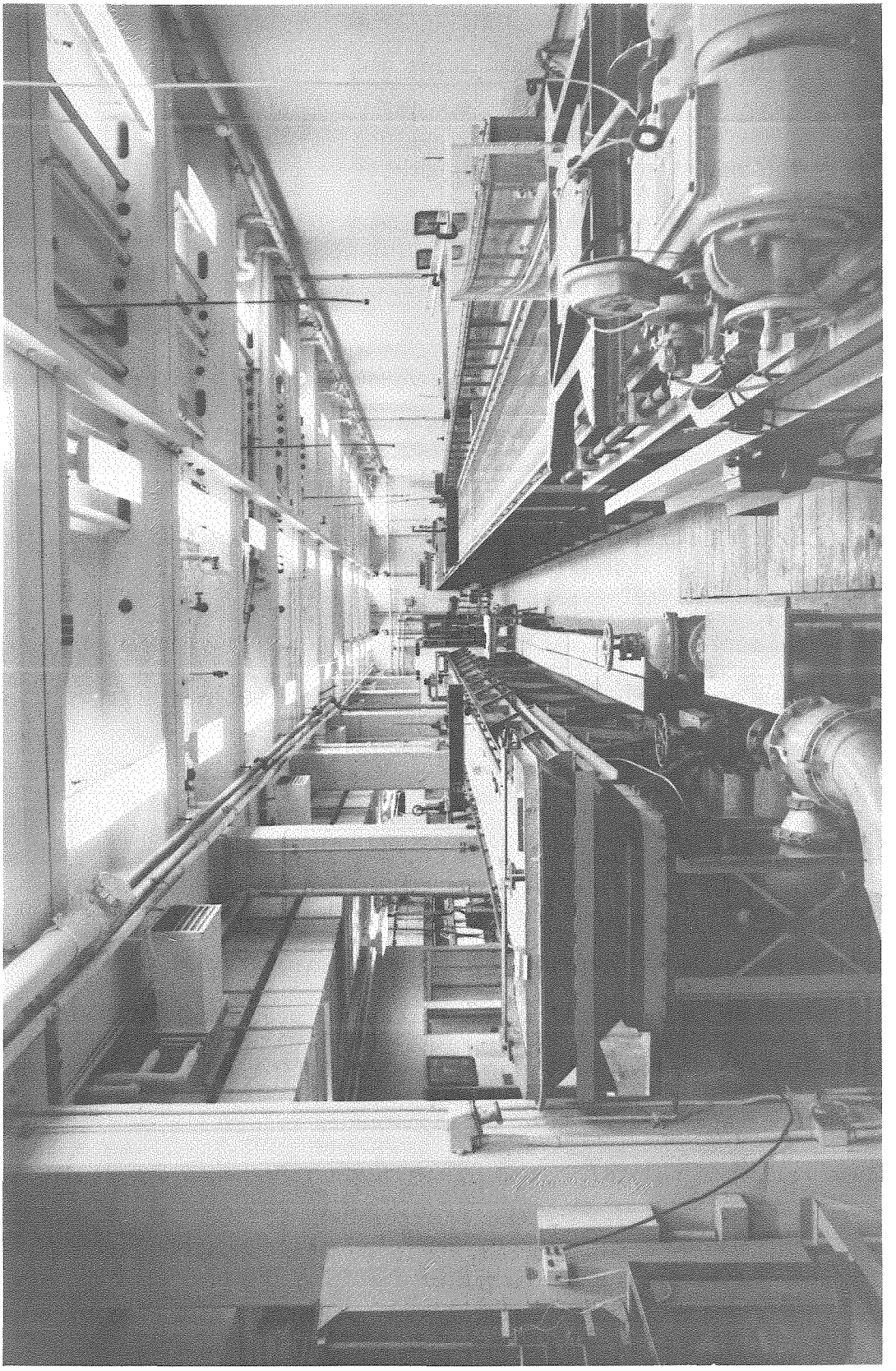

Figure 5-1. The W. M. Keck Hydraulics Laboratory, 60-ft. flume on left.

fixed to the top of one flume wall.

For rigid-wall experiments a false wall was installed within the flume to create a 26.67 cm-wide channel. This off-center arrangement allowed use of the windows in the existing wall. The test-section inlet for this configuration (Figure 5-2a) consisted of a round-edged orifice the same width as the test channel, with a 6 cm high raised ramp at the sand drop area for the sand feeder. The test channel outlet for this configuration (Figure 5-3a) is a free-overfall into the former pump well. A 6 cm-high sill prevented excessive bed erosion at the outlet.

For alluvial-bank channel work a centered trapezoidal inlet was used (Figure 5-2b). Flume outlet for these experiments (Figure 5-3b) was a short 26.67 cm-wide rectangular section with wingwalls to guide the flow. Riprap armor of 0.7 to 1 cm gravel protected the channel end of the inlet from erosion, and a 3 cm-high ramp prevented bed erosion in this outlet.

Inlet water supply. Water supply for the flume is pumped from a 55 m^3 reservoir located under the laboratory floor to a 4.8 m^3 constant-head tank at a rate of .057 m^3/sec. The water surface in the constant-head tank is 7.3 m above the laboratory floor. The constant-head tank supplies a commercial standard 8-inch distribution pipe, which has several outlet locations in the laboratory. All of this equipment is part of existing laboratory facilities. For these experiments, a commercial standard 3-inch pipe with appropriate bell-reducers was used to connect the control valve to the 8-inch distribution line. Because

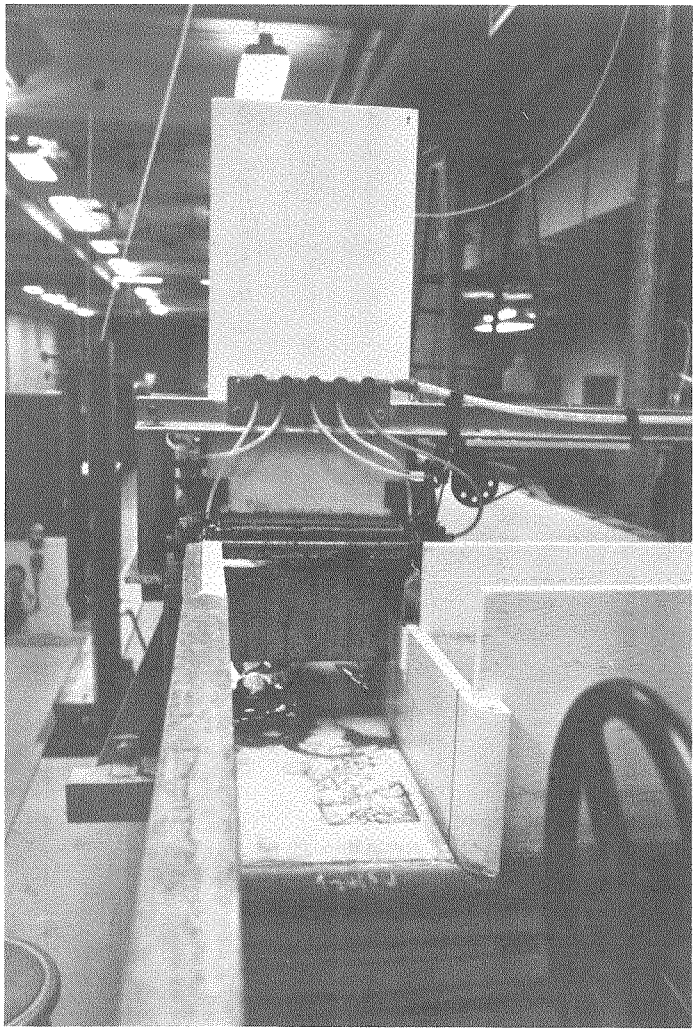

(a) Rigid-wall experiments.

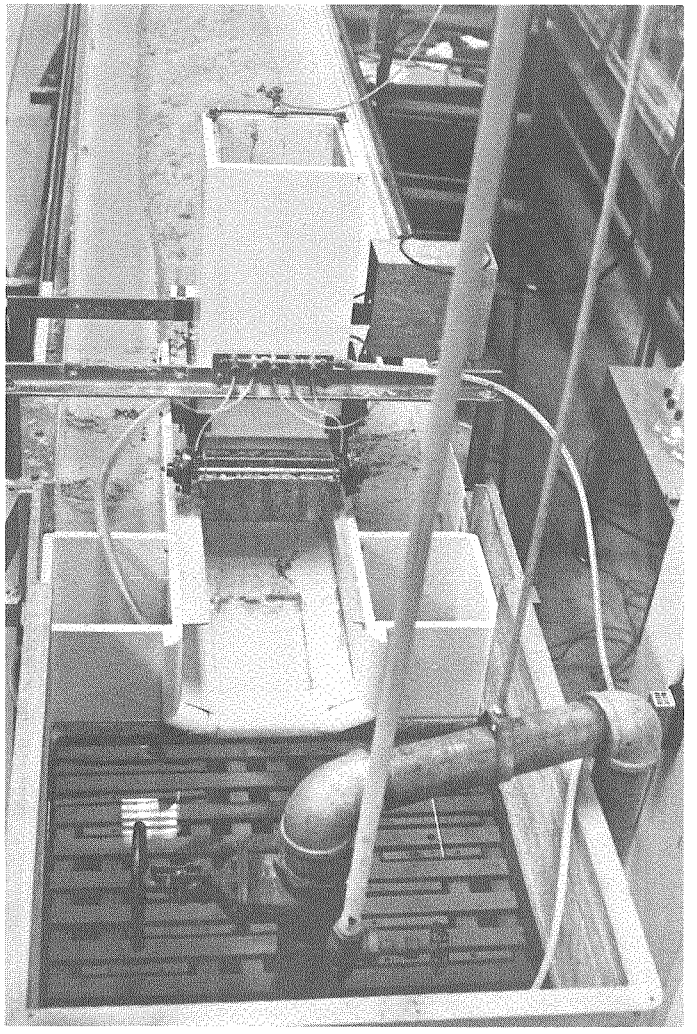

(b) Alluvial-bank experiments.

Figure 5-2. Flume inlets with sand feeder mounted.

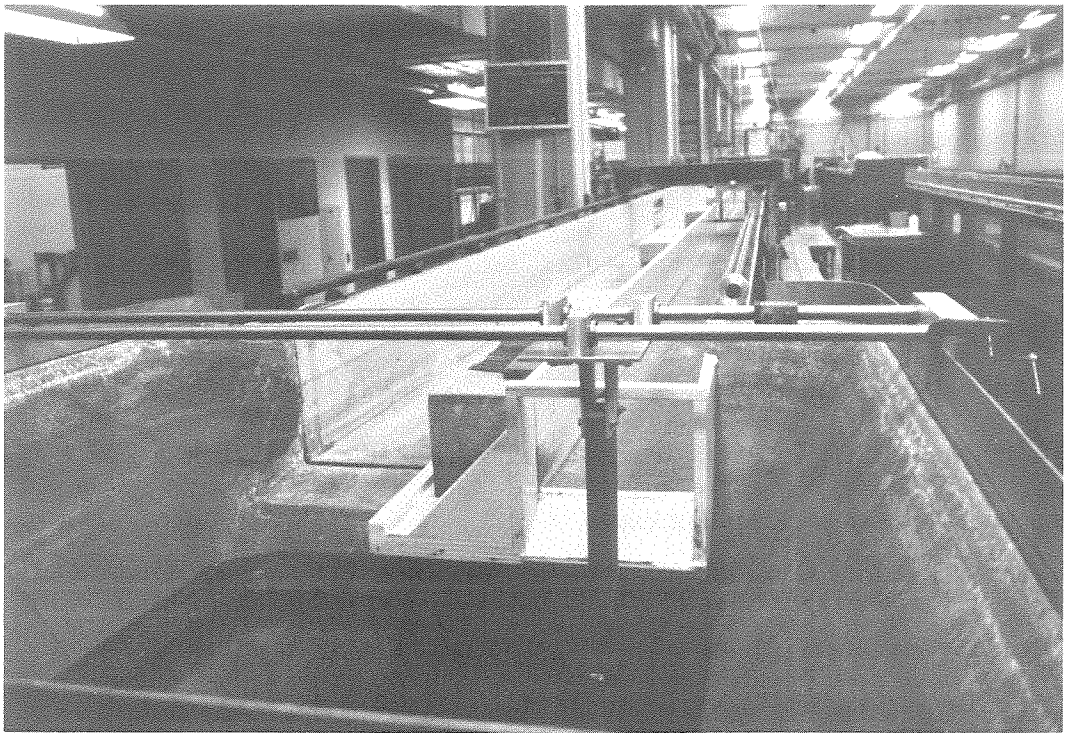

(a) Rigid-wall experiments.

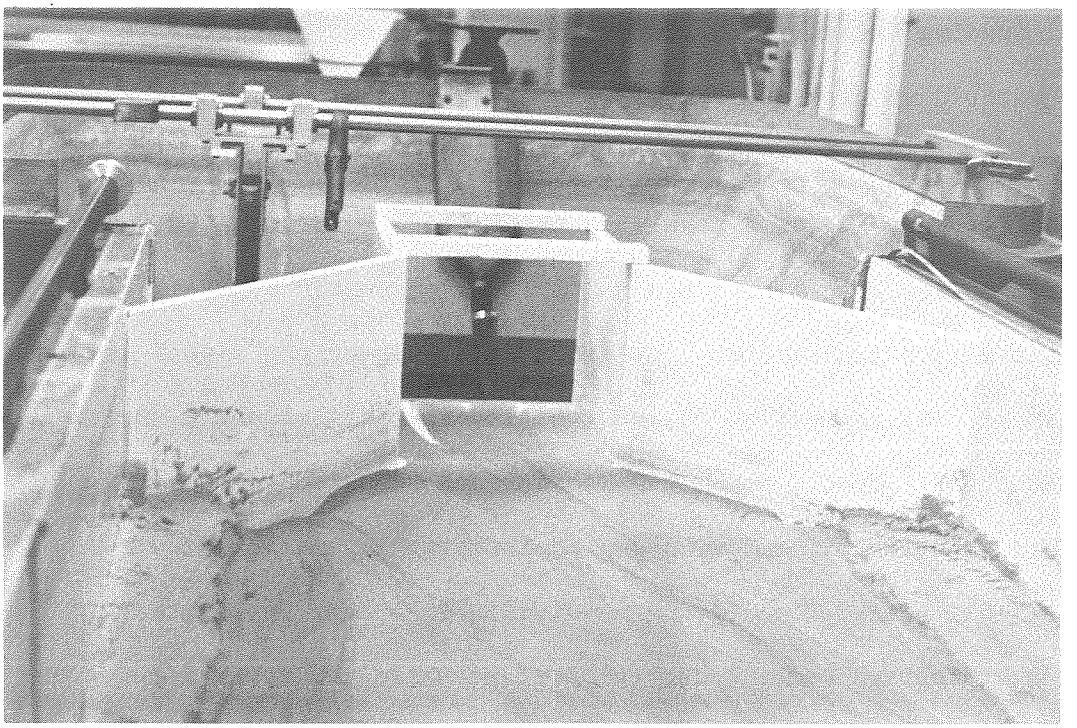

(b) Alluvial-bank experiments.

Figure 5-3. Flume outlets with sediment sampler mounted.

of the large volume in this system, stored in an air-conditioned environment, water temperature shows little seasonal variation.

Discharge measurement. Water discharge into the flume is measured by an orifice meter in the 3-inch inlet line. The meter is situated in a straight section of line, so there are no flow disruptions, and is connected by flange taps to a water manometer and a differential pressure transducer. This meter was calibrated in situ using a 200 ℓ weighing tank and an electric timer.

Control valve and controller. Inlet control is a Fisher pneumatically-actuated globe valve. Valve control is a diaphragm attached to the valve actuator rod and opposed by a spring. Air pressure forces the diaphragm against the spring, moving the actuator rod and opening the valve in proportion to the input air pressure.

A water discharge hydrograph is generated by programming the air pressure supplied to the valve actuator. As shown schematically (Figure 5-4) facility air is first regulated to 60 psig, then supplied to a pneumatic motion transmitter and a 3:1 ratio pneumatic booster. The pneumatic motion transmitter provides a 0-15 psig output signal as a function of displacement of the control lever. This signal is multiplied by a factor of 3 by the pneumatic booster and supplied to the valve actuator. An electric motor, shown in the overall controller view (Figure 5-5), geared down to one revolution in 1 hour 36 minutes, drives a hydrograph cam. A cam follower actuates the control lever of the pneumatic motion transmitter. Once water discharge is determined as a function of cam-follower displacement, any hydrograph shape can be

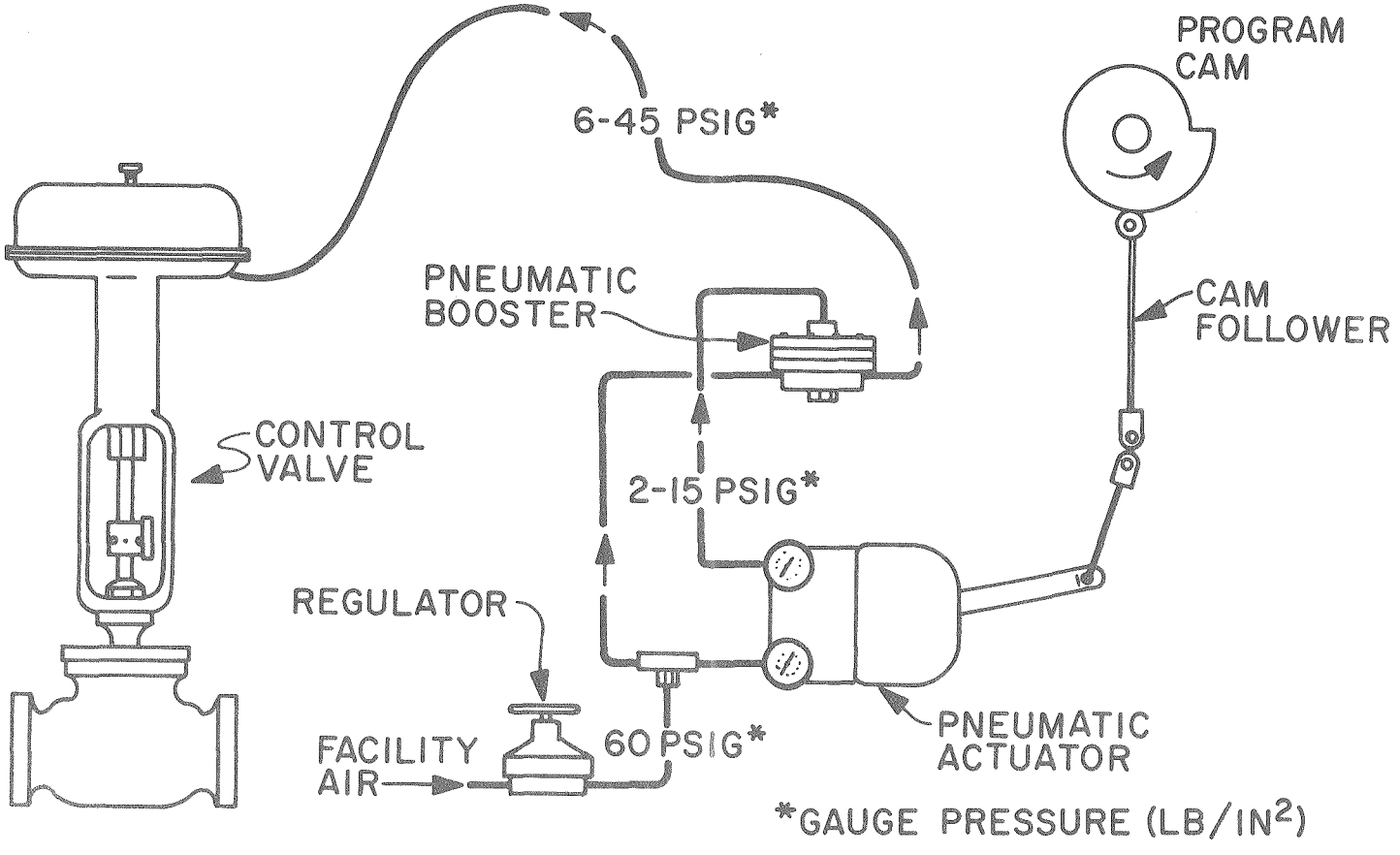

Figure 5-4. Schematic diagram of pneumatic valve-control system.

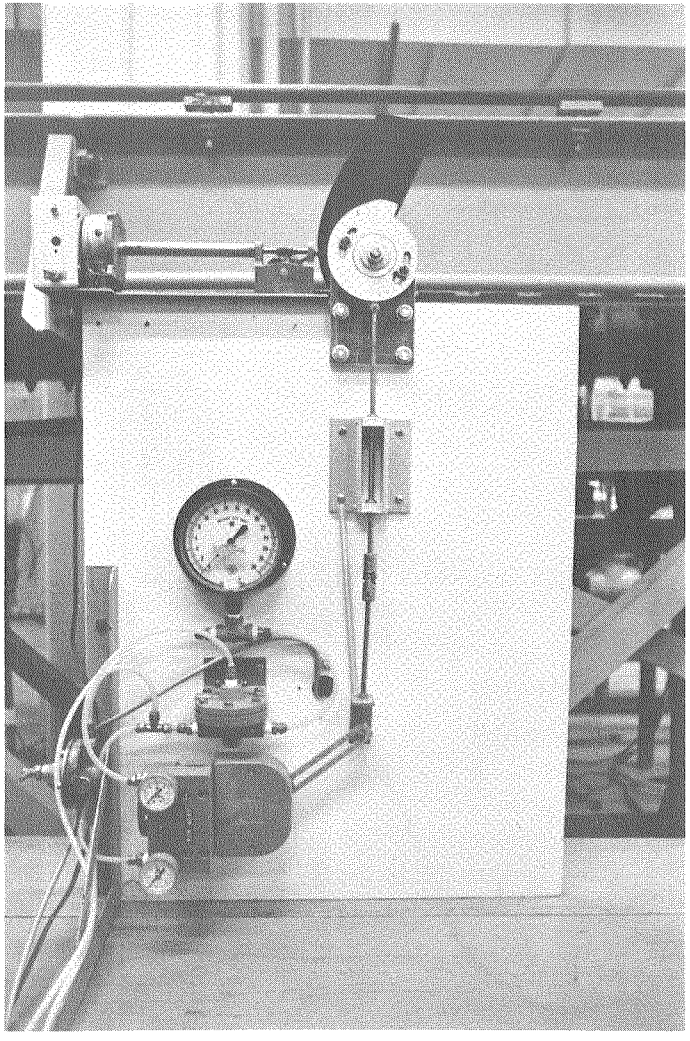

(a) Water discharge controller.

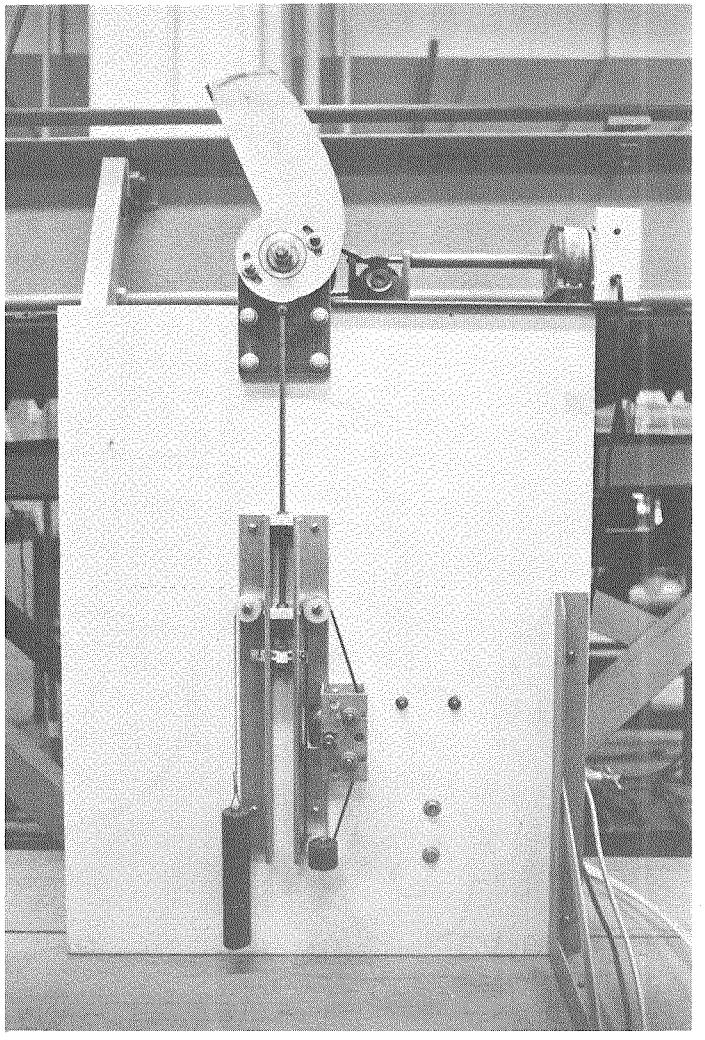

(b) Sediment input-rate controller.

Figure 5-5. Automatic controller for water hydrograph and sediment input rate.

programmed by cutting the appropriate cam. These cams (Figure 5-5) are cut from 6 mm tempered masonite.

Constant-discharge experiments were conducted using a Red Valve pneumatic control valve. Since this valve was not sufficiently stable under progressive throttling to give repeatable hydrographs, it was replaced by a Fisher control valve for variable flow experiments.

Wet sand feeder. For sedimentation experiments in open-circuit flumes, sand must be fed into the flume inlet. Previous sand feeders produced accurate input rates only with dry sand, but the volume of sand recovery and reuse necessary in these experiments made drying between experiments impractical. Therefore, a wet-sand feeder system (Figure 5-6) was designed and built. The straight-walled sand hopper used avoids the problem of wet sand cohesiveness since it does not support the mass except by friction at the walls, and this is easily overcome by weight of the sand. Earlier designs using a conical or tapered hopper proved unsatisfactory because the sloping sidewalls support the mass of cohesive sand despite stirring or vibration and piping and high variability of sand-to-water ratio prevent the use of water to flush out the sand.

In a straight-walled hopper sand must be removed from the entire bottom surface. Within the hopper this is accomplished by a conveyor-belt scraper mechanism (Figure 5-7). An aluminum plate over which the scrapers move supports the sand load. The aluminum scrapers, attached at each end to stainless-steel sprocket-driven roller chains, push the sand across the plate and off the edge. The plate and scrapers

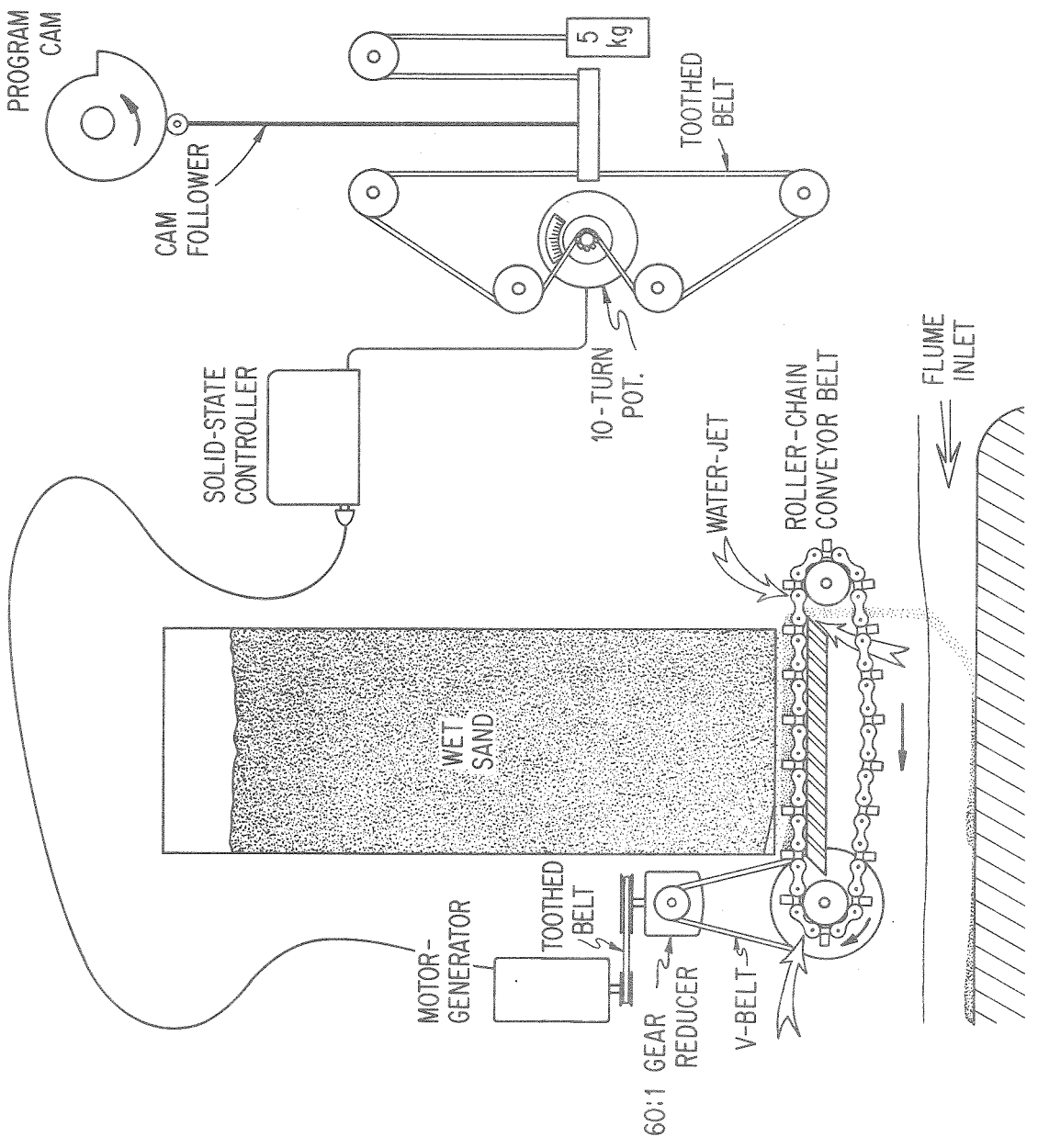

Figure 5-6. Schematic diagram of wet-sand feeder.

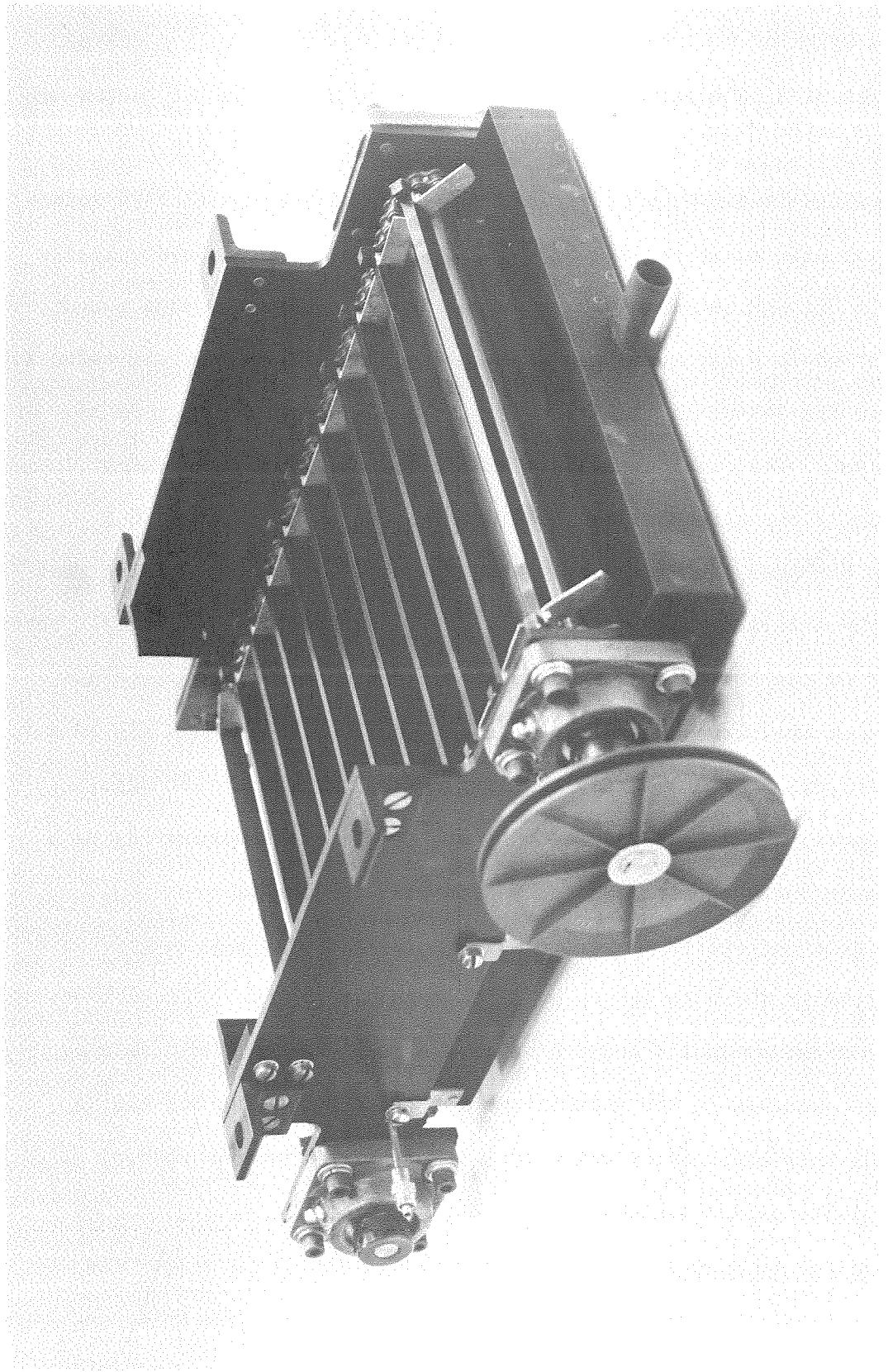

Figure 5-7. Sand feeder mechanism, showing support plate and scrapers.

are the width of the flume inlet so sand is fed to the full width of the inlet at a rate proportional to that at which the roller chains are driven.

The feeder drive-unit (Figure 5-6) is a variable-speed 149W motor-generator with solid-state D.C. controller. The motor is controllable within ± 0.1 RPM between 5 RPM and 3000 RPM at constant torque output, with an absolute minimum speed of slightly over 1 RPM. Overall reduction ratio to the feeder is 1:2542, providing a maximum scraper speed of 1.5 cm/sec. The final drive is a v-belt to protect the system by slipping if the scrapers jam. Calibration reproducibility of 0.5 percent has been achieved. For this accuracy, sand in the hopper must be nearly saturated with water so it fills the scrapers uniformly. Water sprayed on the outlet edge of the support plate assures complete unloading of the scrapers, and a pan under the feeder prevents all sand and water drips from entering the flume except at the outlet edge of the support plate. For continuous operation, it is necessary to wash each chain sprocket with a water jet to prevent jamming.

Direct control of the drive-speed motor is by a 10-turn precision potentiometer which is driven by a cam-actuated pushrod (Figure 5-6). Linear-to-rotary-motion conversion is a no-slip toothed belt driving a pinion attached to the potentiometer shaft. The actuating cam is co-axial with the control valve cam, assuring synchronous control of water discharge and sediment-input rate.

Movable carriage. The flume is equipped with a carriage (Figure 5-8) which can be moved the length of the flume along the rails mounted on top of the flume walls. Mounted on this carriage is a vertically-

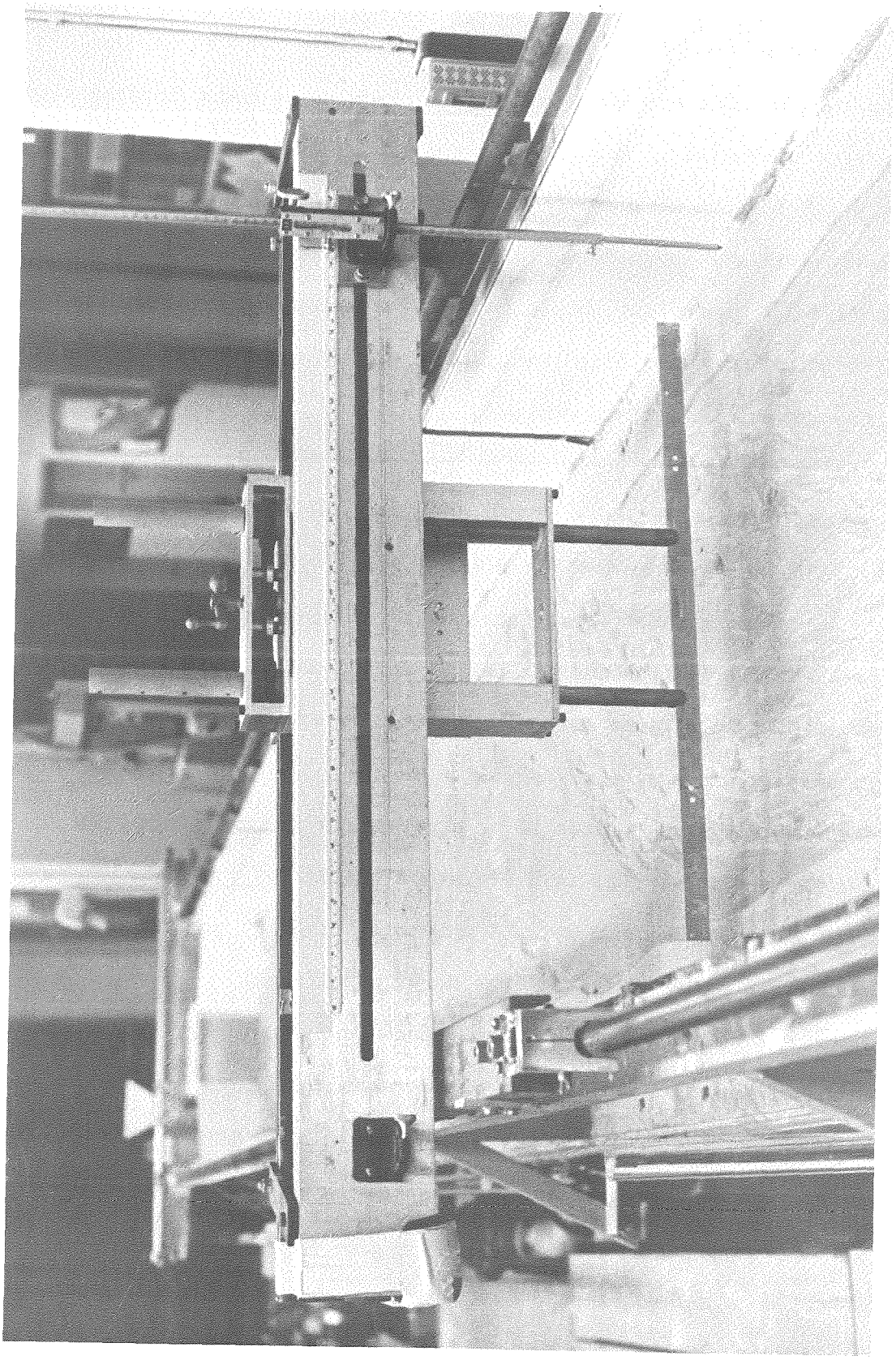

Figure 5-8. Movable carriage.

adjustable point gage which can be read by a vernier to .01 cm, and interpolated to .005 cm. This point gage can also be moved horizontally so relative elevation of any point in the flume can be measured. A static water surface was used to determine the slope-scale datum, and relative elevations on the flume rails, as described in detail by Brooks (1954). Instead of shifting the flume rails, their elevation relative to a "mean rail line" was determined and used to correct point gage measurements at a given station.

An aluminum scraper supported by two threaded brass rods mounted in a nearly-rigid frame attached to the movable carriage is used as a bed leveler. The scraper can be raised and lowered by turning the captive nut on each support rod. These nuts are threaded-hub pulleys attached to a crank handle, so the scraper can be raised and lowered keeping its edge parallel to the flume bottom. The bed leveler can also be moved horizontally from one side of the flume to the other, but it is not provided with either a horizontal or a vertical movement scale. In leveling the bed for a run, rail elevation variations are reproduced on the bed. Since the maximum variation is only slightly greater than the mean sand grain size, it is not considered significant.

Piezometric taps, pressure transducers, and recorders. Following the method of Kennedy (1961), piezometric taps were installed in the flume to measure water surface elevation during high Froude number flows when point gage measurements are grossly inaccurate. The taps (Figure 5-9) were 1/4-inch copper tubing sealed at one end and attached at the other end to a tee threaded into the flume bottom. At two centimeter intervals along the tubes, three one-millimeter holes were drilled

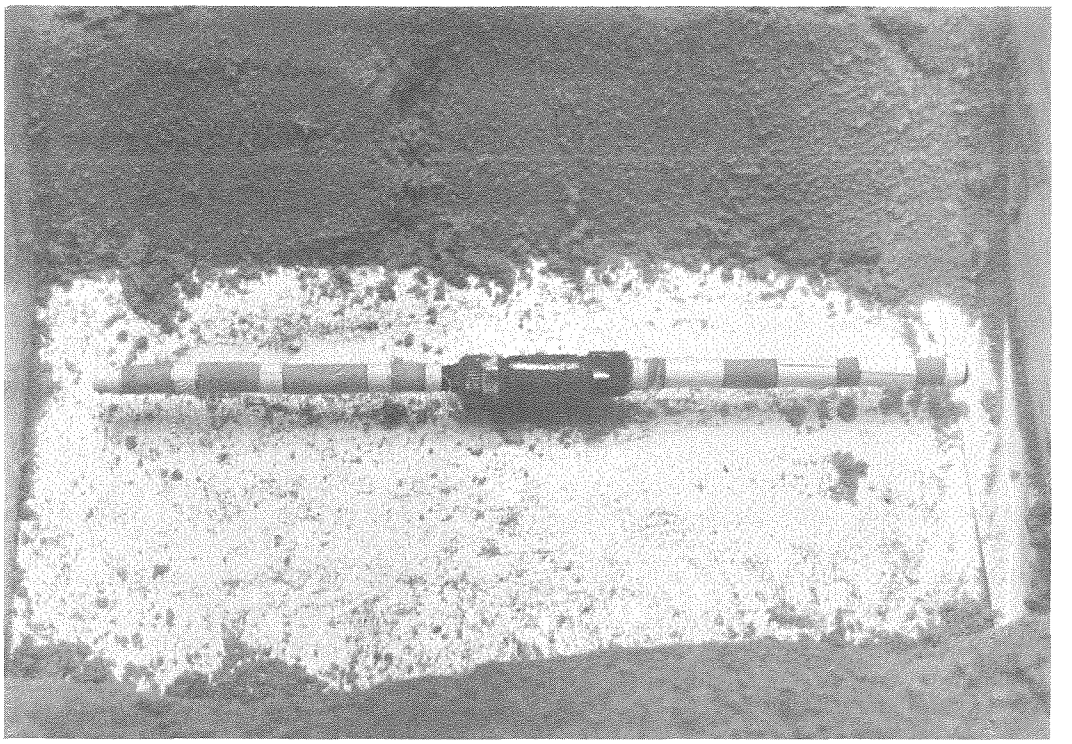

(a) Rigid-wall experiments.

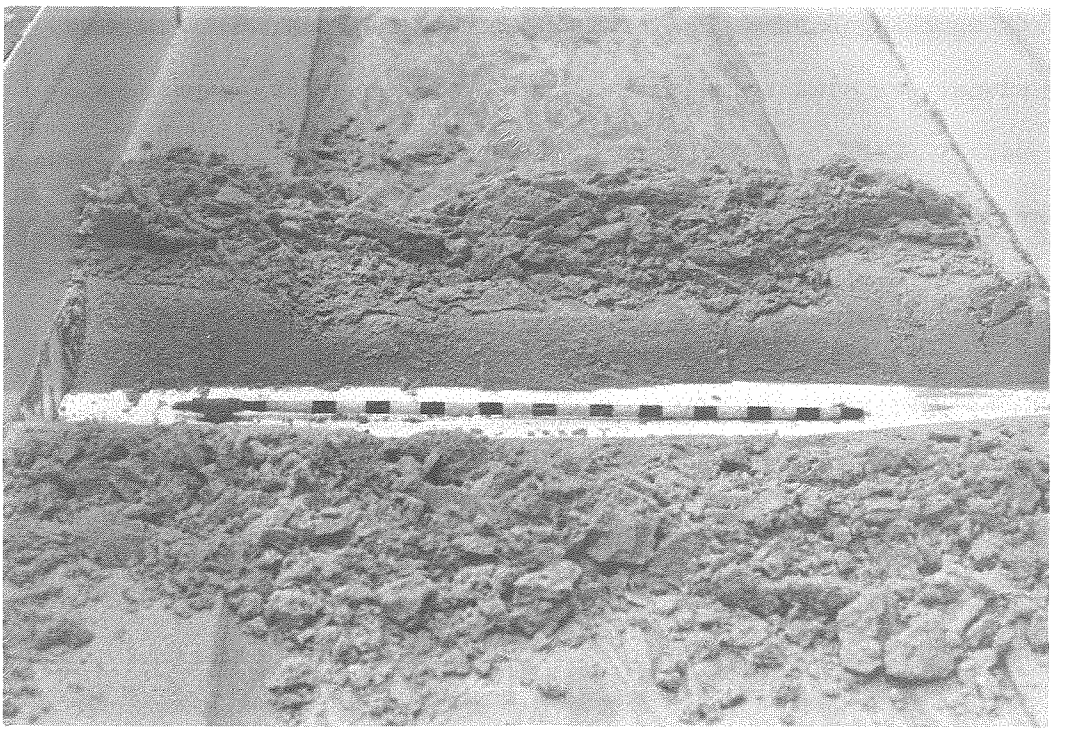

(b) Alluvial-bank experiments.

Figure 5-9. Piezometric taps.

120° apart. The tubes were then wrapped with cloth and taped to prevent sand ingestion. Seven taps were installed at two-meter intervals along the flume. Kennedy (1961) connected the taps to manometer tubes to determine water surface elevations along the flume. With the sand used in these experiments, fine material clogged the taps when any significant water-to-manometer flow occurred. For this reason and also because there was little time during a simulated flood to measure water elevations in the manometers, the taps were connected to pressure transducers, which require negligible water flow and provide a record of level readings which can be reviewed later.

Four of the transducers used were Pace P7D models and three were Validyne DP-7 models. These are identical transducers, the manufacturer simply having changed names and transducer designations. A fifth Pace P7D transducer was used to measure differential pressure across the orifice meter. Operation of these transducers has been described in detail by Hwang (1965) and Brock (1967).

Transducer outputs were measured by Model 150 Sanborn recorders. The transducers were driven by Sanborn 1100 and 1100AS carrier pre-amplifiers, the 1100AS model allowing smoothing of the noisy orifice meter signal. A variable-speed motor-drive was used to advance heat-sensitive record paper, at a minimum speed of .25 mm/sec in these experiments.

It was necessary to calibrate the transducers for each run. After lines and piezometric taps were flushed, recorder zeros were set to the reference zero water elevation in calibrating tubes (Figure 5-10)

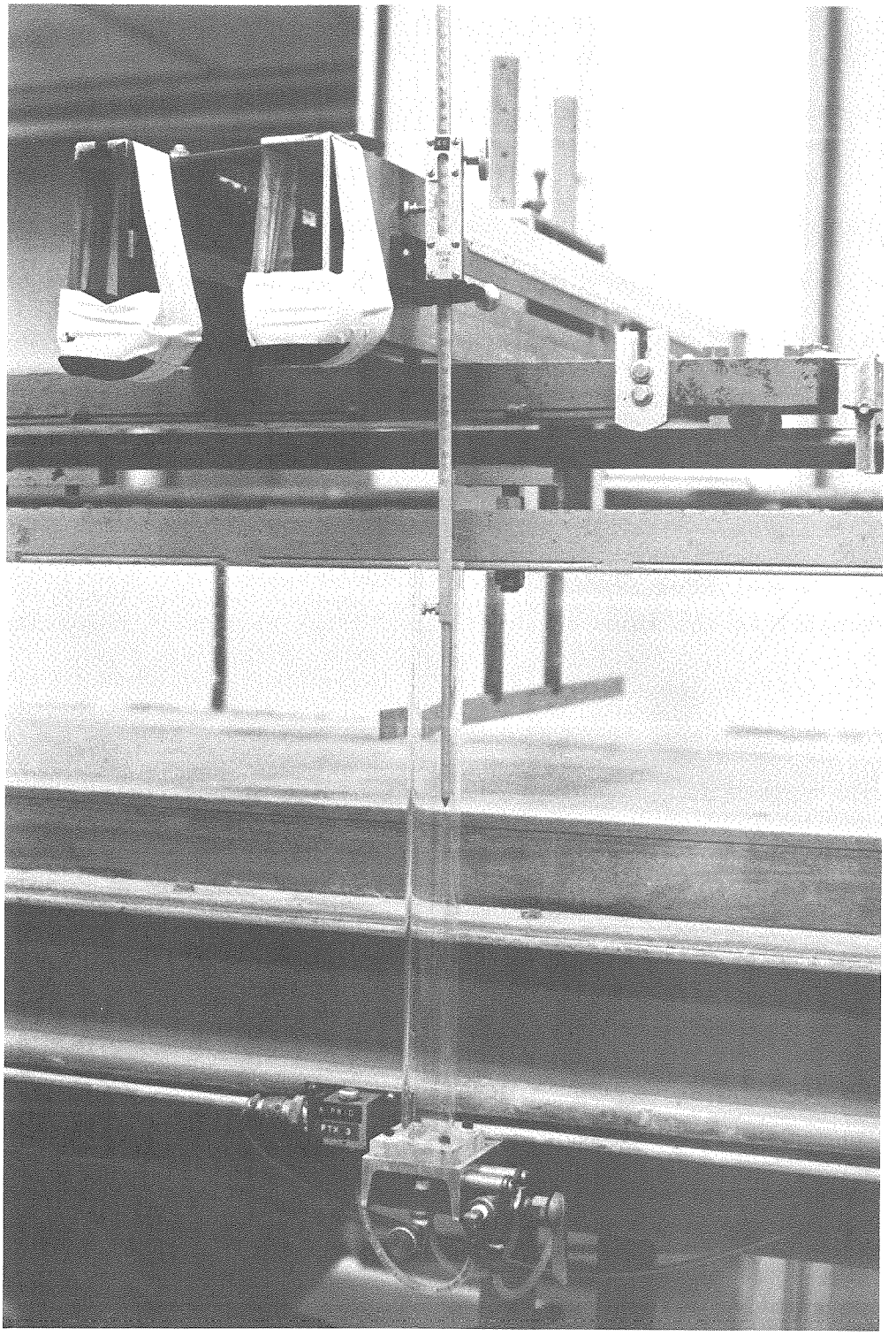

Figure 5-10. Pressure transducer and calibrating tube.

attached to each transducer mounting bracket. Water was then added to the calibrating tube, the water surface elevation in the tube was measured with a point gage attached to the movable carriage, and the recorder pen deflection noted. Several such points defined the recorder deflection-water surface elevation curve for each transducer. A three-way valve allowed rapid change between measuring water pressure in the flume piezometric tap and in the calibrating tube. In this way, the recorder zero could be checked and reset if necessary during a run, and transducer zero shift determined.

Determination of total sediment discharge. A traversing vertical-slot sampler at the flume outlet (Figure 5-11) is used to determine total sediment discharge. The vertical-slot collector is attached to a carriage mounted on transverse rails on the flume outlet box. A tygon tube leads from the collector to a nipple through the side of the outlet box near its base. A tube attached to this nipple (Figure 5-12) allows sample collection in one-liter flasks outside the outlet box. Samples are taken by manually traversing the collector the full width of the channel outlet at a constant transverse speed. Two samplers, with slot widths of 3.2 and 9.5 mm, were used to allow sampling over a wide range of discharges. Transverse speed must be constant so that no part of the flow is favored or neglected in the overall sample. Maximum traverse speed with the wide slot at maximum water discharge was 10 cm/sec, about 12 percent of water velocity at that discharge.

Sample sediment concentrations are determined using a separatory funnel. A sample flask is inverted over the collecting funnel and

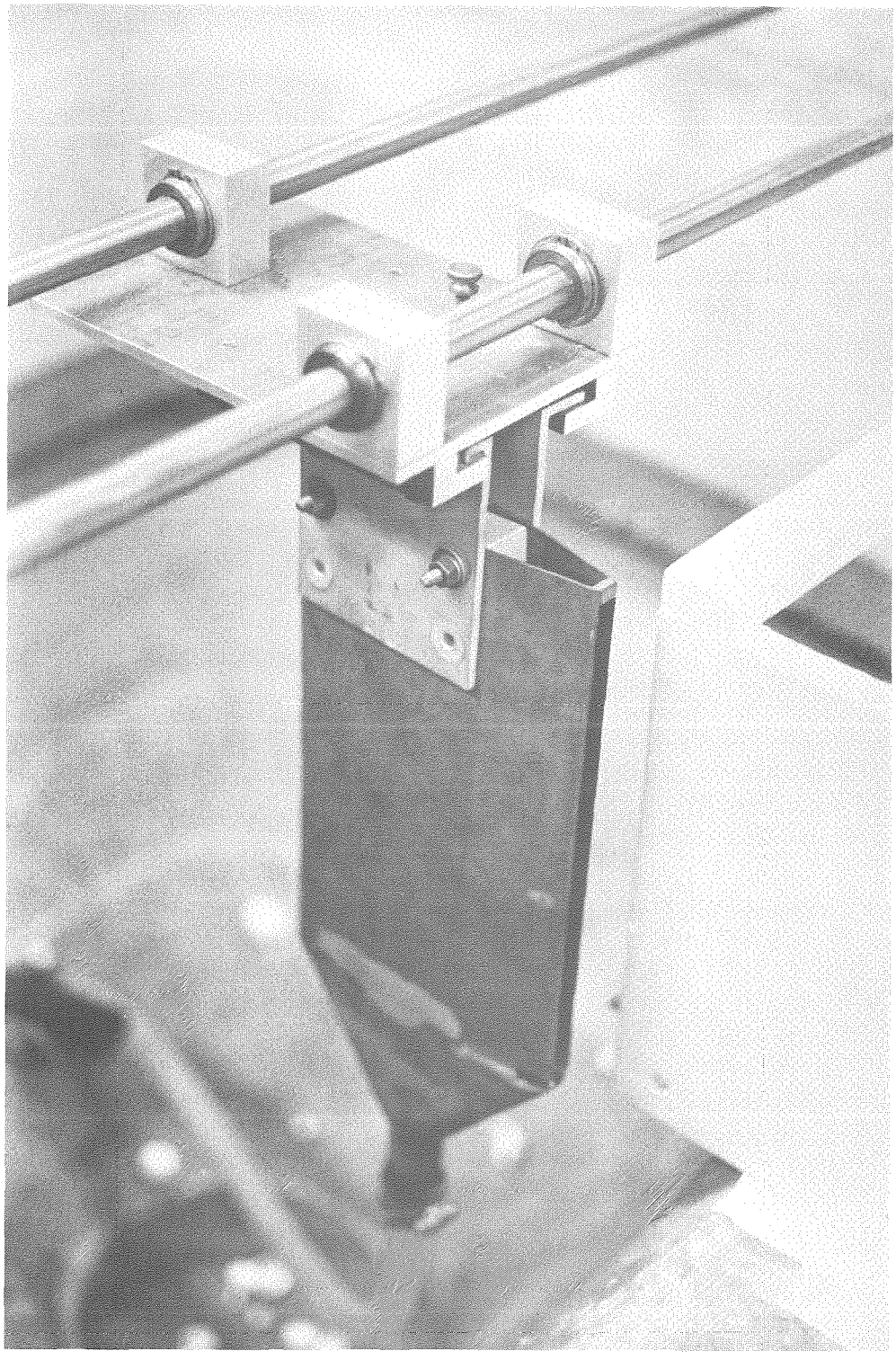

Figure 5-11. Traversing vertical-slot sampler.

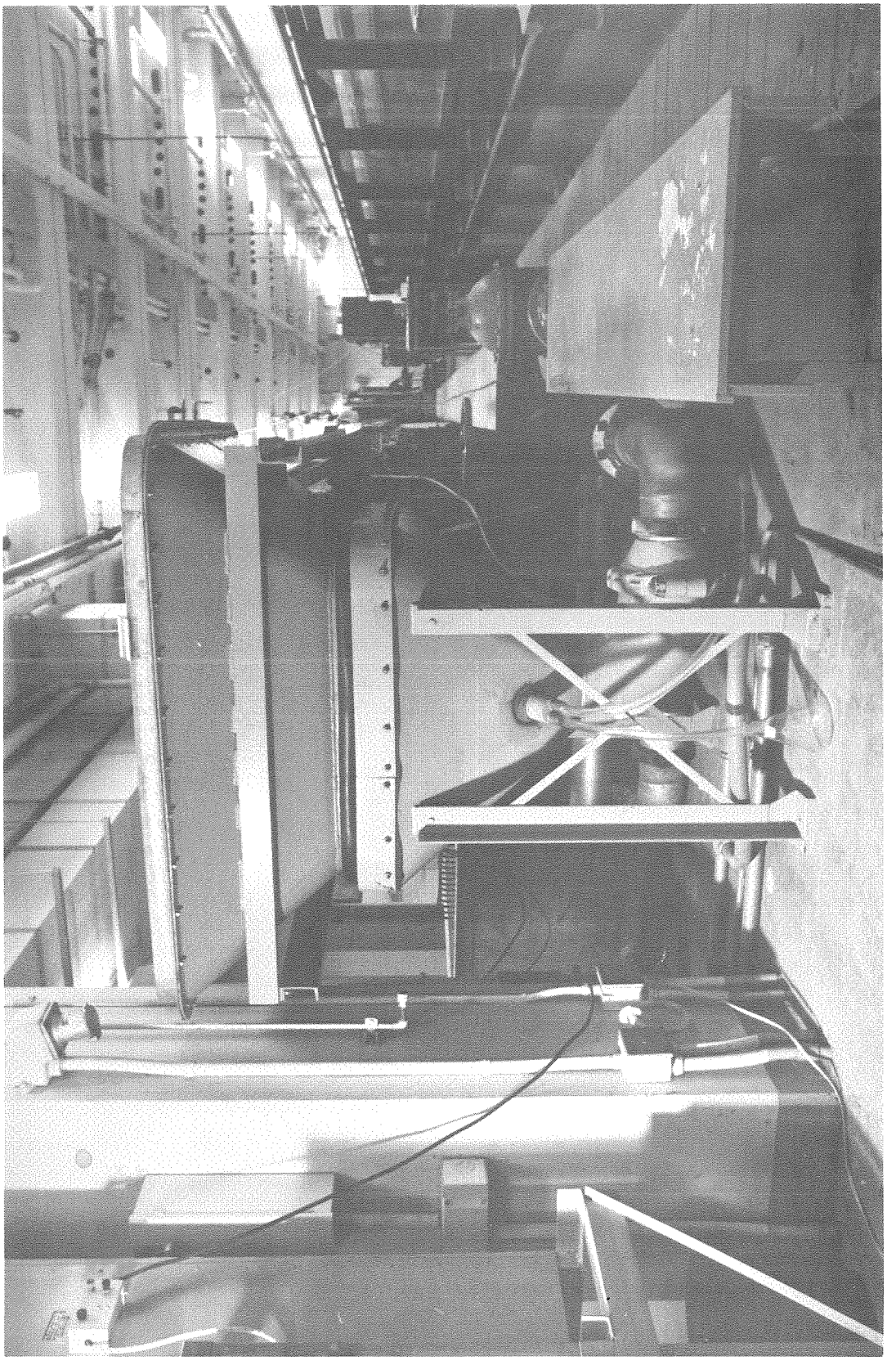

Figure 5-12. Sample outlet tubes.

swirled to remove all sand. After all sand has settled, the stopcock is manipulated to transfer it to a 5 mℓ graduate cylinder. After the sand is compacted by a combination of rotation and vibration, its volume is measured. Sand density using this compaction method is 1.74 gm/cm^3. Excess water is returned to the funnel, and the sand set aside for later size analysis. Sample water volume is measured in a one-liter graduate cylinder. Volumetric sand transport rate is then calculated as the sample-volume concentration of sand multiplied by the outlet discharge. For simulated floods, samples must be noted on the discharge strip-chart so the appropriate discharge can be determined.

Settling tank. A settling tank (Figure 5-13) separates sediment from the flume outlet water so that only clear water is returned to the constant-head tank reservoir. This tank has a working section 91 cm-wide x 61 cm deep x 381 cm-long, and water depth is controlled by a weir at the outlet end. At a discharge of 7500 cm^3/sec, water entering the tank has a maximum residence time of 283 seconds, allowing a theoretical minimum particle fall velocity of 0.22 cm/sec. At 22°C water temperature, this tank theoretically allows natural quartz grains (shape factor of 0.7) as small as .042 mm to be completely settled out, but actually turbulence generated by the inlet reduces effective residence time by a significant although unknown amount. All sand was washed through the flume into the settling tank before being used in experiments. In this way, any turbulence effects acting to selectively remove fine-grained sediment from the settling tank would do so before experiments began so that no sediment size-distribution changes would take place during the experimental program.

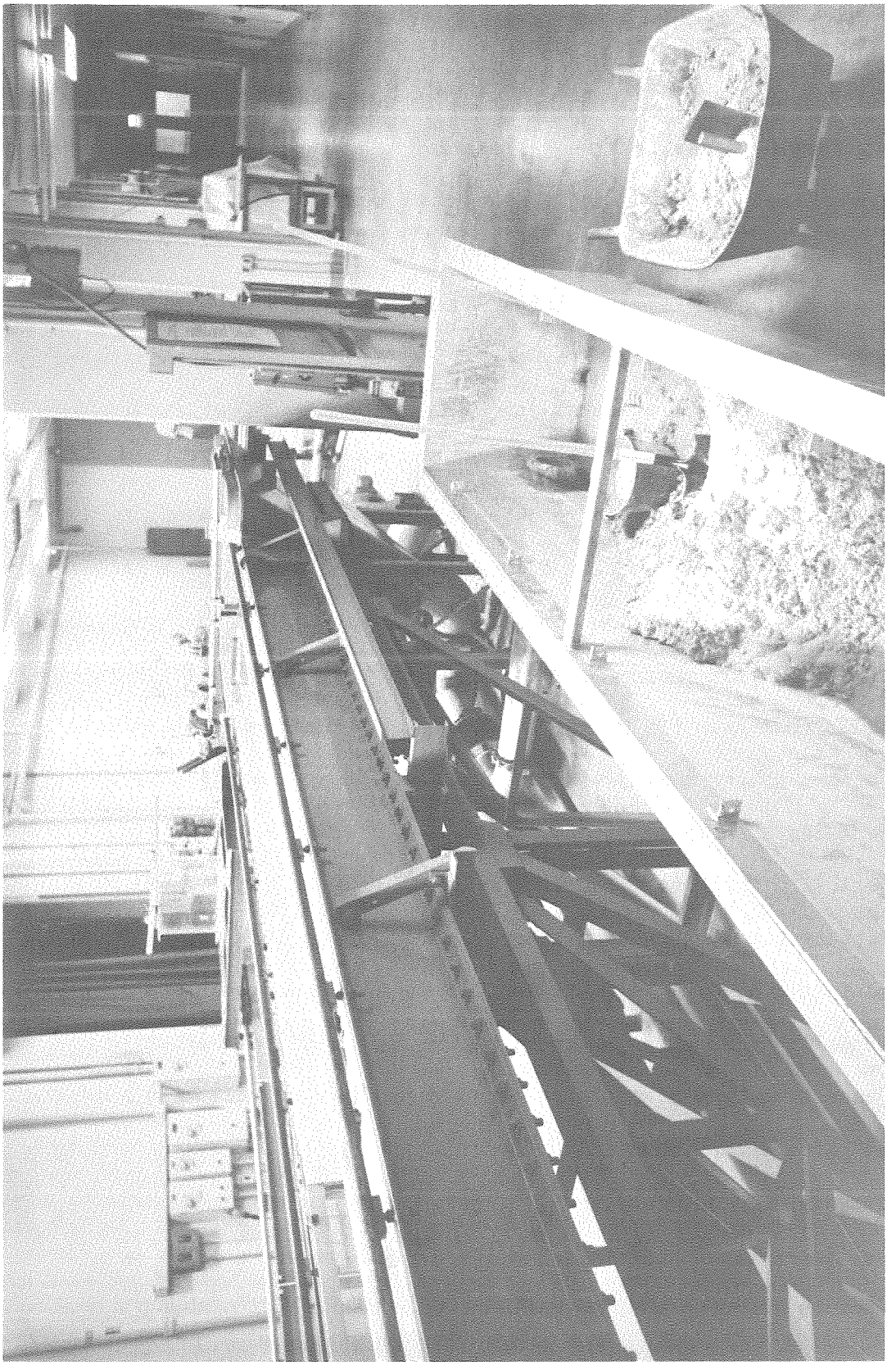

Figure 5-13. Settling tank.

Sand characteristics. Bed and input load material used in these experiments is Nevada 47 sand, available commercially from Silica Products, Inc. of Overton, Nevada. This sand has a mean size of 0.28 mm, and consists almost entirely of sub-rounded to well-rounded quartz grains, with trace magnetite. Figure 5-14 is a size-distribution plot for this sand using both sieve and visual-accumulation tube data. Results of the two analyses differ by only 2 percent, so size data from the sieve analyses used for all experimental determinations can be used interchangeably with fall diameter.

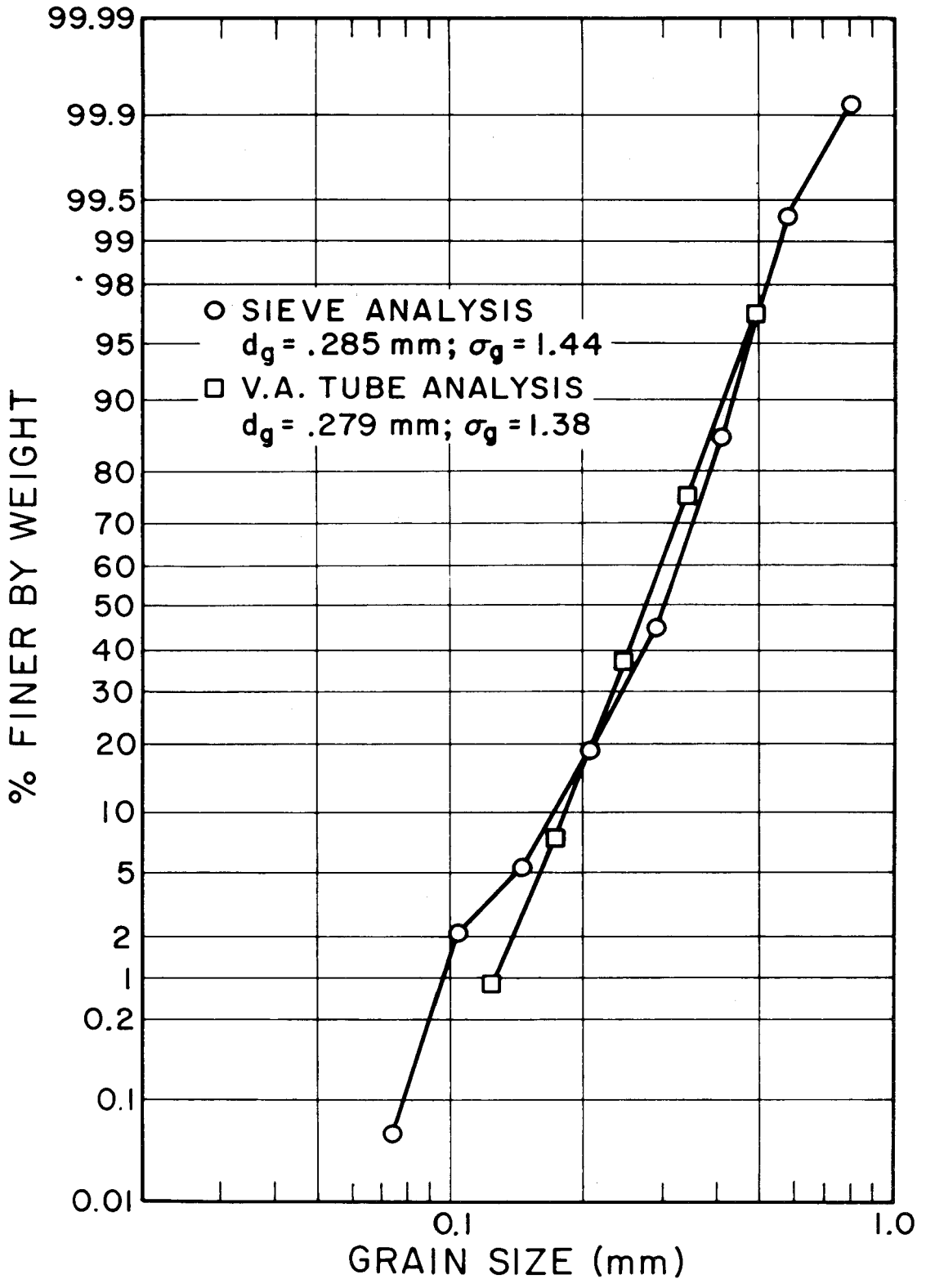

Figure 5-14. Size-distribution of bed sand used in experiments.

CHAPTER 6. LABORATORY EXPERIMENTAL RESULTS

Introductory Statement

Open-circuit laboratory flume experiments executed fall into three categories, steady-state with rigid walls, simulated floods with rigid walls, and alluvial-bank experiments. Steady-state experiments with constant discharge and sediment-input rate are performed for defining equilibrium flow conditions for given channel geometry and input parameters. Rigid-wall simulated floods demonstrate bed behavior in the absence of extraneous effects from eroding or aggrading banks, channel bends, or from changes in channel width. Alluvial-bank experiments qualitatively extend flume data to more realistic field conditions and serve to check the validity of field data.

Steady-State Experiments with Rigid Walls

Two series of steady-state experiments were conducted, the A-series at a slope of .004, and the D-series at a slope of .010. The A-series provided training and experience in flume operation, transducer operation and data reduction, and sediment transport-rate sampling. A further objective was to provide a time-independent sediment transport-rate versus discharge curve for this flume geometry and sand size. The slope used in A-series was chosen for relatively low equilibrium sediment transport rates to minimize the time spent on sand recycling. Initial slope was determined by running the sand feeder at 25 percent of maximum speed and allowing the bed to achieve equilibrium slope at maximum water discharge. At lower discharges, water discharge was set and sand feeder rate adjusted by trial-and-error until the desired slope was attained.

It was found, however, that equilibrium flows at this slope underwent a transition from upper- to lower-regime at a large fraction of the maximum water discharge, and that sediment transport rates at discharges below 50 percent Q_{max} were so low that several hours were required to reach equilibrium conditions. For experiments of this duration, water heating by the constant-head tank pump becomes significant (2 to 4°C) in terms of reconciling the data with those from shorter-duration experiments.

The D-series steady-state experiments were conducted to establish maximum-discharge conditions at the largest flume slope practical, determined as the equilibrium slope at maximum water discharge and 75 percent sand feeder capacity. The larger sediment transport rates at this slope allowed shorter experiment durations so that water temperature increase was negligible. Transition to lower-regime flow was also expected to occur at a much lower fraction of maximum discharge than in the A-series experiments. Because of bed elevation behavior during equilibrium flow and uncertain relationships of steady-state sediment-transport data to simulated flood conditions, to be discussed in later sections, D-series experiments were terminated after uniform flow conditions had been investigated for two discharges at this slope.

Equilibrium criteria. In a real stream, discharge and sediment supply are independent variables, with channel geometry and bed slope dependent variables. In a stable natural stream at equilibrium, the dependent variables are, on the average, constant and the same criteria of equilibrium can apply to laboratory streams. Laboratory channel geometry is fixed by rigid walls, so changes in bed elevation and slope,

and water-surface slope, are the only variable parameters bearing on equilibrium. Bed and water surface slopes are sensitive factors which, fortunately, can be measured accurately. The primary criterion for equilibrium flow conditions in these experiments is that the bed and water surface be parallel within a relative slope of .0002 cm/cm or less. In performing a series of experiments at different discharges on the same slope, the data from an equilibrium experimental run are considered valid only if the average of its bed, water surface, and energy grade line slopes is within ± .0002 cm/cm of the mean. Bed elevation could not be held constant with the slopes and water discharges specified, as explained in a later section.

Determination of water surface elevation. Water surface elevations were measured on pressure transducer recordings (Chapter 5). Figure 6-1 shows part of the pressure transducer record for run D-1-3. This run was at maximum water discharge at the greatest slope used in steady-state experiments, and flow conditions ranged from high-speed flow over a flat bed to violently-breaking trains of stationary waves over antidunes. The relatively flat portions of the transducer traces show times of flat-running water over the piezometric taps. The prominent peaks occur when stationary waves form and break over the piezometric taps. Kennedy (1961) used the average of the maximum water level excursions in a manometer attached to each piezometric tap as the water surface elevation for that location. Since Kennedy did not have a pressure recording system, he was not aware that the water pressure excursions caused by breaking waves are not necessarily representative

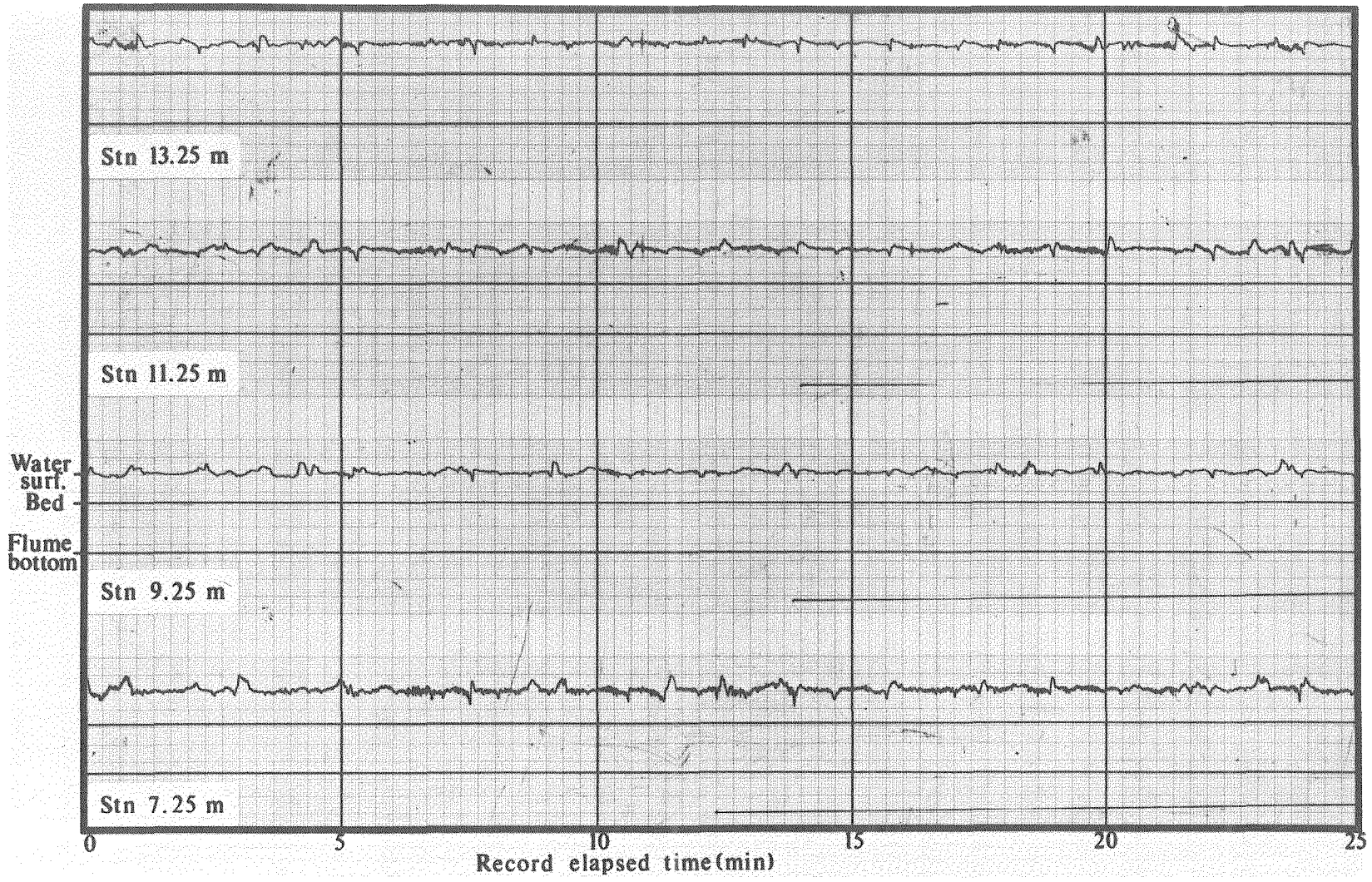

Figure 6-1. Pressure-transducer recorder record for steady-state experiment D-1-3.

of the flow as a whole. For the pressure record of Figure 6-1, three different systems of measurement were tried. Mean recorder-pen deflection for each transducer was measured by; 1) taking the average of the deflection at every 5 mm (20 sec) for the last 5 cm (200 sec) of the run, 2) taking the average of the deflection at every 25 mm (100 sec) for the last 25 cm (1000 sec) of the run, 3) estimating by eye the deflection during flat-water intervals for the last 100 sec of the run. The results of these three methods agree within 1 percent. Since Kennedy was using highly-damped manometers, his measurement technique was similar in effect to methods 1 and 2, and was therefore generally accurate. It is a simple matter to convert strip-chart recorder-pen deflections to water surface elevations for each piezometric tap using previously-determined calibration curves.

Determination of mean bed elevation. Mean bed elevation is determined by leveling the drained bed for an "appropriate interval" centered on each calculation station until all irregularities are removed, and all sand in the interval is used up. This technique is described in detail by Brooks (1954). The "appropriate interval" must be long compared to ripple wavelength. For all experiments, a 1-meter interval centered on each piezometric tap was chosen. In the A-series this is the wavelength of the meandering thalweg that formed between submerged bars alternately on the right and left side of the channel down the flume. In all others, this interval was adequate for the definition of "appropriate interval", and allowed an interval to be leveled between each piezometric tap station also. After leveling, the bed elevation

is measured with the point gage. Brooks (1954) used a strong oblique light to determine when the point gage "touched" its shadow on the sand surface. In these experiments, a saturated bed with no free-standing water has enough surficial inter-grain water to form a meniscus when touched with the tip of the point gage, and the formation of this meniscus is easily seen. Elevation measurements so made are repeatable to 1/20 mm.

Calculation of water depth, mean velocity, and slope of energy gradient. The difference between water surface and mean bed elevations at a piezometric tap station is the mean water depth at that station. Mean water velocity at the station is discharge divided by flow cross-sectional area based on the mean depth. Equivalent height above the flume bottom of the energy grade line at that station is:

$$e = y + \overline{a}\,\frac{V^2}{2g}$$

where

y = elevation of water surface above flume bottom

$\overline{a}$ = coriolis coefficient $\approx$ unity

After water surface elevation, mean bed elevation, water depth, and e are determined, a summary plot is prepared. Figure 6-2 shows such a summary plot for Run D-1-3, a steady-state run at Q = 7500 cm^3/sec and $S \approx .01$. For this energetic run, the bed was apparently affected by inlet disturbance upstream of station 7 m. Further, transducer data at stations 5.25 and 11.25 m are so far out of agreement with the others that their calibrations are suspect. This run was made before it was

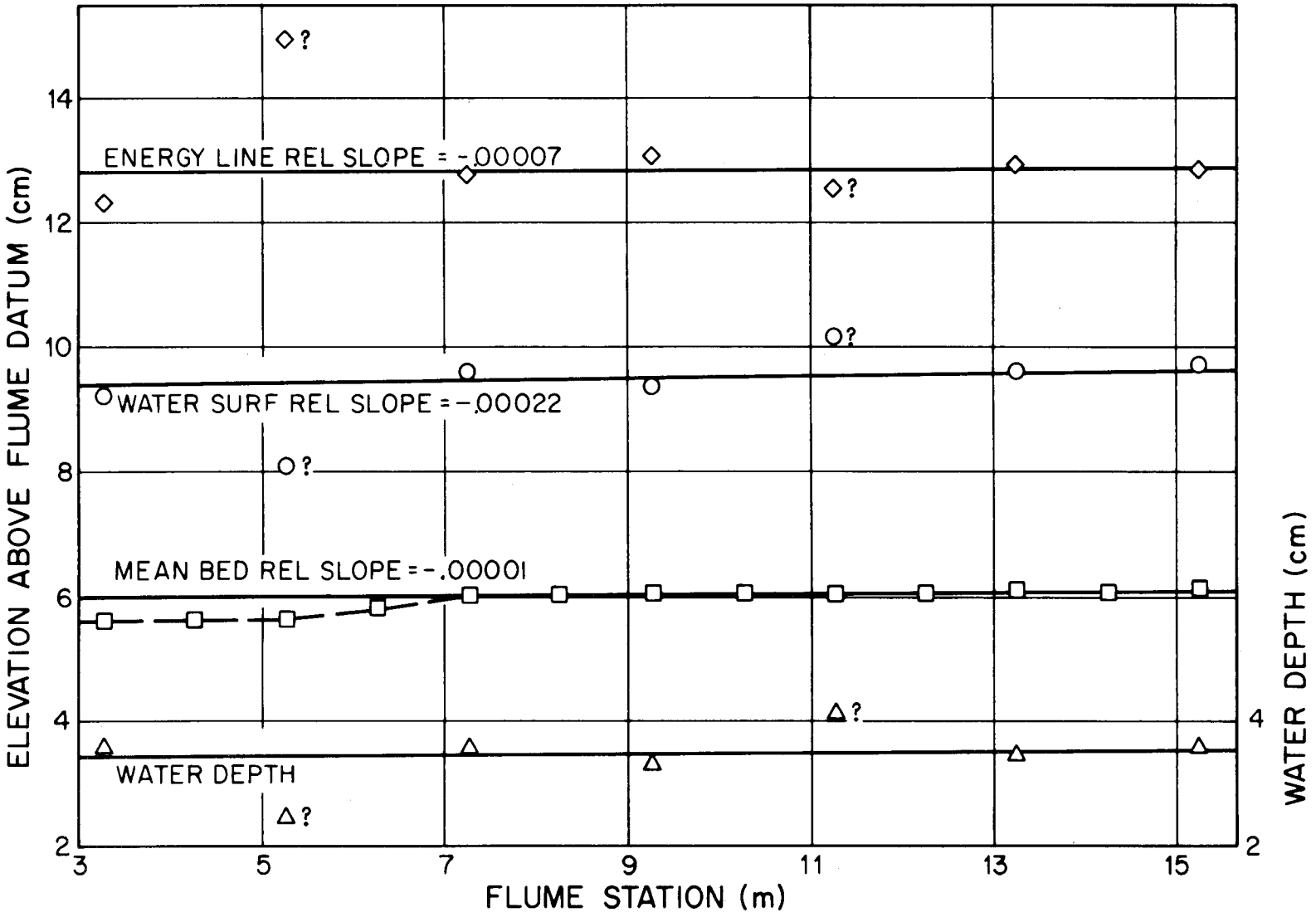

Figure 6-2. Summary plot for steady-state experiment D-1-3.

realized that transducer calibrations were necessary before each experiment. Using remaining data, a straight line was fit to the points. The slopes, relative to the flume, of the energy grade line, water surface, and mean bed elevation were averaged; and average relative slope was used to calculate the slope for the experiment. The small change of water depth relative to the bed is the basis for concluding that this flow was in equilibrium.

Water depth and mean velocity error. A source of systematic error for water-pressure determinations of water-surface elevation is the largely unknown effect of the vertical components of flow velocity on pressure readings (Jayaraman and Sethuraman, 1973). Brock (1967) determined transducer calibrations under actual flow conditions, a method not generally applicable in these experiments. However, during run A-1-3, with a mean flow velocity of 50-58 cm/sec at a depth of 5.61 cm, the mean water depth determined from transducer data was approximately 1 percent less than that determined using Brooks' (1954) point-gage averaging technique. Further, for all experiments with uniform flow where stationary wave wavelengths were measured, the flow velocities determined, using equation 4-3, were less than 2.4 percent higher than those determined from transducer water-depth data, using the continuity equation $V = \frac{Q}{Wd}$. Accuracy of measurement of the stationary wave wavelengths is estimated to be ± 1 cm, which is great enough to accommodate differences between calculated velocities and velocities determined from transducer data. The higher nominal velocities determined from stationary wave data, than calculated from

transducer data, may suggest that mid-channel mean velocities are higher than overall cross-section mean velocities. This problem becomes more severe at the larger width-to-depth ratios encountered in alluvial-bank channels, as discussed later.

Summary of data from steady-state experiments. Observed and calculated data from A-series and D-series experiments are tabulated (Table 6-1) in order that experiments were run. For example, Run D-1-4 is the fourth experiment conducted with Q = 7500 cm^3/sec and G_{so} = 41.0 cm^3/sec, with flume slope set at .01064. Experiments for which water depth and/or mean bed elevation profiles were not obtained are not tabulated because calculated quantities are based on these data. Data from non-equilibrium runs are identified by superscript daggers. They have water-surface and bed relative slopes outside limits earlier specified. The quantities of Table 6-1 are as follows:

Column 1. d = average depth of water in cm in instrumented test section, determined from transducer data.

Column 2. $V = \frac{Q}{Wd}$ = average water velocity in cm/sec in instrumented test section, where W = 26.67 cm = width of flume.

Column 3. Q = water discharge in cm^3/sec, measured by water manometer connected to flange taps on inlet line orifice meter.

Column 4. $F = \frac{V}{\sqrt{gd}}$ = Froude number.

Column 5. $r = \frac{Wd}{W+2d}$ = hydraulic radius in cm.

Column 6. S = slope = mean of slopes of mean bed elevation profile, water surface, and energy grade line. Use of slope of energy grade line alone, although theoretically more desirable, puts too much

TABLE 6-1. SUMMARY OF DATA FROM STEADY-STATE EXPERIMENTS

Run Number	1 d	2 V	3 Q	4 F	5 r	6 S	7 S_r	8 f	9 f_b	10 f_b/f_b'	11 T	12 G_{s_o}	13 G_s	14 Bed-Form*	15 L	16 V_L	17 Bed d_g	18 Material σ_g	19 Load d_g	20 Material σ_g	21 Notes
	Water Depth	Mean Velocity	Discharge	Froude Number	Hydraulic Radius	Slope	Relative Slope	Overall Friction Factor	Bed Friction Factor	Friction Factor Ratio	Water Temperature	Sediment Input Rate	Sediment Discharge		Stationary Wave Wavelength	Stationary Wave Velocity	Geometric Mean Size	Geometric Standard Deviation	Geometric Mean Size	Geometric Standard Deviation	
	cm	cm/sec	cm^3/sec	--	cm	--	--	--	--	--	^oC	cm^3/sec	cm^3/sec	--	cm	cm/sec	mm	--	mm	--	
A-1-3†	5.61	50.39	7540	.68	3.95	.00304	-.00137	.0368	.0407	1.62	22.4	5.2	--	DA	--	--	--	--	--	--	1,3,5,8
A-1-4†	5.43	52.00	7530	.71	3.86	.00331	-.00089	.0369	.0407	1.62	22.4	5.2	7.0^B	DAB	--	--	--	--	--	--	1,3,5,9
A-2-1	3.84	56.05	5740	.88	2.98	.00381	-.00002	.0302	.0310	1.16	22.0	4.0	4.7^B	--	--	--	--	--	--	--	1,3,5,9
A-3-1	4.73	59.73	7535	.88	3.49	.00402	+.00001	.0308	.0320	1.25	22.4	7.1	$7.6^S/7.6^B$	DAB	23	59.92					1,3,5,9
A-3-2	4.71	59.96	7532	.89	3.48	.00401	+.00007	.0302	.0312	1.20	22.0	7.1	8.0^B	--	--	--	.290	1.38	.286	1.42	1,3,5,9
A-5-2	3.74	57.05	5690	.94	2.92	.00437	+.00008	.0307	.0316	1.17	22.0	4.0	7.3^B	--	--	--	--	--	--	--	1,3,5,10
A-5-4†	3.85	53.66	5510	.87	2.99	.00423	+.00073	.0344	.0364	1.35	22.0	3.0	6.1^B	--	--	--	--	--	--	--	1,3,6,10
A-6-6	3.58	38.80	3705	.65	2.82	.00394	+.00002	.0579	.0661	2.36	22.4	1.4	1.8^B	DA	10	39.51	--	--	--	--	2,4,6,10
A-7-1	4.38	57.18	6680	.87	3.30	.00391	+.00016	.0310	.0321	1.24	23.2	5.8	$4.8^B/3.7^B$	--	--	--	--	--	--	--	2,4,6,10
A-7-2	4.59	54.57	6680	.81	3.41	.00374	+.00012	.0336	.0357	1.38	23.0	5.8	3.8^B	DA	20	55.87	--	--	--	--	2,4,6,10
D-1-2†	3.67	76.66	7500	1.28	2.88	.01064	-.00038	.0409	.0446	1.75	22.5	41.0	$36.9^B/45.0^B$	AB	40	79.01	.291	1.36	.293	1.41	2,4,6,11
D-1-3	3.49	80.58	7500	1.38	2.77	.01054	-.00021	.0353	.0373	1.40	22.0	41.0	44.2^B	--	--	--	--	--	--	--	2,4,6,12
D-1-4	3.53	79.66	7500	1.35	2.79	.01021	-.00010	.0352	.0372	1.43	22.0	41.0	$43.1^B/46.1^B$	--	--	--	--	--	.276	1.45	2,4,6,12
D-2-1	3.05	69.15	5625	1.26	2.48	.00999	+.00010	.0406	.0436	1.56	22.4	23.1	29.1^B	AB	31	69.56	--	--	--	--	2,4,6,12
D-2-2	2.95	72.07	5670	1.34	2.42	.00995	+.00010	.0364	.0384	1.43	22.4	29.1	27.0^B	AB	--	--	--	--	--	--	2,4,6,12
D-2-4	3.15	66.96	5625	1.20	2.55	.01063	-.00010	.0474	.0521	1.93	22.4	25.0	$37.8^B/37.2^B$	--	--	--	--	--	.274	1.45	2,4,7,12

*BEDFORMS: A = ANTIDUNES
AB = ANTIDUNES WITH BREAKING SURFACE WAVES
DA = "ANTIDUNES" MOVING DOWNSTREAM
DAB = "ANTIDUNES" MOVING DOWNSTREAM WITH BREAKING SURFACE WAVES
-- = NOT OBSERVED

†NOT AN EQUILIBRIUM RUN

dependence on transducer data when bed slope data may be more accurate. For uniform flow, the slopes should all be equal anyway.

Column 7. $S_r = S_{water} - S_{bed}$ = relative slope of water surface with respect to mean bed elevation profile.

Column 8. $f = \frac{8grS}{V^2}$ = Darcy-Weisbach friction factor.

Column 9. $f_b = f + \frac{2d}{W}(f-f_w)$ = bed Darcy-Weisbach friction factor, where $f_w = .0275$ = flume wall friction factor determined experimentally.

Column 10. f_b/f_b' = friction factor ratio, where f_b' is bed grain-roughness friction factor determined from Moody pipe-friction curves for pipe diameter = $4r$, pipe roughness length = d_g, and Reynolds number = $\frac{4rV}{\nu}$.

Column 11. T = water temperature in °C.

Column 12. G_{so} = sediment input rate in cm^3/sec.

Column 13. G_s = sediment discharge in cm^3/sec. Superscript ^{s} denotes rate determined from outlet sampling. Superscript ^{B} denotes rate determined from mean bed elevation change over a known period of time.

Column 14. Bedform.

Column 15. L = wavelength of stationary waves, in cm.

Column 16. $V_L = \sqrt{\frac{gL}{2\pi}}$ = inferred stationary wave velocity using Kennedy's (1961) two-dimensional equation, since the transverse wavelength is not known.

Columns 17 and 18. d_g, σ_g = geometric mean grain size in mm and geometric standard deviation of bed material sampled after experiment.

Columns 19 and 20. d_g, σ_g = geometric mean grain size in mm and

geometric standard deviation of load material sampled during experiment.

Column 21. Notes are as follows:

1. Red Valve control valve.
2. Fisher control valve.
3. Four pressure transducer locations.
4. Seven pressure transducer locations.
5. Outlet with 6 cm-high flat sill, 8-mesh screen.
6. Outlet with 6 cm-high ramped sill, 8-mesh screen.
7. Outlet with 6 cm-high ramped sill, no screen.
8. Flume slope = .00256.
9. Flume slope = .00299.
10. Flume slope = .00397.
11. Flume slope = .01194.
12. Flume slope = .01064.

Missing entries for runs in Table 6-1 indicate data that were not obtained during those experiments.

Reproducibility of results. Table 6-1 includes data from three pairs of experiments in which flume slope, discharge, and sediment input rate were the same for both runs in each pair. Table 6-2 summarizes the differences in several flow parameters between the two runs in each pair.

TABLE 6-2. EXPERIMENTAL REPRODUCIBILITY

Run Pair	Δd(%)	ΔV(%)	ΔF(%)	Δr(%)	ΔS(%)	Δf_b(%)	ΔG_s(%)
A-3-1/A-3-2	0.4	0.4	1.1	0.3	0.3	2.6	5.3
A-7-1/A-7-2	4.8	4.8	7.4	3.3	4.6	11.2	2.7
D-1-3/D-1-4	1.2	1.2	2.2	0.7	3.2	0.3	4.3

The data of Table 6-1 show that all of these flows are in the transition or upper flow regime, having Froude numbers in the range 0.81 to 1.38 and friction factor ratios less than 2. For the simulated flood experiments, discussed in a later section, experimental reproducibility cannot be expected to be better than the quantities in Table 6-2, which do not include any discharge-change dynamic effects.

Bed elevation stability. In none of the experiments tabulated in Table 6-1 were sediment transport rates equal to sediment input rates. Consequently, even the runs which had uniform flow conditions did not maintain constant mean bed elevations. Furthermore, attempts to achieve uniform flow with sediment input and transport rates equal by adjusting sediment input rate of a second experiment to equal transport rate measured in a first experiment at the same discharge and slope usually resulted in uniform flow with sediment transport rate different from either of the sediment input rates and from the previously measured transport rate. This result can be seen for runs D-2-1 and D-2-2. In other instances, the sediment input rate necessary to attain the desired slope differed from the mean transport rate.

Kennedy (1971, Table 2-F.2) indicates that a flume system with discharge, slope, and channel width specified as independent variables, as in these experiments, is not over-constrained. However, the functional relationships defining dependent variables, such as sediment transport rate, may be multiple-valued for some ranges of the independent variables. In A-series experiments for which equilibrium criteria were met at a slope of .0040 ± .0002 (Figure 6-3) the data, although widely scattered, show a reasonable fit to a discontinuous sediment transport

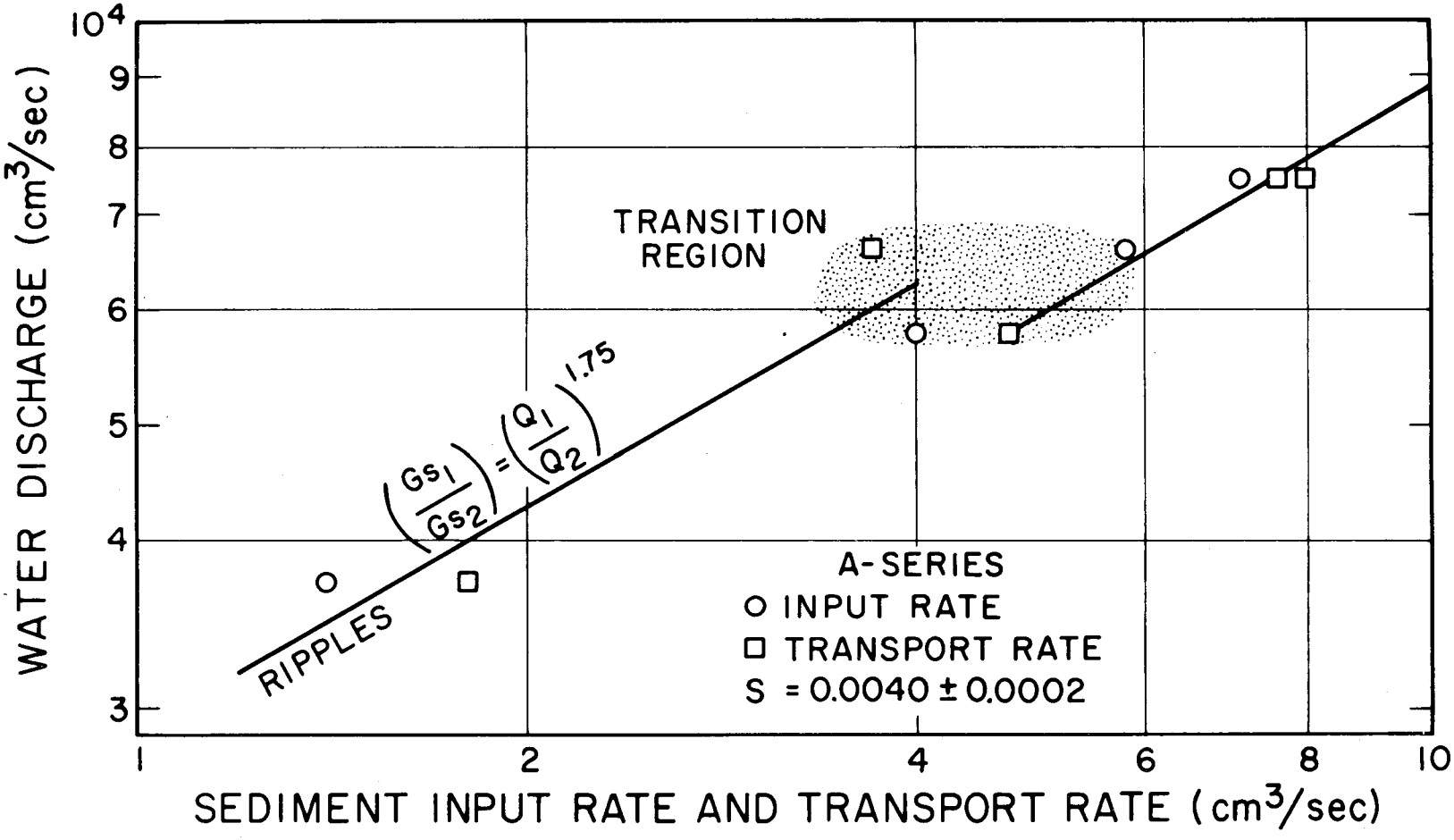

Figure 6-3. Sediment transport behavior for A-series experiments.

relation of the form $G_s \propto Q^{1.75}$. The relatively high friction factor ratio for run A-6-6 (Table 6-1) indicates it is probably in the lower flow regime, while all other A-series runs are in the upper regime. At the discharges, slope, and channel width of these experiments, there are two possible sediment transport relations, and experimental conditions do not really stabilize at either one within the duration of these experiments, although the friction factor ratios indicate that all runs except A-6-6 behave like upper-regime flows.

Sediment input-transport rate behavior is similar in the D-series experiments. There are not enough points to demonstrate that the data represent a transition region of a discontinuous sediment-transport relation at the discharges used in the D-series. Presumably, if a transition occurs it is at a lower discharge, and the D-series transport data can be fit by a single-valued relationship of the form $G_s \propto Q^{1.54}$ (Figure 6-4).

Simulated Flood Experiments with Rigid Walls

The changing slope and bed elevation resulting from a multiple-valued sediment transport relationship cannot be tolerated in steady-state experiments. Changing conditions are incompatible with the definition of a steady-state experiment, and physical limitations of experimental equipment prohibit the changes from continuing for an indefinite period of time. However, a multiple-valued sediment transport relationship is acceptable in a simulated flood experiment as long as the sum of changes occurring during the flood does not exceed the physical limits of the flume. If the steady-state sediment transport relationship

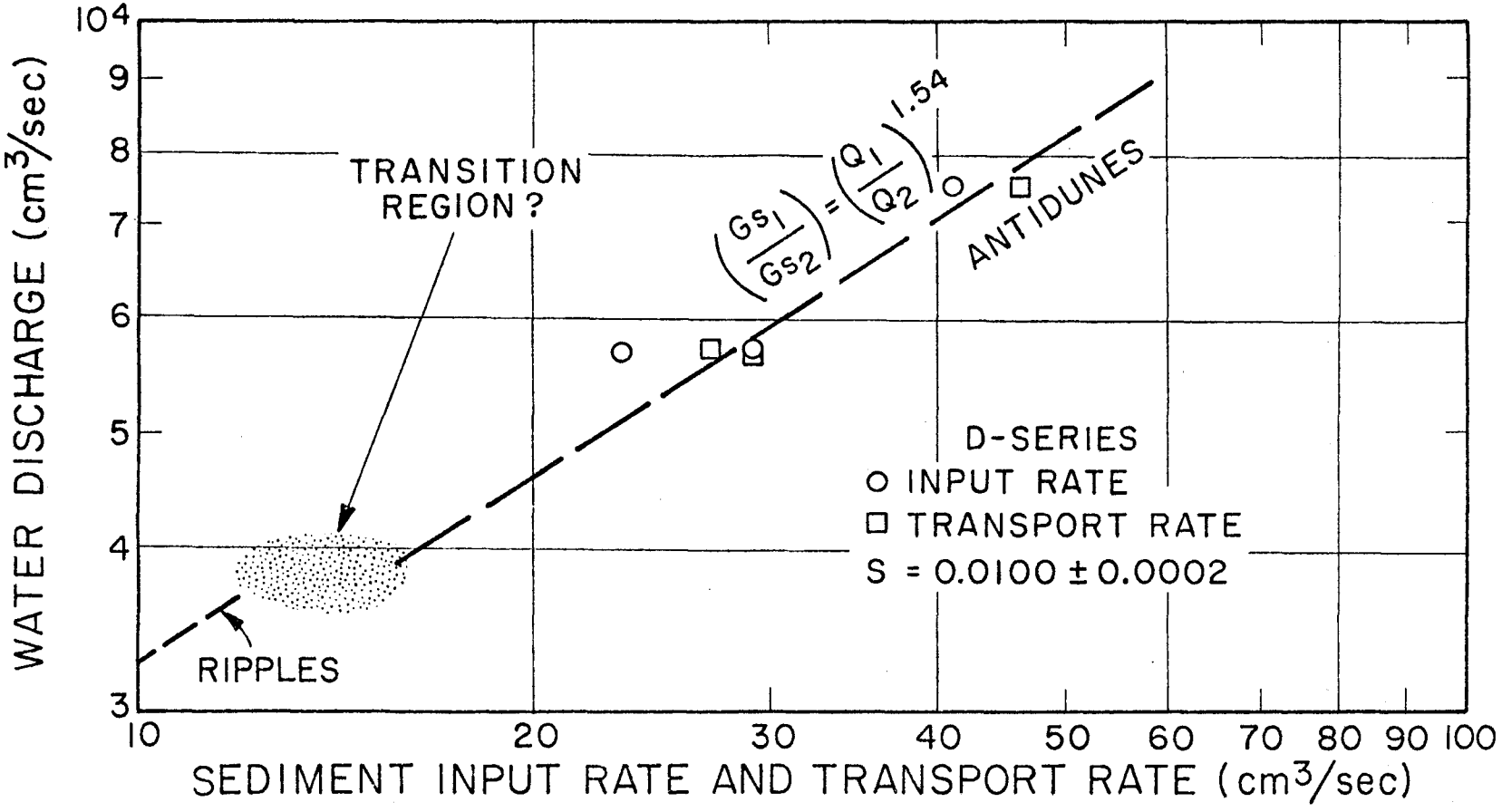

Figure 6-4. Sediment transport behavior for D-series experiments.

had been single-valued, there still would have been the dilemma of applicability to time-varying discharge conditions. This dilemma, and the problem of a multi-valued relationship, compel adoption in simulated floods, of an ad hoc sediment-transport relationship based on field observations.

Selection of hydrograph. Laboratory simulated floods were not designed to model field conditions in Quatal Creek. However, for relevance it is necessary that the style of the laboratory flood be similar to a field runoff event. For this reason, an ephemeral stream or "flash flood" hydrograph was chosen, of the dimensionless form:

$$o<t<t_o; \quad Q = Q_{max} \text{ (flattop peak)}$$

$$t_o<t<t_{max}; \quad Q = Q_{max} \exp\left[-\frac{3(t-t_o)}{(t_{max}-t_o)}\right]$$

where $t_o = 0.1\ t_{max}$

t_{max} = 1 hour = duration of run

$Q_{max} = 7500\ cm^3/sec$

For early experiments, a linear decay from $Q_{max} \cdot e^{-3}$ to zero was used from t_{max} to 72 minutes. Figure 6-5 shows this hydrograph, with overplots of the actual hydrographs run in this experimental series.

The exponential tail of this hydrograph is representative of the falling limbs of surface runoff hydrographs of ephemeral streams in California (Gupta and Moin, 1974). The flattop peak and short, nearly linear rise are similar to those of the Alamogordo Creek watershed (Renard and Keppel, 1966). This very sharp rise to maximum discharge,

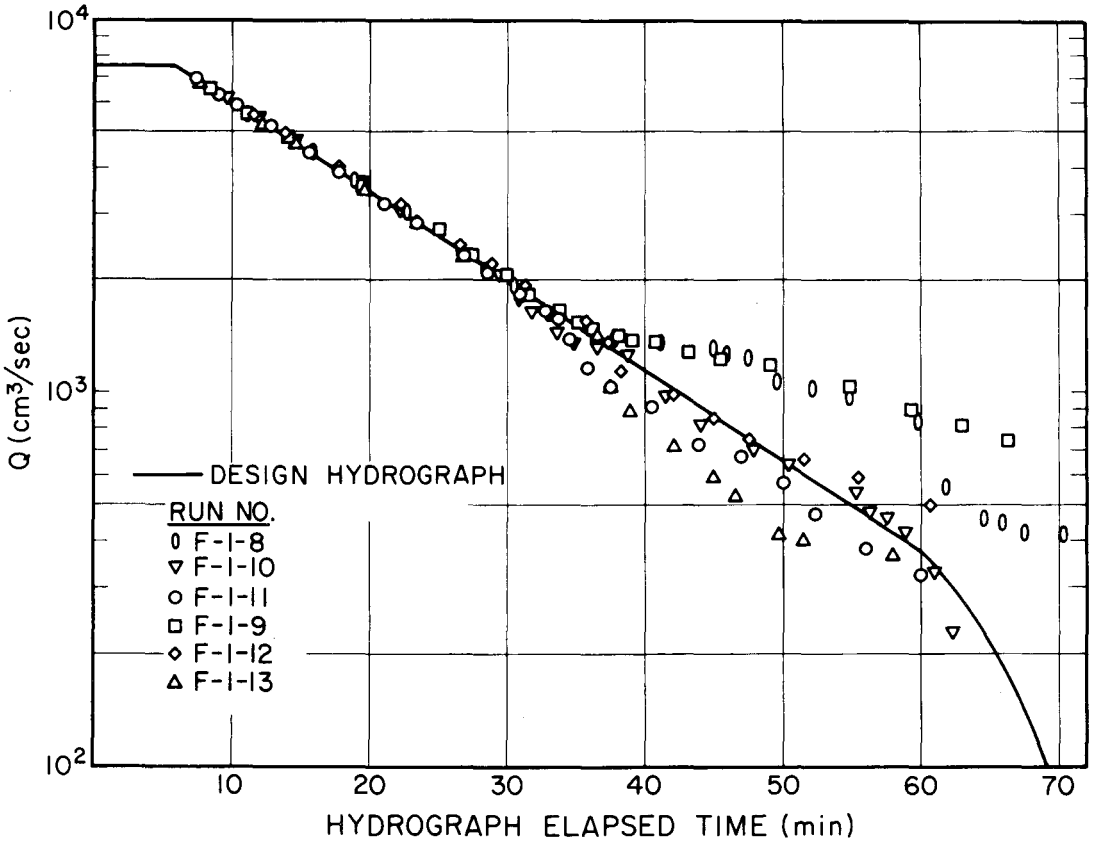

Figure 6-5. Design and actual hydrographs for simulated floods.

requiring less than 10 seconds, along with the antecedent wet bed condition, produces an abrupt translatory wave as the leading edge of the laboratory flash flood. The single "wall of water" translatory wave is thought by Renard and Keppel (1966) to be relatively uncommon in the field; a series of translatory waves of small amplitude building to full flood depth is the general occurrence. The laboratory flood wave increases in height as it passes through the inlet section and the upper part of the test section, indicating a behavior qualitatively similar to the general field observation, but of such a small scale and short duration that individual translatory waves do not occur.

Selection of sediment input relation. Since water discharge and sediment input rate are independent variables in these open-circuit experiments, any sediment input relation is possible. For differing water-source circumstances in the field, such as snowmelt, thunderstorm, or steady rain, there will be greatly varying relations between rate of water input and rate of sediment input. Modeling this process is beyond the scope of this research. A relevant sediment transport relation can be derived from field observations (Bennett and Sabol, 1973):

$$G_{so} = \alpha Q^{\beta} \text{ where } \alpha \text{ and } \beta \text{ are constants.}$$

For Rio Grande data with sand grain-size similar to these experiments (Nordin, 1964), a fit of all data in his Figures 16 and 17 gives $1.8 \leq \beta \leq 2.4$. Bennett and Sabol (1973) find that the best fit to field data is obtained by a zero-intercept quadratic relation of the form:

$$G_{so} = \gamma Q^2 + \delta Q \quad \text{where } \gamma \text{ and } \delta \text{ are constants.}$$

For these experiments, a compromise sediment-input relation of the form:

$$G_{so} = \alpha Q^2 \quad \text{was chosen,}$$

with $G_{so_{max}} = 41.1$ cm^3/sec at $Q_{max} = 7500$ cm^3/sec. In this way, the constant α or γ is determined from the conditions of steady-state experiment series D-1, $\beta = 2$, and $\delta = 0$. The design and actual sediment input curves are shown in Figure 6-6.

Mean bed elevation determination. Following a simulated flood, mean bed elevations along the flume can be determined in the same manner used in steady-state experiments. It has not been possible to measure directly mean bed elevations while the water is running. For this reason, mean bed elevation for the flume as a whole is determined at any time during a flood by dividing the known volume of bed sand in the flume by the bed area. The volume of sand in the flume is determined by sampling total sediment discharge at the outlet, subtracting it from known sediment input rate, and integrating the difference as a function of time. A basic assumption of this method is that there are not persistent or propagating discontinuities in mean bed elevation, such as a scour or fill "wave". No such discontinuities were observed during simulated floods, so this assumption is valid for discontinuities of greater than about 5 mm amplitude.

In practice, total sediment discharge sampling is difficult. Sediment discharge fluctuates wildly, particularly during the high-discharge part of the flood, requiring frequent sampling to achieve a

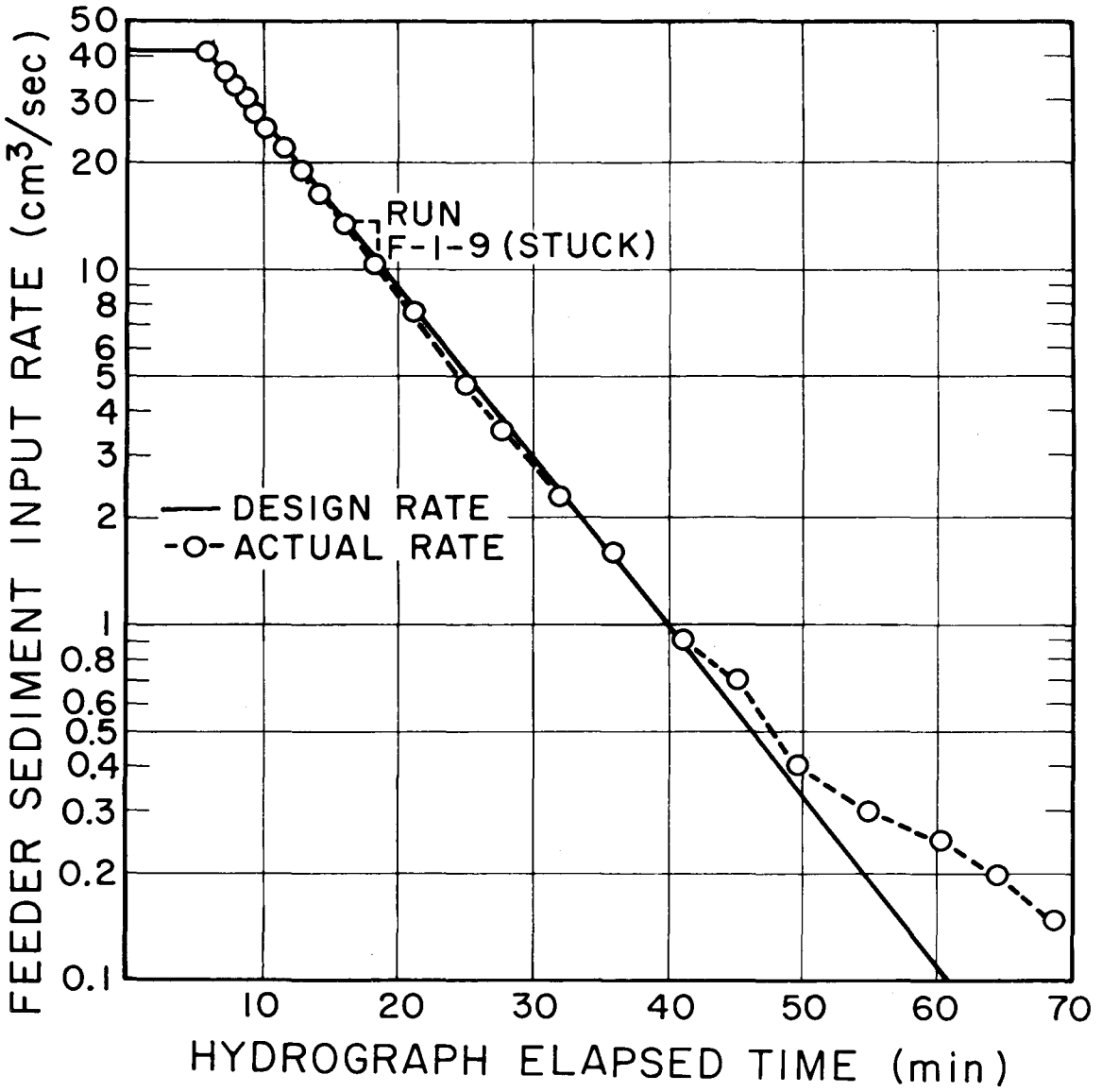

Figure 6-6. Design and actual sediment-input rates for simulated floods.

meaningful average. Equipment constraints limited the total number of one-liter samples for each experiment to 30. Because of this it is necessary to include more than one sample, defined as the water and sand recovered from one pass of the sample slot, in each sample flask. Sampling experiments conducted during the steady-state series of experiments indicate that the narrow sampling slot gives discharge measurements systematically higher than those of the wide slot and those calculated from bed elevation changes. This difference indicates an inlet flow problem with the narrow-slot sampler, thus it was not used in simulated flood experiments.

Trial-and-error usage of the wide-slot sampler indicates that the optimum sampling interval during simulated floods is 30 seconds, with operator judgment determining the duration of each sample traverse. The sample traverses must be timed so the samples pooled in a one-liter sample flask are of nearly equal volume to provide a meaningful average sediment discharge, with the further constraints that the volume of pooled samples is greater than 500 mℓ for accuracy, but does not exceed flask capacity. Minimum difference between mean bed elevation change calculated from sample data and that measured at the end of a simulated flood was obtained for the sampling procedure using:

1 sample every 30 seconds

2 samples per flask for first 9 samples

4 samples per flask for next 11 samples

8 samples per flask for next 4 to 10 samples

This procedure has the advantage of averaging samples over a shorter

period of time when conditions of discharge and sediment discharge are changing rapidly, and over a longer period of time later in the flood when conditions are changing slowly. This procedure was used for runs F-1-9, 11, 12, 13 as described below. Unacceptable differences were obtained for sampling procedures used in runs F-1-8 and F-1-10. In F-1-8, one sample was taken every 2 minutes for the first 30 minutes of the flood and every 4 minutes thereafter, with just one sample in each sample flask. This procedure was apparently not sufficient to describe accurately initial average sediment discharge. In F-1-10, a sample was taken every 20 seconds with the same sample-flask change interval used in the successful procedure described above, but with 3, 6, and 12 samples in each sample flask depending on the location in the sample sequence. This procedure produced a difference which indicates that the sample-slot transverse velocity necessary to get so many samples in each sample flask was so high that inertial inlet effects affected the accuracy of the samples, making measured discharges systematically low.

It must be emphasized that this sampling procedure measured only sediment concentration at the outlet. To calculate sediment discharge, it is necessary to know water discharge at the outlet. Hydrograph water discharge at the inlet is known, but the discharge hydrograph at the outlet suffers time lag from inlet discharge as water discharge decreases. This time lag is the flume length divided by the flood-wave speed, c. From Henderson (1966, p.365-366),

$$c = V + d \frac{dV}{dd}$$

Using equation 4-1:

$$c = V + \left[\frac{V}{2} - \frac{Vd}{f}\frac{df}{dd}\right]$$

The functional relationship between f and d is not known, and $\frac{df}{dd}$ may be positive or negative at different times in a simulated flood. This uncertainty means that c cannot be calculated directly. For this reason, the approximation $c \approx V$ will be used, with the neglected term $d\frac{dV}{dd}$ contributing to sampling errors already large because of flow and sediment concentration fluctuations at the outlet. Thus, the water discharge at the outlet is: $Q_{outlet}(t) = Q_{inlet}(t-\Delta t)$ where t is elapsed time in the hydrograph and $\Delta t(t) = \frac{\text{flume length}}{V(t-\Delta t)}$. The packet velocity is $V = \frac{Q}{Wd}$ where d is determined from transducer data. Determining Δt from $V(t-\Delta t)$ is a time-consuming iterative process since Δt is unknown. However, Q(t) and V(t) change slowly enough that a good approximation of outlet discharge is obtained by using

$$\Delta t(t) \approx \frac{\text{flume length}}{V(t)} .$$

Equilibrium simulated flood criteria. A natural stream is considered in equilibrium or at grade (Mackin, 1948), if it is not, on the average, aggrading, degrading, changing slope, or rapidly altering its banks. Short-term fluctuations caused by different flows are permitted, if the variations balance. Since all flood hydrographs in these laboratory experiments are the same, no fluctuations are acceptable. Thus, the equilibrium criteria for rigid-walled simulated flood experiments are that mean bed elevation and slope are the same before and after the flood.

In practice, a .0003 cm/cm variation in slope is not considered significant. Equilibrium was achieved in the experiments by adjusting flume slope between floods until the slope equilibrium criterion was met. Achievement of stability of mean bed elevation required running two more floods after slope equilibrium was achieved, apparently because of bed armoring and inlet and outlet geometry. These effects will be discussed in a later section.

Summary of data from simulated flood experiments. Following run F-1-7, the seventh attempt of the F-1 series, bed slope was within equilibrium criterion limits, and full-scale data collection was begun. Observed and calculated data for runs F-1-8 through F-1-13 are tabulated in Tables 6-3 through 6-8. The quantities in each column of these tables, including tabulated entries for the pooled samples described above, are as follows:

Column 1. t = time in minutes elapsed since beginning of hydrograph.

Column 2. d = average depth of water in cm in instrumented test section, determined as the difference between transducer water-surface elevation determinations and mean bed elevations determined by linear interpolation between initial and final measured mean bed elevations.

Column 3. $Q(t)$ = water discharge in cm^3/sec, measured as a function of t by water manometer connected to flange taps on inlet line orifice meter.

Column 4. $V = \frac{Q}{Wd}$ = average water velocity in cm/sec in instrumented test section, where $W = 26.67$ cm = width of flume.

TABLE 6-3. DATA SUMMARY FOR RUN F-1-8

1 t min	2 d cm	3 Q(t) cm^3/sec	4 V cm/sec	5 Δt min	6 $t-\Delta t$ min	7 $Q(t-\Delta t)$ cm^3/sec	8 $G_{so}(t)$ cm^3/sec	9 $G_s(t)$ cm^3/sec	10 $\Delta G_s(t)$ cm^3/sec	11 $\Delta d(t)$ cm
1.00	3.9	7500	72.1	.42	.58	7500	41.10	49.86	-8.76	-.006
3.00	3.9	7500	72.1	.42	2.58	7500	41.10	33.34	7.76	.013
5.00	3.9	7500	72.1	.42	4.58	7500	41.10	48.26	-7.16	-.005
7.00	3.7	7200	73.0	.41	6.59	7400	35.40	27.34	8.06	.015
9.00	3.5	6410	68.7	.44	8.56	6610	30.00	52.68	-22.68	-.041
11.00	3.4	5750	63.4	.47	10.53	5870	24.10	23.08	1.02	-.039
13.00	2.9	5080	65.7	.46	12.54	5220	19.80	27.04	-7.24	-.057
15.00	2.9	4550	58.8	.51	14.49	4660	15.80	21.60	-5.80	-.071
17.00	2.7	4070	56.5	.53	16.47	4200	12.70	20.82	-8.12	-.092
19.00	2.6	3700	53.4	.56	18.46	3800	10.20	17.50	-7.30	-.112
21.00	2.3	3340	54.5	.55	20.45	3410	8.15	11.03	-2.88	-.119
23.00	2.2	2995	51.0	.59	22.41	3070	6.50	10.02	-3.52	-.128
25.00	2.2	2670	45.5	.66	24.34	2730	5.10	6.58	-1.49	-.132
27.00	2.0	2370	44.4	.68	26.32	2440	4.06	4.19	- .13	-.132
29.00	1.7	2130	47.0	.64	28.36	2170	3.28	3.13	.15	-.132
33.00	1.7	1650	36.4	.83	32.17	1730	2.25	4.00	-1.75	-.140
38.25	1.7	1400	30.9	.97	37.28	1430	1.33	3.60	-2.27	-.155
42.00	1.7	1340	29.6	1.02	40.98	1360	.87	2.09	-1.22	-.161
46.00	1.7	1295	28.6	1.05	44.95	1320	.75	2.52	-1.77	-.170
50.00	1.7	1070	23.6	1.27	48.73	1140	.40	3.08	-2.68	-.183
54.00	1.7	985	21.7	1.38	52.62	1030	.30	1.05	- .75	-.187
57.75	1.7	890	19.6	1.53	56.22	924	.28	.18	.10	-.187
61.75	1.7	550	12.1	2.47	59.28	855	.25	1.33	-1.08	-.192
65.75	1.2	447	14.0	2.15	63.60	490	.20	.05	.15	-.191
70.00	1.2	420	13.1	2.29	67.71	420	.15	.03	.12	-.191

Measured Δd (72 min) = -.06 cm

TABLE 6-4. DATA SUMMARY FOR RUN F-1-9

1 t min	2 d cm	3 Q(t) cm^3/sec	4 V cm/sec	5 Δt min	6 $t-\Delta t$ min	7 $Q(t-\Delta t)$ cm^3/sec	8 $G_{so}(t)$ cm^3/sec	9 $G_s(t)$ cm^3/sec	10 $\Delta G_s(t)$ cm^3/sec	11 $\Delta d(t)$ cm
1.25	4.18	7500	67.28	.45	.80	7500	41.10	37.42	3.68	.004
2.25	4.18	7500	67.28	.45	1.80	7500	41.10	36.07	5.03	.010
3.25	4.18	7500	67.28	.45	2.80	7500	41.10	35.00	6.10	.018
4.25	4.18	7500	67.28	.45	3.80	7500	41.10	39.57	1.53	.020
5.25	4.18	7500	67.28	.45	4.80	7500	41.10	40.24	.86	.021
6.25	4.15	7400	66.86	.45	5.80	7500	38.00	48.98	-10.98	.007
7.25	4.13	7000	63.55	.47	6.78	7150	33.50	39.49	-5.99	-.001
8.25	3.98	6650	62.65	.48	7.77	6760	30.25	33.88	-3.63	-.005
9.25	3.65	6300	64.72	.46	8.79	6400	26.85	36.54	-9.69	-.017
10.75	3.57	5720	60.08	.50	10.25	5900	25.25	21.43	3.82	-.010
12.75	3.38	5150	57.13	.53	12.22	5340	18.70	17.57	1.13	-.007
14.75	3.13	4610	55.22	.54	14.21	4800	14.60	18.08	-3.48	-.016
16.75	3.00	4140	51.74	.58	16.17	4310	13.70	15.76	-2.06	-.021
18.75	2.89	3710	48.13	.62	18.13	3880	13.70	13.85	-.15	-.022
20.75	2.69	3380	47.11	.64	20.11	3490	7.50	12.66	-5.16	-.034
22.75	2.60	3100	44.71	.67	22.08	3160	5.88	10.17	-4.29	-.045
24.75	2.42	2760	42.76	.70	24.05	2860	4.60	6.73	-2.13	-.050
26.75	2.32	2430	39.27	.76	25.99	2570	3.68	5.23	-1.55	-.054
28.75	2.26	2120	35.17	.85	27.90	2260	2.96	7.22	-4.26	-.065
30.75	2.28	1895	31.16	.96	29.79	2040	2.47	4.00	-1.53	-.069
33.50	2.15	1680	29.30	1.02	32.48	1760	1.95	4.64	-2.69	-.078
37.50	2.04	1430	26.28	1.14	36.36	1470	1.20	3.89	-2.69	-.092
41.50	2.10	1320	23.57	1.27	40.23	1370	.88	2.56	-1.68	-.100
45.50	2.08	1220	21.99	1.37	44.13	1245	.60	2.01	-1.41	-.107
49.50	2.19	1160	19.86	1.51	47.99	1190	.37	2.03	-1.66	-.115
53.50	2.20	1060	18.07	1.66	51.84	1100	.30	1.87	-1.57	-.123
57.50	2.23	946	15.91	1.89	55.61	1010	.20	1.38	-1.18	-.129
61.50	2.14	840	14.72	2.04	59.46	890	.19	.87	-.68	-.132
65.50	2.05	760	13.90	2.16	63.34	800	.13	.75	-.62	-.135
69.50	1.98	685	12.97	2.31	67.19	725	.13	.81	-.68	-.139

MEASURED Δd(72 min) = -.18 cm

TABLE 6-5. DATA SUMMARY FOR RUN F-1-10

1 t min	2 d cm	3 Q(t) cm^3/sec	4 V cm/sec	5 Δt min	6 t-Δt min	7 Q(t-Δt) cm^3/sec	8 $G_{sQ}(t)$ cm^3/sec	9 $G_s(t)$ cm^3/sec	10 $\Delta G_s(t)$ cm^3/sec	11 $\Delta d(t)$ cm
1.33	3.72	7540	76.00	.39	.94	7540	41.10	30.20	10.90	.013
2.32	3.72	7540	76.00	.39	1.93	7540	41.10	28.96	12.14	.028
3.32	3.72	7540	76.00	.39	2.93	7540	41.10	31.71	9.39	.040
4.30	3.72	7540	76.00	.39	3.91	7540	41.10	34.88	6.22	.047
5.30	3.72	7540	76.00	.39	4.91	7540	41.10	31.27	9.83	.059
6.30	3.69	7450	75.70	.40	5.90	7540	39.10	36.04	3.06	.063
7.28	3.54	7040	74.57	.40	6.88	7195	34.70	25.14	9.56	.075
8.28	3.40	6720	74.11	.40	7.88	6850	30.99	29.51	1.48	.077
9.28	3.27	6390	73.27	.41	8.87	6500	27.90	24.37	3.53	.081
10.77	3.10	5900	71.36	.42	10.35	6000	23.12	17.54	5.58	.092
12.75	2.99	5290	66.34	.45	12.30	5420	19.20	16.50	2.70	.098
14.75	2.89	4730	61.37	.49	14.26	4870	15.09	13.36	1.73	.103
16.73	2.69	4220	58.82	.51	16.22	4350	12.80	13.26	-.46	.102
18.73	2.48	3790	57.30	.52	18.21	3890	9.65	11.60	-1.95	.097
20.72	2.30	3360	54.78	.55	20.17	3490	7.74	9.08	-1.34	.093
22.70	2.20	3000	51.13	.59	22.11	3130	6.09	10.15	-4.06	.083
24.70	2.09	2755	49.43	.61	24.09	2820	4.80	8.23	-3.43	.075
26.68	2.00	2450	45.93	.65	26.03	2560	3.80	6.45	-2.65	.068
28.67	1.98	2170	41.09	.73	27.94	2270	3.11	6.34	-3.23	.060
31.63	1.83	1695	34.73	.86	30.77	1820	2.34	3.87	-1.53	.054
35.60	1.64	1340	30.64	.98	34.62	1370	1.61	2.44	-.83	.050
39.60	1.71	1150	25.22	1.19	38.41	1170	1.00	1.87	-.87	.046
43.57	1.68	850	18.97	1.58	41.99	935	.83	1.52	-.69	.043
47.55	1.59	720	16.98	1.77	45.78	768	.48	.71	-.23	.041
51.52	1.50	612	15.30	1.96	49.56	665	.31	.55	-.24	.040
55.50	1.43	500	13.11	2.29	53.21	563	.25	.47	-.22	.039
59.50	1.20	378	11.81	2.54	56.96	474	.20	.07	.13	.040
63.50	.96	230	8.98	3.34	60.16	360	.15	.03	.12	.040

MEASURED Δd(66 min) = -.17 cm

TABLE 6-6. DATA SUMMARY FOR RUN F-1-11

1 t min	2 d cm	3 Q(t) cm^3/sec	4 V cm/sec	5 Δt min	6 $t-\Delta t$ min	7 $Q(t-\Delta t)$ cm^3/sec	8 $G_{sQ}(t)$ cm^3/sec	9 $G_s(t)$ cm^3/sec	10 $\Delta G_s(t)$ cm^3/sec	11 $\Delta d(t)$ cm
1.25	3.77	7550	75.09	.40	.85	7550	41.10	36.37	4.73	.005
2.25	3.77	7550	75.09	.40	1.85	7550	41.10	38.65	2.45	.008
3.25	3.77	7550	75.09	.40	2.85	7550	41.10	31.92	9.18	.020
4.25	3.77	7550	75.09	.40	3.85	7550	41.10	46.34	-5.24	.013
5.25	3.77	7550	75.09	.40	4.85	7550	41.10	32.42	8.68	.024
6.25	3.71	7450	75.29	.40	5.85	7550	39.90	35.57	4.33	.029
7.25	3.64	7050	72.62	.41	6.84	7200	35.25	44.85	-9.60	.017
8.25	3.50	6620	70.92	.42	7.83	6840	31.30	29.56	1.74	.019
9.25	3.39	6210	68.69	.44	8.81	6400	28.35	33.77	-5.42	.013
10.67	3.25	5780	66.68	.45	10.22	5900	23.70	23.47	.23	.013
12.67	3.05	5200	63.93	.47	12.20	5330	19.55	16.33	3.22	.021
14.67	2.88	4660	60.67	.49	14.18	4800	15.35	13.98	1.37	.025
16.67	2.68	4150	58.06	.52	16.15	4280	12.30	14.20	-1.90	.020
18.67	2.51	3700	55.27	.54	18.13	3800	9.90	12.96	-3.06	.012
20.67	2.37	3300	52.21	.57	20.10	3400	7.90	11.42	-3.52	.003
22.67	2.25	2970	49.49	.61	22.06	3050	6.20	8.44	-2.24	-.002
24.67	2.15	2660	46.39	.65	24.02	2740	4.85	7.97	-3.12	-.010
26.67	2.07	2380	43.11	.70	25.97	2460	3.85	5.02	-1.17	-.013
28.67	2.00	2100	39.37	.76	27.91	2190	3.12	3.94	-.82	-.015
30.67	1.94	1920	37.11	.81	29.86	1980	2.57	5.22	-2.65	-.022
33.67	1.79	1575	32.99	.91	32.76	1660	2.00	3.12	-1.12	-.026
37.67	1.76	1030	21.94	1.37	36.30	1140	1.22	1.44	-.22	-.027
41.75	1.72	840	18.31	1.64	40.11	975	.89	1.32	-.43	-.029
46.25	1.61	682	15.88	1.89	44.36	715	.60	.69	-.09	-.030
50.50	1.55	545	13.18	2.28	48.22	629	.35	.57	-.22	-.031
55.50	1.31	392	11.22	2.67	52.83	455	.28	.32	-.04	-.031

MEASURED $\Delta d(60\ min) = 0.00$ cm

TABLE 6-7. DATA SUMMARY FOR RUN F-1-12

1 t min	2 d cm	3 Q(t) cm^3/sec	4 V cm/sec	5 Δt min	6 t-Δt min	7 Q(t-Δt) cm^3/sec	8 $G_{s_Q}(t)$ cm^3/sec	9 $G_s(t)$ cm^3/sec	10 $\Delta G_s(t)$ cm^3/sec	11 Δd(t) cm
1.25	3.72	7610	76.70	.39	.86	7610	41.10	47.68	-6.58	-.007
2.25	3.72	7610	76.70	.39	1.86	7610	41.10	43.76	-2.66	-.010
4.25	3.72	7610	76.70	.39	3.86	7610	41.10	40.34	.76	-.008
5.25	3.72	7610	76.70	.39	4.86	7610	41.10	48.57	-7.47	-.018
6.25	3.70	7480	75.80	.40	5.85	7610	39.80	39.15	.65	-.017
7.25	3.52	7080	75.42	.40	6.85	7210	35.20	35.76	- .56	-.018
8.25	3.37	6700	74.55	.40	7.85	6850	31.30	21.30	10.00	-.005
9.25	3.19	6390	75.11	.40	8.85	6500	28.40	31.20	-2.80	-.009
10.25	3.00	6005	75.05	.40	9.85	6160	24.87	22.66	2.21	-.006
11.75	2.93	5550	71.02	.42	11.33	5700	21.20	26.17	-4.97	-.015
13.75	2.74	5000	68.42	.44	13.31	5130	17.24	17.10	.14	-.015
15.75	2.56	4590	67.23	.45	15.30	4680	13.60	14.80	-1.20	-.018
17.75	2.38	4150	65.38	.46	17.29	4140	10.85	12.39	-1.54	-.022
19.75	2.18	3690	63.47	.47	19.28	3800	8.70	12.65	-3.95	-.032
21.75	2.07	3280	59.41	.50	21.25	3380	6.93	7.95	-1.02	-.034
23.75	1.99	2920	55.02	.55	23.20	3005	5.48	9.44	-3.96	-.044
25.75	1.91	2600	51.04	.59	25.16	2695	4.28	6.13	-1.85	-.049
27.75	1.84	2295	46.77	.64	27.11	2395	3.42	6.40	-2.98	-.056
29.75	1.79	2050	42.94	.70	29.05	2100	2.80	5.91	-3.11	-.064
32.75	1.68	1800	40.17	.75	32.00	1870	2.13	4.79	-2.66	-.074
36.75	1.53	1430	35.04	.86	35.89	1540	1.40	2.14	-.74	-.077
40.75	1.46	1040	26.71	1.12	39.63	1070	.94	1.46	-.52	-.080
44.75	1.60	860	20.15	1.49	43.26	920	.79	1.50	-.71	-.084
48.75	1.52	720	17.76	1.69	47.06	766	.40	.70	-.30	-.085
52.75	1.42	635	16.77	1.79	50.96	672	.30	1.23	-.93	-.090
56.75	1.31	563	16.11	1.86	54.89	595	.22	.27	-.05	-.090
60.00	1.28	512	15.00	2.00	58.00	543	.20	.54	-.34	-.092

MEASURED Δd(60 min) = -.18 cm

TABLE 6-8. DATA SUMMARY FOR RUN F-1-13

1 t min	2 d cm	3 Q(t) cm^3/sec	4 V cm/sec	5 Δt min	6 t-Δt min	7 Q(t-Δt) cm^3/sec	8 $G_{s_0}(t)$ cm^3/sec	9 $G_s(t)$ cm^3/sec	10 $\Delta G_s(t)$ cm^3/sec	11 $\Delta d(t)$ cm
1.25	3.67	7520	76.83	.39	.86	7520	41.10	35.82	5.28	.006
2.25	3.67	7520	76.83	.39	1.86	7520	41.10	37.56	3.54	.010
3.25	3.67	7520	76.83	.39	2.86	7520	41.10	39.80	1.30	.012
5.25	3.67	7520	76.83	.39	4.86	7520	41.10	43.37	-2.27	.006
6.25	3.60	7390	76.97	.39	5.86	7520	39.80	44.38	-4.58	.000
7.25	3.47	7000	75.64	.40	6.85	7150	35.20	38.85	-3.65	-.004
8.25	3.32	6610	74.65	.40	7.85	6800	31.30	44.04	-12.74	-.020
9.25	3.16	6220	73.80	.41	8.84	6400	28.40	28.41	-.01	-.020
10.25	3.01	5870	73.12	.41	9.84	6000	24.87	32.87	-8.00	-.030
11.25	2.95	5550	70.54	.43	10.82	5680	22.30	23.90	-1.60	-.032
14.75	2.66	4610	64.98	.46	14.29	4730	15.20	15.30	-.10	-.033
16.75	2.49	4110	61.89	.48	16.27	4230	12.16	13.69	-1.53	-.036
18.75	2.31	3660	59.41	.50	18.25	3760	9.75	13.01	-3.26	-.045
20.75	2.15	3300	57.55	.52	20.23	3370	7.80	12.08	-4.28	-.055
22.75	2.00	3005	56.34	.53	22.22	3090	6.12	10.55	-4.43	-.066
24.75	1.88	2660	53.05	.57	24.18	2780	4.80	10.97	-6.17	-.082
26.75	1.81	2300	47.65	.63	26.12	2420	3.80	6.58	-2.78	-.089
28.75	1.79	2080	43.57	.69	28.06	2160	3.08	5.07	-1.99	-.094
30.75	1.73	1895	41.07	.73	30.02	1960	2.54	3.60	-1.06	-.096
33.75	1.60	1635	38.32	.78	32.97	1695	1.99	3.05	-1.06	-.100
37.75	1.44	1030	26.82	1.12	36.63	1400	1.21	2.21	-1.00	-.105
41.75	1.33	780	21.99	1.36	40.39	851	.88	.72	.16	-.105
45.50	1.29	570	16.57	1.81	43.69	746	.65	.64	.01	-.104
49.50	1.10	420	14.32	2.10	47.40	493	.39	.18	.21	-.103
53.50	.99	380	14.39	2.08	51.42	411	.28	.11	.17	-.103
57.50	.88	335	14.27	2.10	55.40	380	.23	.13	.10	-.102

MEASURED Δd(60 min) = -.185 cm

Column 5. $\Delta t \approx \frac{\text{flume length}}{V}$ = time lag in minutes between Q_{inlet} and Q_{outlet}.

Column 6. $t-\Delta t$ = time in minutes for which Q_{outlet} is determined using Q_{inlet} vs. t curve.

Column 7. $Q(t-\Delta t)$ = outlet water discharge in cm^3/sec at time t.

Column 8. $G_{so}(t)$ = feeder sediment input rate in cm^3/sec.

Column 9. $G_s(t)$ = outlet sediment discharge in cm^3/sec, measured as described above.

Column 10. $\Delta G_s(t) = G_{so}(t) - G_s(t)$ = time rate of change of amount of sand in flume in cm^3/sec.

Column 11. $\Delta d(t) = \frac{\Delta G_s(t)}{W \times \text{flume length}} \times \tau$ = change in mean bed elevation from initial value, in cm, where τ = time elapsed since previous sample.

Figure 6-7 is a plot of $\Delta d(t)$ versus t for these experiments. As noted above, the difference between calculated mean bed elevation change and measured change is excessive for runs F-1-8 and F-1-10, for reasons attributable to sampling procedures. For these reasons, the sample data points are shown but the curves are not lined in. Data from these two experiments will not be used in further discussions.

Reproducibility of results. The calculated mean bed-elevation change curves (Figure 6-7) include three for identical initial conditions, runs F-1-9, 12, 13. In these runs, the pre-run bed was filled with sediment input material and leveled to the elevation of the inlet and outlet sills. Plots of the hydrographs for these experiments (Figure 6-5) show little difference for discharges above 1500 cm^3/sec. Inlet

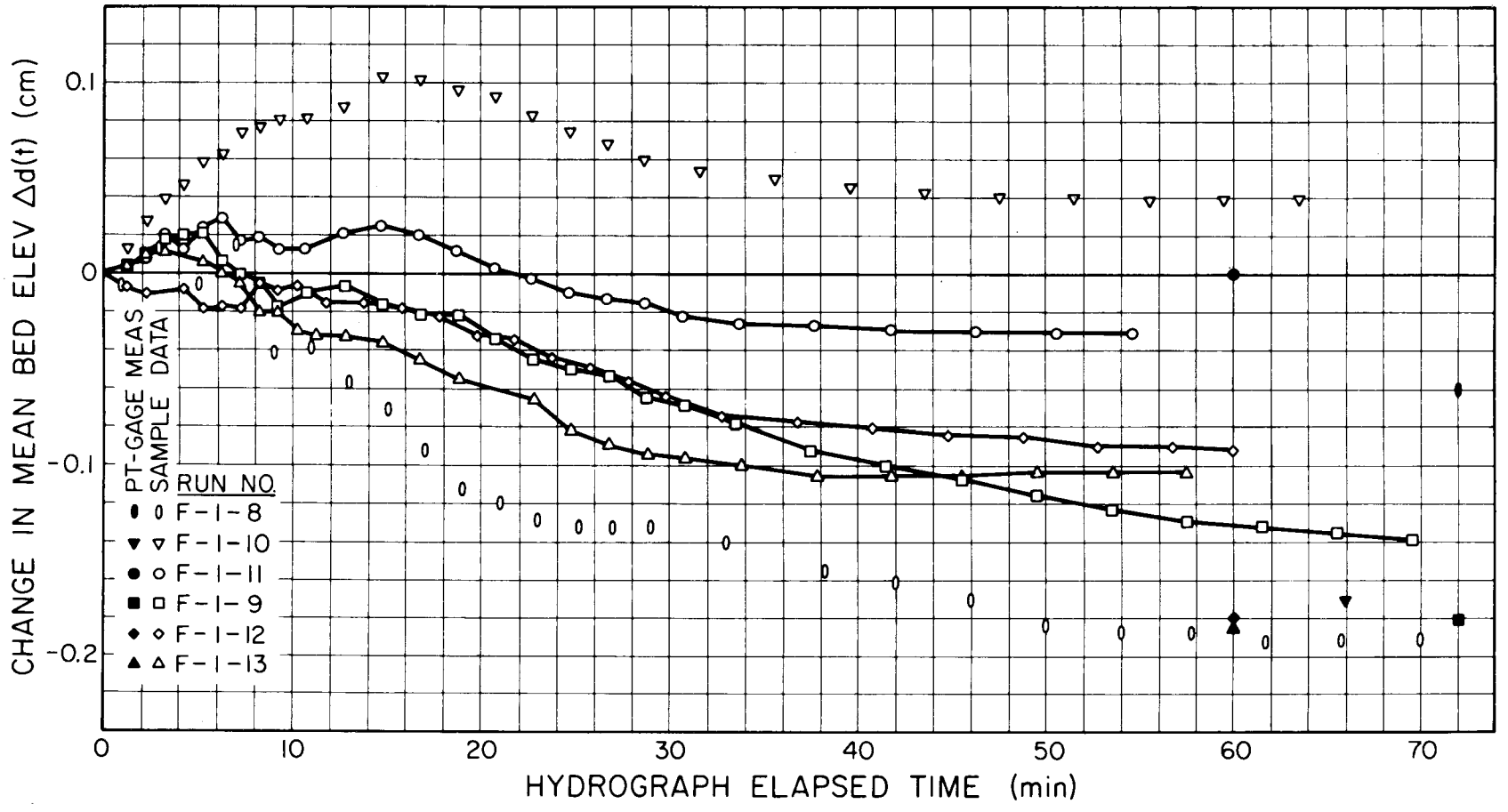

Figure 6-7. Calculated changes in mean bed elevation during simulated floods.

control valve actuator friction became important at discharges below 1500 cm^3/sec, resulting in the low-discharge divergence of the actual hydrographs. Sediment input curves for these three simulated floods were the same except for a short plateau in run F-1-9 (Figure 6-6) caused by a jammed control pushrod.

Final bed condition results are tabulated in Table 6-9, including data for run F-1-11. For runs F-1-9, 12, 13, the .005 cm difference

TABLE 6-9. SIMULATED FLOOD EXPERIMENTAL REPRODUCIBILITY

Run	F-1-9	F-1-12	F-1-13	F-1-11
Measured change in mean bed elevation (cm) (limit of resolution is .005 cm)	$-.18_0$	$-.18_0$	$-.18_5$	0.00_0
Calculated change in mean bed elevation (cm)	-.139	-.092	-.102	-.031
Final bed slope relative to flume	+.00030	+.00023	+.00032	+.00020
Difference between measured mean bed elevation change and change calculated from sediment discharge data (cm)	-.041	-.088	-.083	+.031
(% of calc. change)	29	96	81	-100

between measured mean bed elevation changes is within the limit of resolution of point gage measurements. Differences between final bed slopes relative to the flume are within equilibrium criteria. Only the calculated mean bed elevation changes show significant variability, with final errors up to 100 percent and differences during the floods up to a factor of 2 (Figure 6-7). Because the directly measured results of runs F-1-9, 12, 13 are nearly identical, the variability of calculated mean bed elevation change between those experiments can be used as an

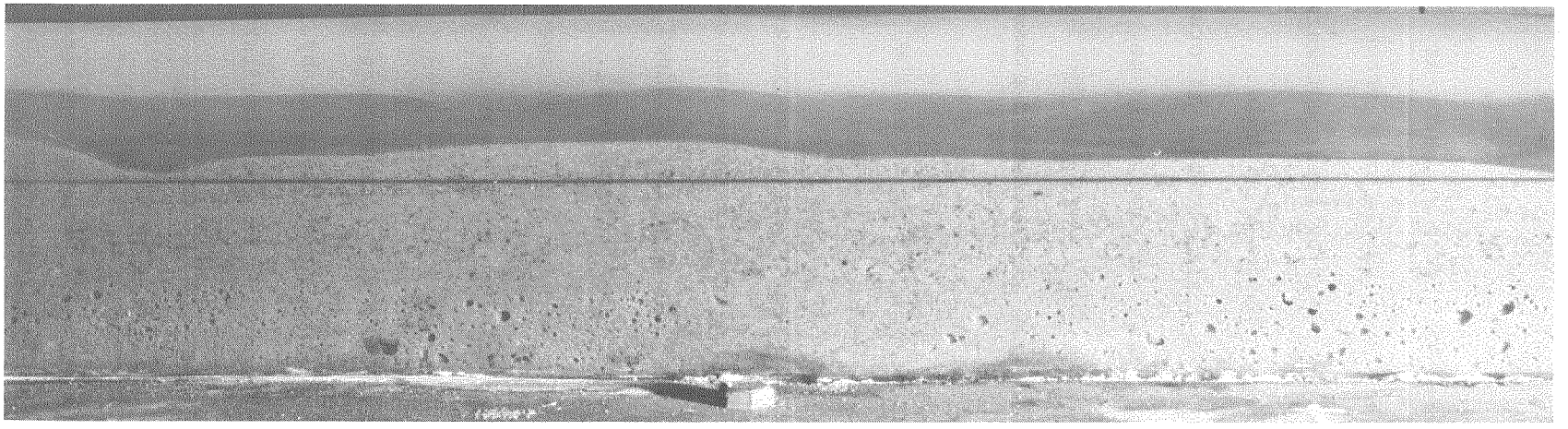

(a) Antidune crossbeds, water surface not shown, sand layer about 6 cm thick.

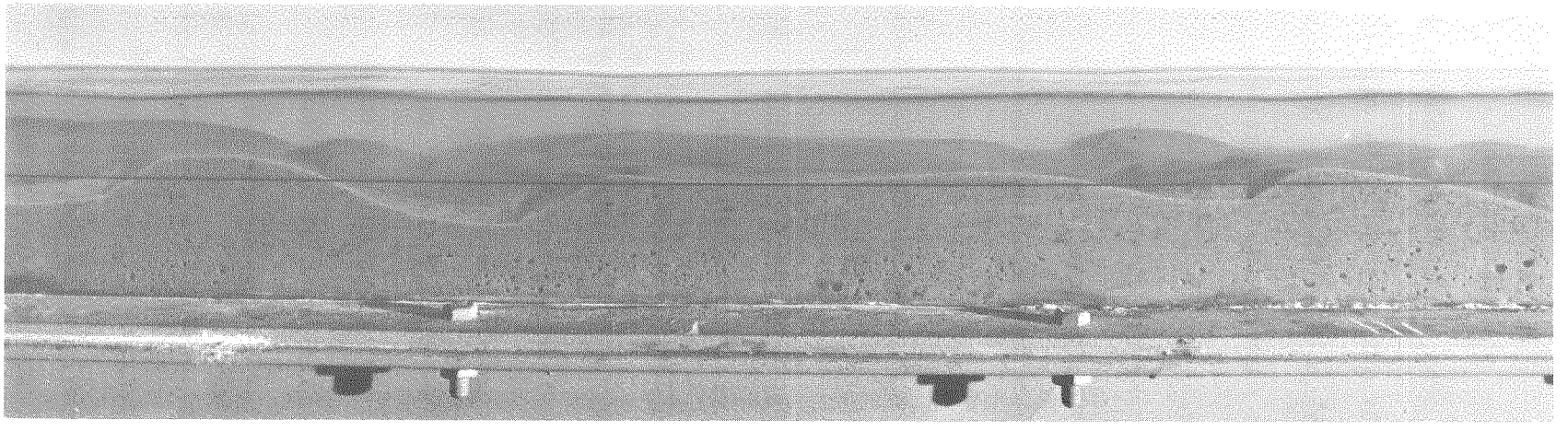

(b) Ripple crossbeds, sand layer about 6 cm thick.

Figure 6-8. Sedimentary structures produced by bedforms in flume (flow from right to left).

indication of probable variability for the stable run F-1-11. The calculated mean bed elevation change of run F-1-11 may be in error at any point by a factor of 2, in addition to the known 100 percent error in the final result. However, the maximum error given by these estimates is only one sand grain diameter for run F-1-11. The cause of this variability is probably the use of $\Delta G_s(t)$ in calculating $\Delta d(t)$. Errors in $G_s(t)$ make the final result less accurate than that that could be obtained by subtracting the total amount of sand transported, as measured at the outlet, from the input amount. However, the latter method gives no more insight into the chronology of scour and fill than would be obtained from measurement of mean bed elevation by leveling after the run.

Bed reworking and sedimentary structures. Development of sedimentary structures during simulated floods was easily seen in cross-section against the flume windows. Antidune migration produced poorly-defined lens-shaped crossbeds dipping upstream and downstream (Figure 6-8a). Downstream migrating antidunes modified only the uppermost part of the antidune crossbeds, because bedform amplitudes in this regime were small. Ripple cross-beds, usually of the small-scale trough cross-lamination type, destroyed all previous cross-laminations because of their large amplitude. The depth of bed reworking by ripples was made evident by coarse grain-size segregation on ripple slipfaces, and by the elimination of air bubbles trapped in the artificially emplaced bed sand (Figure 6-8b). In cross-sections as seen through the flume window, the top of the bubbles clearly marks the limit of bed reworking by migrating ripples.

Channel armoring. In runs F-1-9, 10, 11, the sand bed was leveled between each experiment, but no new material was added. Mean bed elevation decreased 0.18 cm in F-1-9, 0.17 cm in F-1-10, and was stable for F-1-11. As has been discussed above, bed elevation decreases of 0.18 cm were experienced in runs F-1-12, 13 where new bed material was added each time to duplicate F-1-9 initial conditions. These bed elevation changes may reflect at least two influences. First, armoring occurs as fine material is selectively removed progressively increasing the residual mean grain size and the resistance to transport, until a stable bed was achieved by the third consecutive run. Second, inlet and outlet disturbances may produce a bed at grade 3.5 mm lower than the inlet and outlet sills.

The armoring hypothesis is not supported by sediment size data for runs F-1-9 through F-1-13 (Table 6-10). Although there is considerable scatter, the general trend is for the bed material to be slightly finer than input material and the transported material to be slightly coarser. Kennedy (1961, p.110) found that transported material was slightly coarser than bed material for antidune flow with 0.549 mm sand, and slightly finer with .233 mm sand. These data suggest the possibility that a change from load-finer to load-coarser could occur at a sand size between .233 mm and .28 mm, which is consistent with size analyses for the early phase of run F-1-9. However, in a ripple regime transported material is usually finer than bed material (e.g., Hwang, 1965, p.90-91). The armoring hypothesis would thus be consistent with bed evolution under a ripple regime. Even if the coarse fraction were segregated at the

TABLE 6-10. SIMULATED FLOOD SEDIMENT ANALYSES

Run	Input Sand d_g mm	Input Sand σ_g	Transported Sand d_g mm	Transported Sand σ_g	Bed Sand After Run d_g mm	Bed Sand After Run σ_g	Comment
F-1-9	.291	1.44	.338	1.331			1.0 - 5.5 minutes into hydrograph
			.259	1.53			6.0 - 9.5 minutes
			.313	1.40			10.0 - 31.5 minutes
			.278	1.37			32.0 - 72.0 minutes
					.270	1.38	Bed surface (upper 1 cm)
					.248	1.41	Upper 3 cm of bed
F-1-10	.291	1.44	.296	1.44			1.0 - 15.5 minutes
			.289	1.41			16.0 - 66.0 minutes
					.294	1.35	Bed surface (upper 1 cm)
F-1-11	.291	1.44	.298	1.42	---	---	
F-1-12	.291	1.44	.294	1.43	.269	1.35	Bed surface (upper 1 cm)
F-1-13	.291	1.44	.299	1.41	.285	1.33	Bed surface (upper 1 cm)

bottom of the ripple-worked layer, as in Hooke's (1968) granule-armor experiments, it would have been reflected in the deep bed sample taken after run F-1-9.

The fact that transported material is slightly coarser than bed material suggests most bed grain-size evolution was caused by antidune reworking. This hypothesis is contradicted by the observation that the major part of bed reworking was by ripples, which would have resulted in relatively coarser bed material if armoring had been important. Since an armor layer or a progressive increase in bed mean grain size from run F-1-9 and F-1-11 is not detected, bed stability at 3.5 mm below the sills must be due to inlet and outlet flow disturbances, accompanied by possible minor selective removal of coarse material from the bed. This latter apparent effect could also be caused by preferential collection of coarser grains by the sediment sampler.

Experiments with Alluvial-Bank Channels

Behavior of the hydrograph used in rigid-wall experiments was investigated in a series of experiments in a channel with erodible banks. The false wall was removed, and a channel excavated down the center of the flume in the bed material used in rigid-wall experiments. At a water depth of 4 cm, this channel had the same cross-sectional area as the rigid-wall experiments at the same depth. Initial side-wall stability required that the banks have a slope no greater than a 1:2. The initial channel was thus trapezoidal 4 cm deep, with widths of 18.7 cm at the bottom and 34.7 cm at the top. Mean bed elevation change could not be calculated for alluvial bank experiments because of the variable

effects of bank erodibility. In rigid-wall experiments differences between input and output sediment discharges were reflected in the amount of sand in the bed. When the alluvial banks suffered erosion or deposition and when the channel became braided or meandering, sediment discharge measurements at the outlet reflected combined bed and bank erosion or deposition and sediment concentration measurements were not suitable for determining mean bed elevation.

Nonetheless, the qualitative behavior of simulated floods in an unconfined channel has some use. Field techniques can be scaled to a laboratory stream. For example, scour-chain data taken concurrently with width, depth, and stationary wave measurements allow a comparison of scour and fill with bedform parameters. This procedure permits direct comparison between measured and predicted flow parameters, derived from equations 4-1 through 4-6.

Channel morphology development. Bed and bank material for these experiments has about 0.2 percent silt-clay. Extrapolating Schumm's (1961) data (Figure 3-3), a stable channel in such sediment should have a width-depth ratio of 1450. Assuming that the flow Froude number is unity at maximum discharge, stable channel width at a maximum discharge of 7500 cm^3/sec should be about seven meters, with a flow depth of .5 cm. At this shallow depth, it is unlikely that the Froude number would be as high as unity, so stable channel width is probably several meters. Since the flume width is only 85 cm, the fully developed channel cannot be accomodated.

During a simulated flood, bank erosion and channel filling occur

in three separate phases. If the initial channel is trapezoidal, initial flow is approximately the same as in the rigid-wall experiments. The channel runs bank-full with actively breaking stationary waves. Sediment transport is greatest near actively eroding banks, and least in the deep central part of the trapezoidal channel where rapid deposition occurs. Bank erosion is initially by traction, impingement, and sapping, with impingement and sapping during overbank flow being the predominant causes of bank erosion in early stages of the flood. This occurs owing to sudden flow resistance created by a train of large breaking stationary waves in the center of the channel which diverts flow laterally against and over the banks. This produces local embayments in both banks, which eventually coalesce with other embayments of similar origin farther upstream or downstream. As flow decreases on the waning flood, amplitudes of breaking stationary waves diminish, and lateral and overbank flows decrease.

A second phase of active bank sapping begins on the waning flood as channel bores develop. These quasiperiodic bores (to be discussed in more detail in Appendix 2) with amplitudes up to 1 cm are poorly understood but seem to be caused by the release of water "stored" by trains of the low amplitude, downstream-migrating stationary waves. If the stationary waves begin breaking at the downstream end of a train, each breaking wave appears to release a small part of the flow. This produces a small downstream wave and also causes the next wave upstream to break. As a result the train of stationary waves "unravels" upstream, producing a series of small waves traveling downstream. However,

if the stationary wave at the upstream end of a train breaks first, the disturbance causes the next wave downstream to break, and so on. The small downstream-traveling wave released by the first stationary wave joins those released by the second and subsequent breaking waves downstream, finally resulting in a bore to about 1 cm in amplitude. This bore rushes downstream, overflowing and sapping the banks all along the channel. This second phase of bank sapping and channel widening tends to straighten the scalloped banks produced by the first phase. Figure 6-9 shows a typical channel bore during an alluvial-channel flood.

As the discharge decreases further, true bed ripples begin to develop, and the channel begins to meander near the flume outlet. Flow diversions caused by these meanders quickly erode the banks on the outsides of the curves until the flume walls are exposed. Flow disturbances are propagated upstream inducing meandering progressively in that direction and stopping only when the flood ends. A second flood run in the wide, rough channel produced by the first flood starts at a flow velocity much lower than the initial velocity of the first flood, causing immediate overbank flow and rapid bank sapping. Little, if any, bank is left to be attacked by the second and third phases of bank erosion. To counterbalance this, flume slope was set at .015 in an effort to increase low-discharge velocities and slow the development of meanders.

Several simulated floods were run at a maximum discharge of 3750 cm^3/sec with characteristics and sediment input conditions as shown in Figure 6-10. With this reduced flow, three floods could be run in succession before bank erosion and meander development required channel

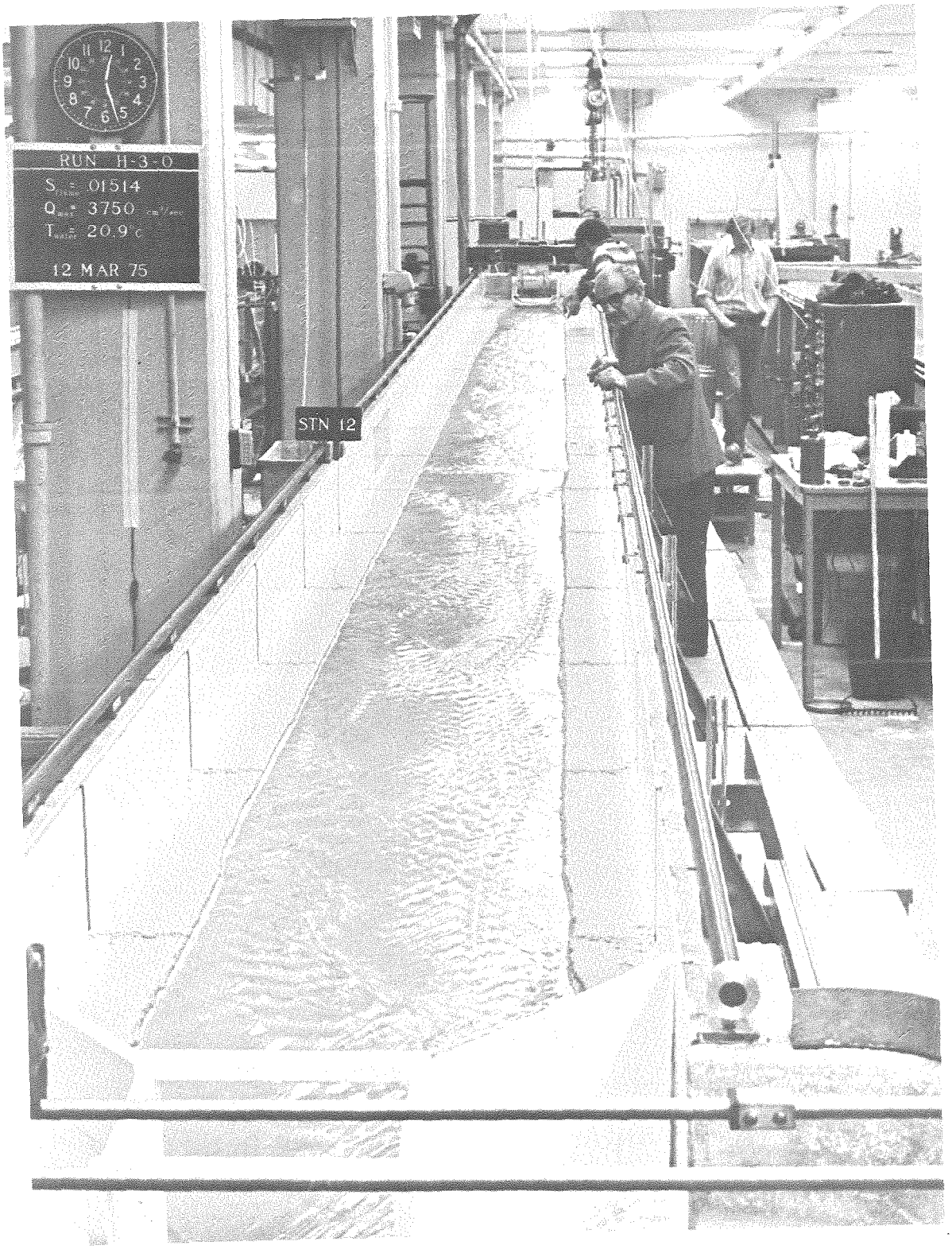

Figure 6-9. Typical channel bore in alluvial-bank experiment.

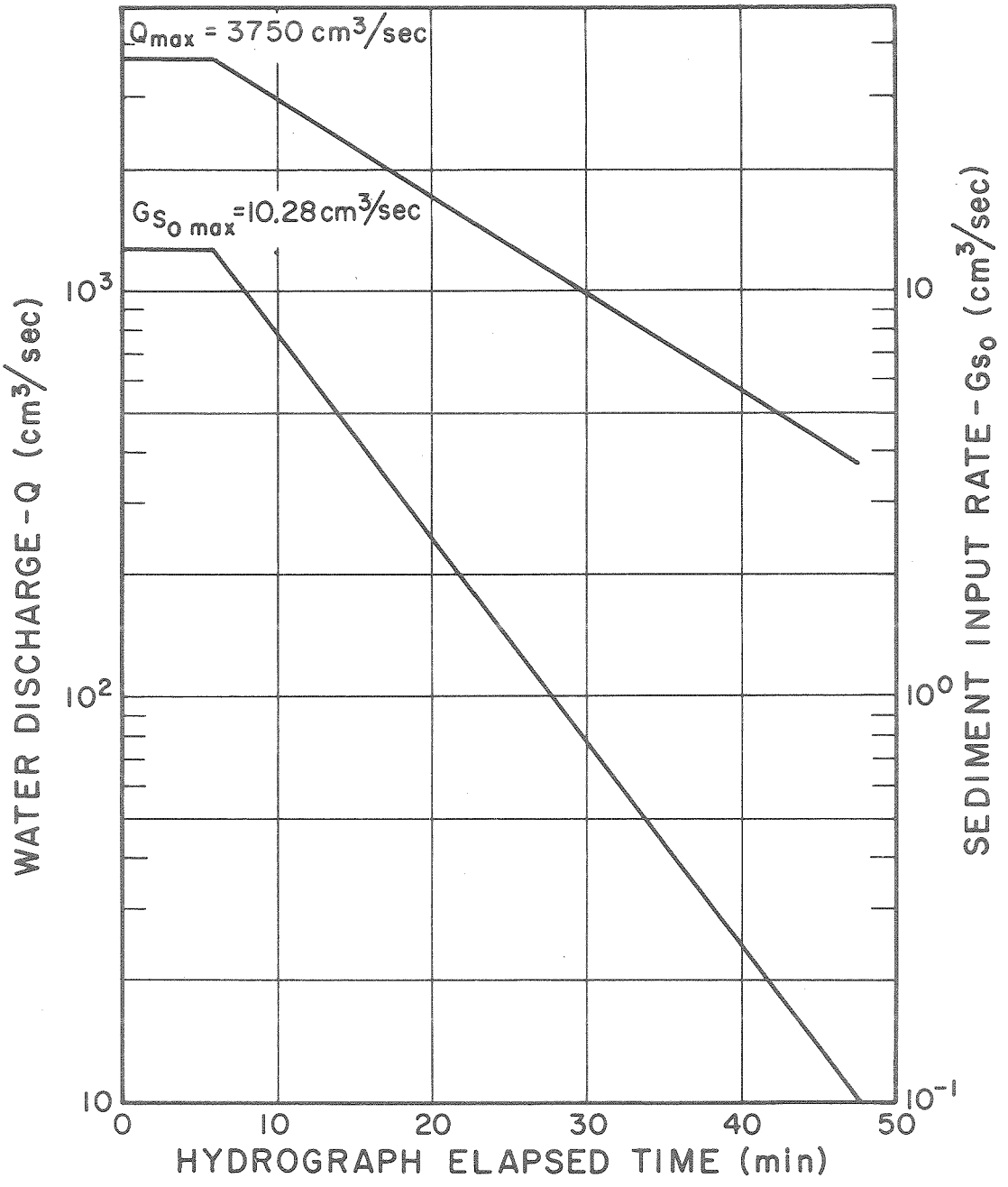

Figure 6-10. Water discharge and sediment-input rate relations for alluvial-bank experiments.

reconstruction. Figure 6-11 shows channel morphological development during the first run of such a series, and Figure 6-12 is a planimetric map of the channel resulting from this run. This channel was used for scour-chain experiments.

Model scour-chain experiments. The experiment series I-2-1, 2, 3 measured bed reworking by means of small scour-chains along with discharge, stationary wave wavelengths, water depth and surface slope, channel width, and initial and final mean bed elevations. Bed reworking in these experiments was compared to bed form amplitude, and flow conditions were compared to those predicted from equations 4-1 through 4-6. Experiment I-2-1, run at a slope of .015 with input parameters as shown in Figure 6-10, produced the channel shown in Figure 6-12. Six model scour-chains (Figure 6-13) were buried in the bed at 5-cm intervals in a line across the channel (Figure 6-12). Experiments I-2-2 and I-2-3 were run, with bed and maximum-scour elevations measured at each scour chain location. Before-and-after mean bed elevations were measured at the scour-chain line and the transducer stations immediately upstream and downstream. General flow data from these two experiments are summarized in Table 6-11. Both runs were stopped before ripple formation began, so all bed reworking was by antidunes.

Maximum scour from initial bed elevation was 1.16 ± .1 cm in run I-2-2 and 0.64 ± .1 cm in I-2-3. Scour-chain exposure occurred only in the troughs of antidunes. Figure 6-14 shows bed reworking inferred from scour-chain measurements and maximum water depths for these experiments. Maximum scour is taken from initial bed elevation rather

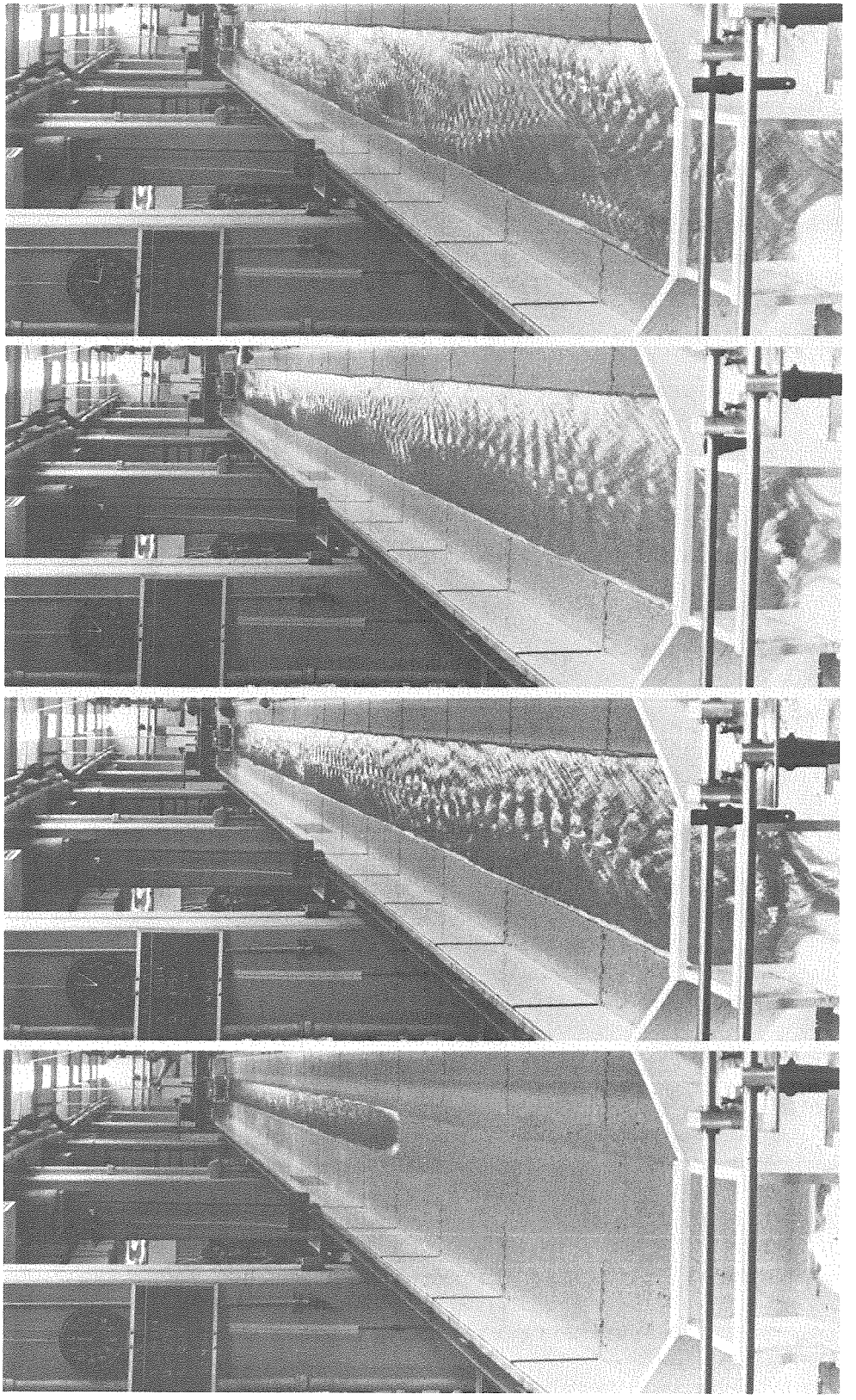

(a) (b) (c) (d)

Figure 6-11. Channel morphological development during a simulated flood.

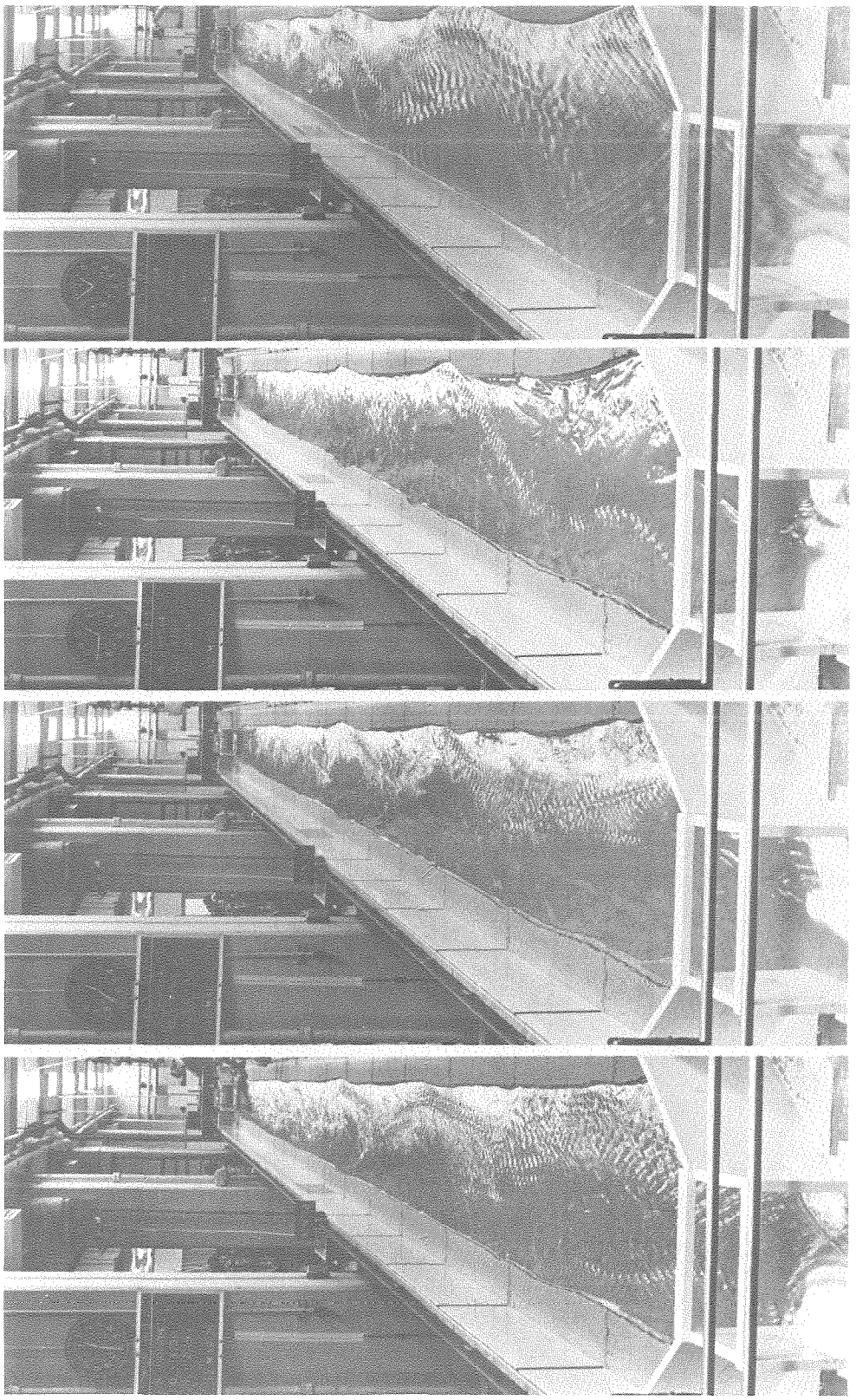

(e) (f) (g) (h)

Figure 6-11, continued. Channel morphological development during a simulated flood.

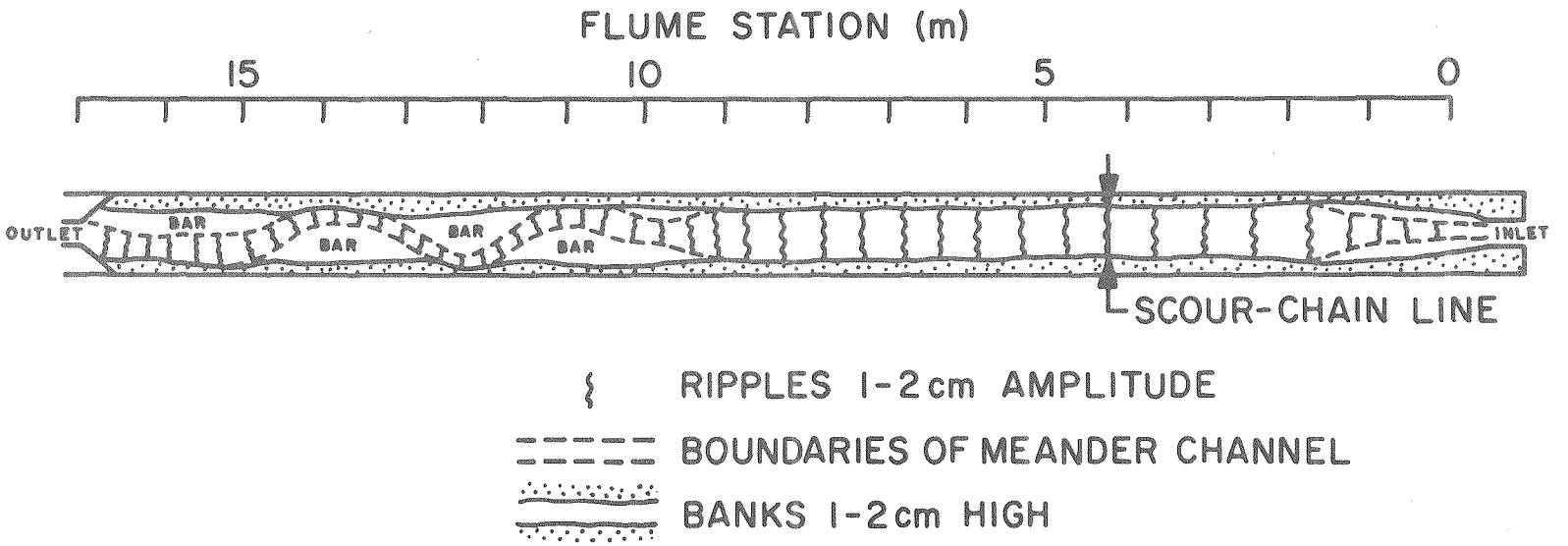

Figure 6-12. Initial channel configuration for scour-chain experiments.

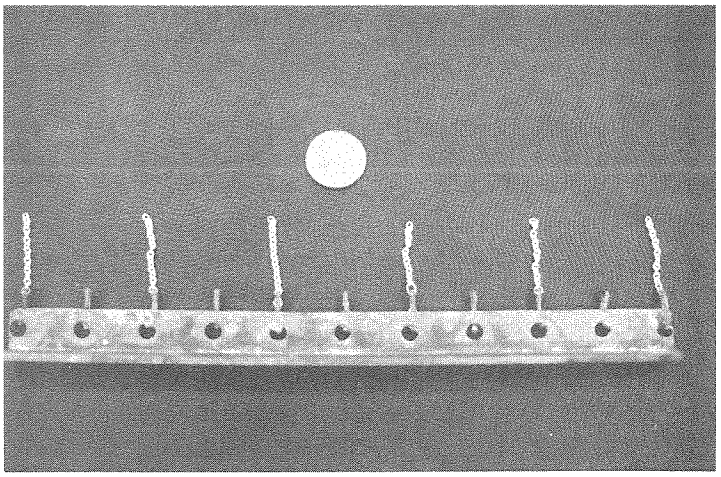

(a) Scour-chains attached to 2.5x2.5x0.3 cm brass angle.

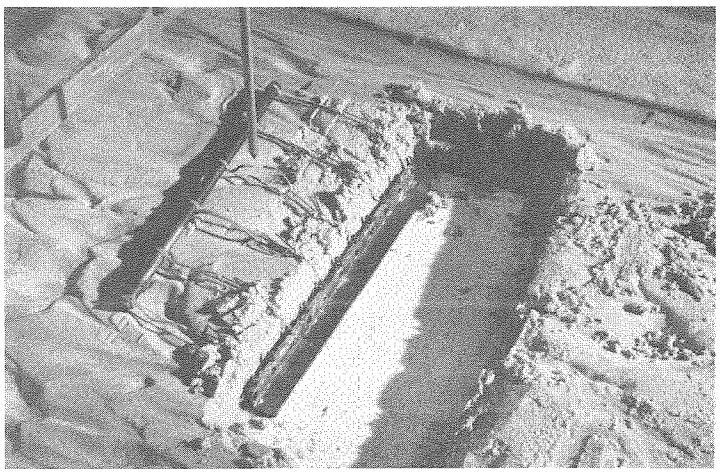

(b) Installation in flume showing pre-burial support hooks.

(c) Installed scour-chains with excess length turned upstream.

Figure 6-13. Scour-chains used in model experiments.

TABLE 6-11. SCOUR-CHAIN EXPERIMENT DATA SUMMARY

t	d	b	Q	V	F	L	B	V_L	r	f	f_L	ϵ_s/d	R_e	R_{e_L}	f_b'	f_{b_L}'	f/f_b'	f_L/f_{b_L}'
Elapsed Time	Water Depth	Channel Width	Discharge	Mean Velocity $\frac{Q}{bd}$	Froude Number $\frac{V}{\sqrt{gd}}$	Stationary Wave Wavelength	Stationary Wave Transverse Wavelength	Stationary Wave Velocity $\left(\frac{gL}{2\pi}\right)^{1/2}\left[1+\left(\frac{L}{B}\right)^2\right]^{1/4}$	Hydraulic Radius	Overall Friction Factor $\frac{8grS}{V^2}$	Antidune Friction Factor $\frac{8grS}{V_L^2}$	Equivalent Pipe Friction Relative Roughness $\frac{d}{4r}$	Equivalent Overall Pipe Friction Reynolds Number $\frac{4rV}{\nu}$	Equivalent Antidune Pipe Friction Reynolds Number $\frac{4rV_L}{\nu}$	Overall Bed Roughness Friction Factor	Antidune Bed Roughness Friction Factor	Overall Friction Factor Ratio	Antidune Friction Factor Ratio
min	cm	cm	cm^3/sec	cm/sec		cm	cm	cm/sec	cm									
RUN I-2-2 S = .01356; T = 21°C																		
3.32	1.44	58.5	3440	40.84	1.09	16	~16	59.42	1.37	.0874	.0413	.0051	2.28×10^4	3.32×10^4	.0340	.0331	2.57	1.25
4.00	1.47	59.5	3440	39.33	1.04	--	--	--	1.40	.0963	--	.0050	2.25	--	.0340	--	2.83	--
5.32	1.43	60.2	3440	39.96	1.07	15	~15	57.53	1.37	.0913	.0440	.0051	2.23	3.22	.0341	.0332	2.68	1.33
5.83	1.44	60.5	3440	39.49	1.05	--	--	--	1.37	.0935	--	.0051	2.21	--	.0341	--	2.74	--
6.77	1.44	60.8	3420	39.06	1.04	15	~15	57.53	1.37	.0955	.0440	.0051	2.18	3.22	.0342	.0333	2.79	1.32
7.32	1.41_5	61.0	3310	38.35	1.03	--	--	--	1.35	.0977	--	.0052	2.11	--	.0343	--	2.85	--
8.40	1.40	61.3	3100	36.12	.97	13	~13	53.56	1.34	.1093	.0497	.0052	1.98	2.93	.0345	.0334	3.17	1.49
8.88	1.38	61.5	3010	35.47	.96	--	--	--	1.32	.1116	--	.0053	1.91	--	.0348	--	3.21	--
10.30	1.28	61.5	2755	35.00	.99	11	~11	49.27	1.23	.1068	.0539	.0057	1.76	2.47	.0353	.0343	3.03	1.57
10.92	1.24	61.5	2660	34.88	1.00	--	--	--	1.19	.1041	--	.0059	1.69	--	.0360	--	2.89	--
RUN I-2-3 S = .01368; T = 21°C																		
2.70	1.32	66.0	3410	39.14	1.09	12	~12	51.47	1.27	.0890	.0515	.0055	2.03×10^4	2.67×10^4	.0350	.0340	2.54	1.51
3.32	1.29	67.0	3410	39.45	1.11	--	--	--	1.24	.0855	--	.0056	2.00	--	.0353	--	2.42	--
3.90	1.28	67.0	3410	39.76	1.12	12	~12	51.47	1.23	.0835	.0498	.0057	2.00	2.58	.0353	.0342	2.37	1.46
4.53	1.27	67.0	3410	40.08	1.14	--	--	--	1.22	.0815	--	.0057	2.00	--	.0353	--	2.31	--
5.25	1.25_5	67.5	3410	40.25	1.15	12	~12	51.47	1.21	.0802	.0490	.0058	1.99	2.54	.0355	.0345	2.26	1.42
5.83	1.24	68.0	3410	40.44	1.16	--	--	--	1.20	.0788	--	.0058	1.98	--	.0355	--	2.22	--
6.67	1.23	68.3	3400	40.47	1.17	10	~10	46.99	1.19	.0780	.0578	.0059	1.97	2.28	.0356	.0350	2.19	1.65
7.17	1.20	68.5	3290	40.02	1.17	--	--	--	1.16	.0777	--	.0060	1.89	--	.0358	--	2.17	--

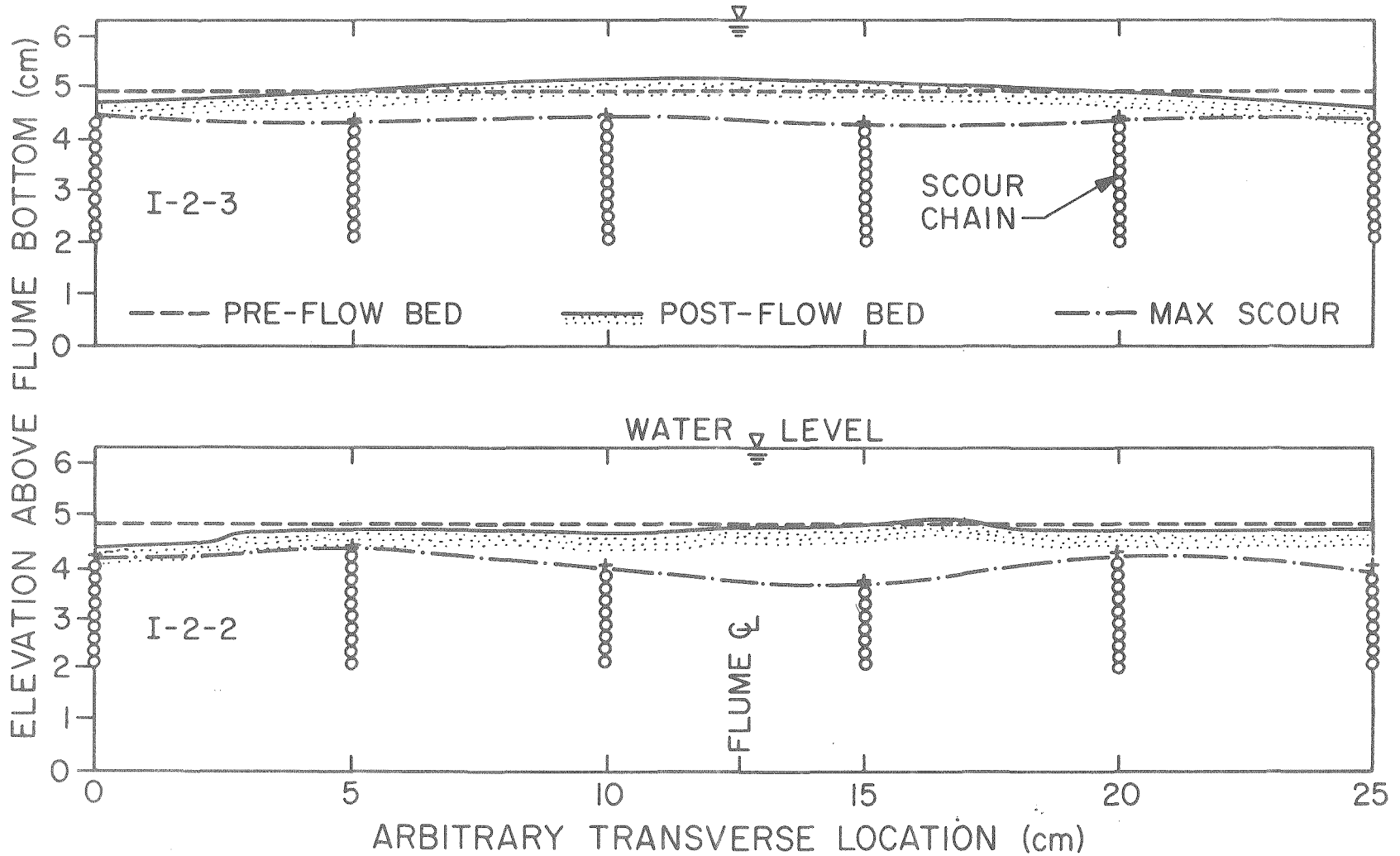

Figure 6-14. Results of model scour-chain experiments.

than final elevation because stationary wave wavelengths, hence antidune amplitudes, were greatest near the beginning of each flood.

Data in Table 6-11 indicate that stationary wave velocities, calculated using equation 4-4, are as much as 48 percent higher than mean cross-section velocities, suggesting that the stationary wave trains measured were formed in subchannels of above-average velocity within the body of the flow. Two experiments were conducted with styrofoam floats to test for possible differences in surface-velocity. Figure 6-15a is a view of the styrofoam floats just after dropping from a transverse hopper. Flow is from left to right, and the scales at the top and bottom of the photo are in cm. The bottom scale is the flume station scale, and the mark "M4", near lower left center is station 4.000 m. Figure 6-15b shows a line of floats approximately one second after drop. In this instance maximum float displacement from initial drop point is 26.5 percent greater than minimum displacement. Repeated float experiments show that floats are poor indicators of surface velocity for a flow with stationary waves. The stationary waves can seriously impede progress of a float running down the axis of the train if the waves are near their breaking height, and in a flow with stationary waves the floats do not hit the water so an initially straight transverse arrangement can be established.

Figure 6-15b shows several lines of stationary waves, with wavelengths varying from 4.75 cm to 11.25 cm. Stationary wave velocities calculated from these wavelengths (equation 4-4) are 30.63 cm/sec and 49.83 cm/sec, a difference of 53.9 percent. This difference is great

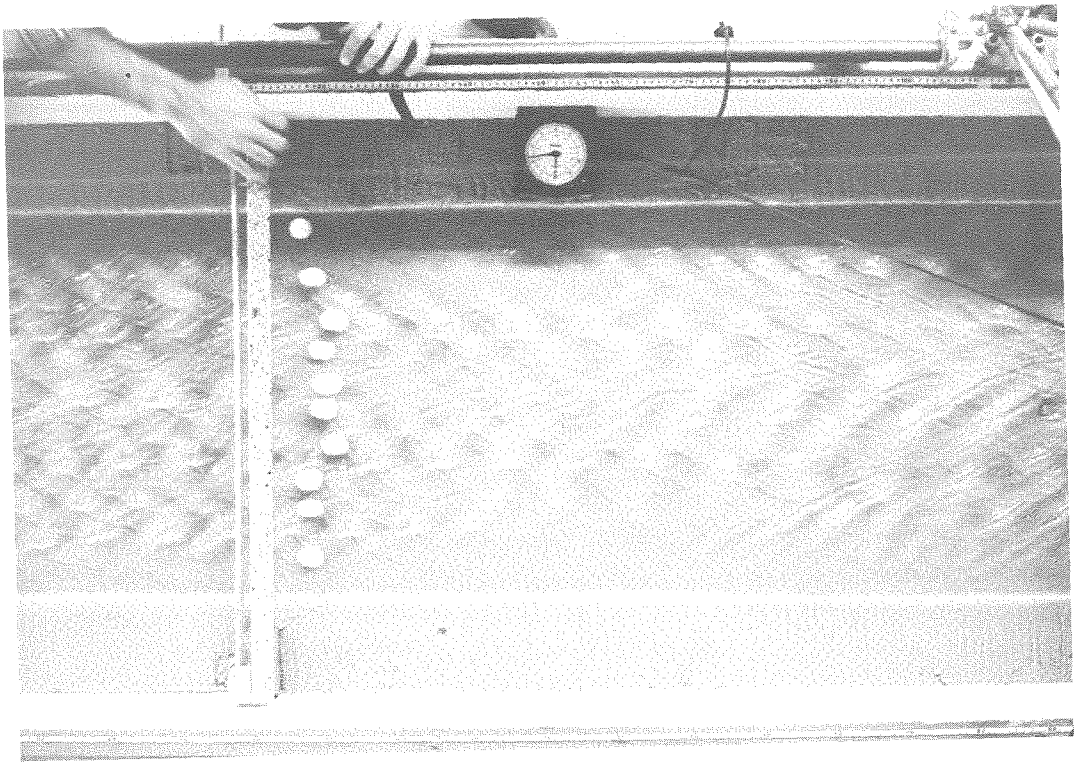

(a) Floats dropped across width of channel.

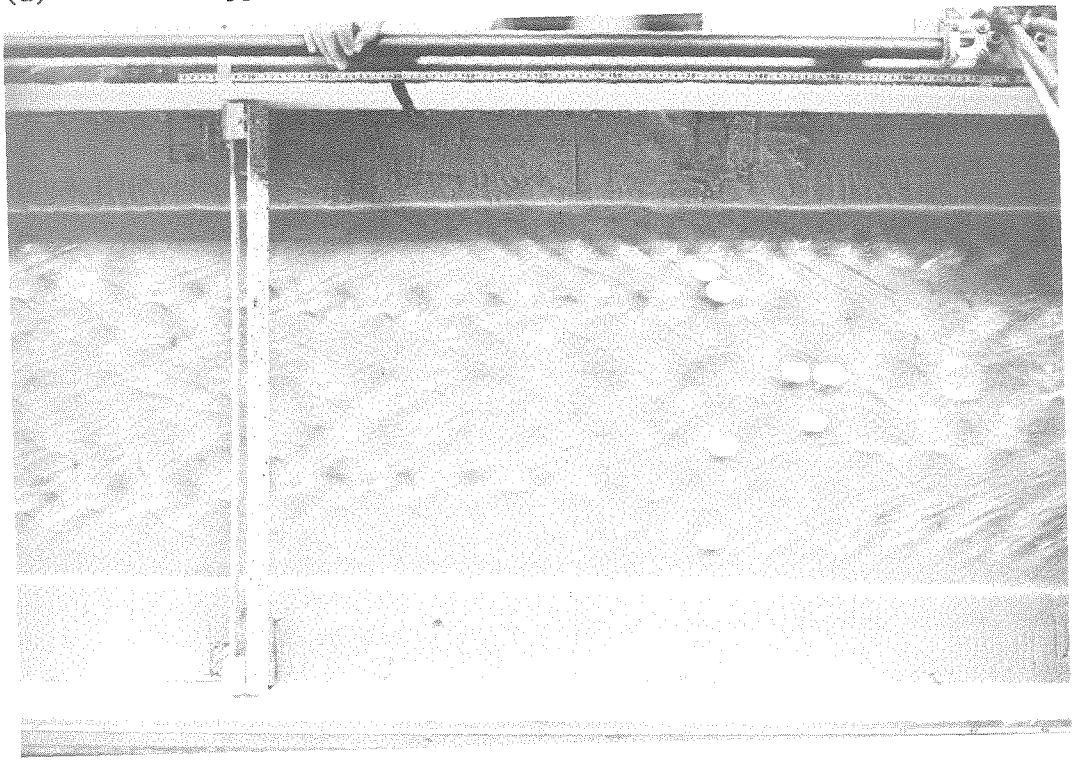

(b) Floats approximately 1 sec. after drop.

Figure 6-15. Transverse velocity distribution experiments.

enough to account for the velocity variations seen in runs I-2-2 and I-2-3 provided the high velocity zone is confined to a small part of the flow. For run I-2-2, the higher-velocity zone was near the center of the channel and maximum scour (Figure 6-14) for I-2-2 is greatest near the center of the flume, reflecting the larger amplitude of stationary waves forming in the faster flow. As banks erode, channel width increases and the higher-velocity zone broadens, lessening the difference between maximum stationary wave velocity and mean velocity. The more uniform maximum scour for run I-2-3 (Figure 6-14) shows this effect.

Observations of model scour-chain behavior. During model scour-chain experiments, water in the flume was clear enough to allow direct observation of exposed scour-chains. Scour-chains exposed in antidune troughs invariably fell straight downstream, and were straight when buried (Figure 6-16a). This behavior was a result of bottom currents oriented uniformly downstream in the antidune flow regime, and relatively rapid burial of the scour-chains after exposure. Flow disturbances caused by breaking stationary waves did not seem to affect scour-chain alignment.

During flow in the ripple regime, scour-chains were exposed in ripple troughs. Secondary flows near the bottoms of these troughs are strong, and oriented transverse or even counter to the general flow. Scour-chains exposed and reburied in these troughs rarely pointed downstream, and were usually contorted because of shifting of currents during the relatively slow burial (Figure 6-16b). These observations

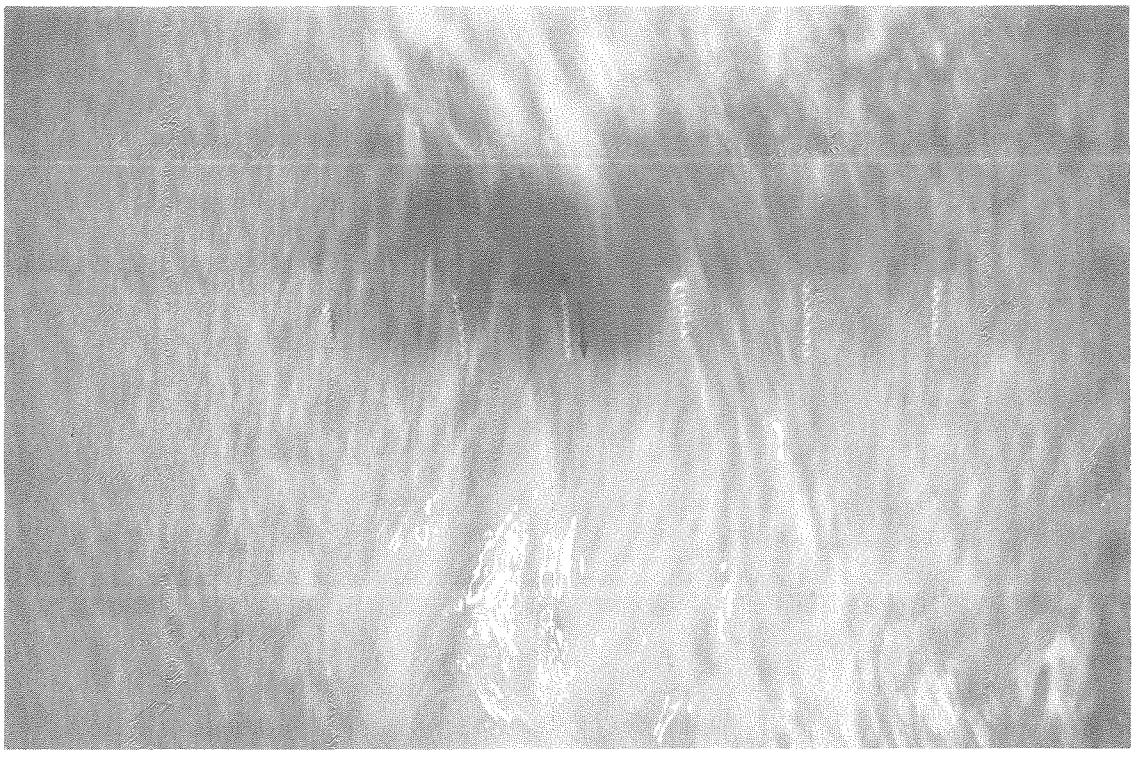

(a) Antidune-regime flow, arrow shows orientation of scour-chains.

(b) Ripple-regime flow, arrow shows orientation of scour-chain.

Figure 6-16. Scour-chain behavior during antidune- and ripple-regime flow (flow from top to bottom).

suggest that a recovered scour-chain lying fairly straight downstream probably reflects upper-regime flow. A chain that is contorted and inclined upstream or transverse to the stream, rarely downstream, reflects a dune-covered bed at the time maximum bed-reworking occurred.

CHAPTER 7. DISCUSSION OF LABORATORY RESULTS

Introductory Statement

Statements in previous chapters emphasize that these laboratory experiments have been conducted to investigate a phenomenon and not to model a specific field situation. Interpretation of natural scour and fill and related flow parameters is restricted in quantitative application to conditions and geometry similar to those used in the laboratory. Some hydraulic scale effects have been identified, and this chapter will discuss the applicability of laboratory results to field relationships, with emphasis on the field data analysis presented earlier.

Scour and Fill in a Rigid-Wall Channel

Figure 7-1a is a plot of the deviation of mean-bed elevation from its initial value against time for run F-1-11, the only stable simulated flood. The mean-bed elevation change has been adjusted .031 cm in two ways to match the end result measured by point gage. The open-circle points in Figure 7-1a represent an adjusted curve in which the mean-bed elevation change between each point is reduced by the total change, .031 cm, divided by the number of points. This linear correction assigns the same error to each point and results in a curve with the minimum positive mean-bed elevation change during the run. However, the largest errors in mean-bed elevation change between points should occur during the early phase of the flow when transport rate and transport rate fluctuations are the greatest. The solid-circle points in Figure 7-1a show an adjusted curve in which a body shift of + .031 cm has been made to the initial curve. This adjustment assigns all of the error to the

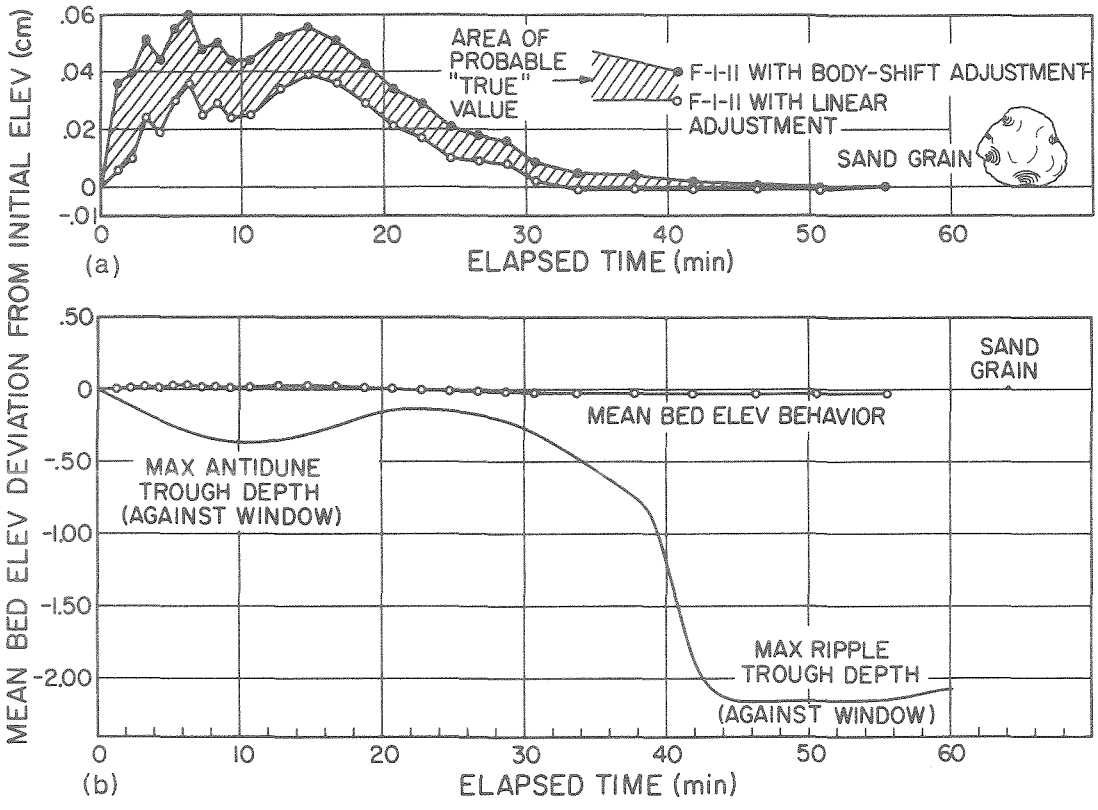

Figure 7-1. Calculated mean bed elevation change during run F-1-11; (a) Adjusted curve, (b) Unadjusted curve with bedform reworking added.

first point and results in a curve with the maximum positive mean-bed elevation change during the run. Spreading the error over the first five or ten points is more realistic and would result in a "true" curve in the hatchured area between the two adjusted curves. A sense of proportion in this magnified vertical-scale plot is provided by a sand grain shown to scale. For this equilibrium run, maximum mean-bed elevation change during the flood is but one to two sand grain diameters of fill followed by scour to the initial mean-bed elevation. By comparison, Figure 7-1b shows unadjusted F-1-11 data plotted on a less exaggerated vertical scale along with minimum depth of bed reworking by bedforms plotted to the same scale. This bed reworking depth was measured as the minimum elevation of the bottoms of bedform troughs seen in cross-section against the flume window. Bedform trough depths in the center of the channel, particularly antidunes, will be considerably greater than the ones measured at the window. Figure 7-1b shows clearly that mean-bed elevation fluctuations are less than 3 percent of bed reworking by bedforms when the worst-case adjusted data are used.

The fill-and-scour style of mean bed elevation behavior must be explained, particularly since it does not agree with the classical scour-and-fill bed-behavior concept. Two probable causes of mean-bed elevation fluctuations, the arbitrary sediment-input relation and unsteady flow effects, can now be treated in light of relevant laboratory data.

Effect of sediment input relation on mean-bed elevation behavior. Steady-state experiments described in Chapter 6 have an effective sediment transport relation of the form $G_s \propto Q^{1.54}$. Figure 6-4 suggests that

there may be at least two curves of this form, with different intercepts, that describe the sediment transport rate as a function of different discharges. Steady-state experiments indicate that flow conditions do not necessarily stabilize on either of the two curves. However, the general behavior of sediment transport rate in steady-state experiments is to vary as the 1.54-power of discharge, with an ill-defined transition between two flow regimes.

Sediment input rate for simulated floods is of the form $G_s \propto Q^2$. With flume slope adjusted to .01064, this sediment input rate will give conditions similar to runs D-1-3, 4 at maximum discharge. Thus, for the first six minutes of the flood there will be approximately equilibrium flow. However, when the exponential decay of the flood begins, the input sediment rate will drop as the square of the discharge while the transport rate drops as roughly the 1.5-power. This difference will result in scour for the remainder of the flood unless the transition to the lower sediment transport rate temporarily decreases transport rate below input rate. For an equilibrium flood, this behavior required that flume slope be lowered to .00876 so that fill takes place in the first six minutes of the flood to balance the scour occurring later. This balancing results in mean-bed fill and scour, but time-dependent hydraulic effects may produce similar results.

Time-dependent hydraulic effects. The depth-velocity curve for run F-1-11 (Figure 7-2) exhibits a transition from upper flow regime to lower flow regime as depth and mean velocity decrease. This discontinuity is of the type first described in the laboratory by Brooks (1958) and in

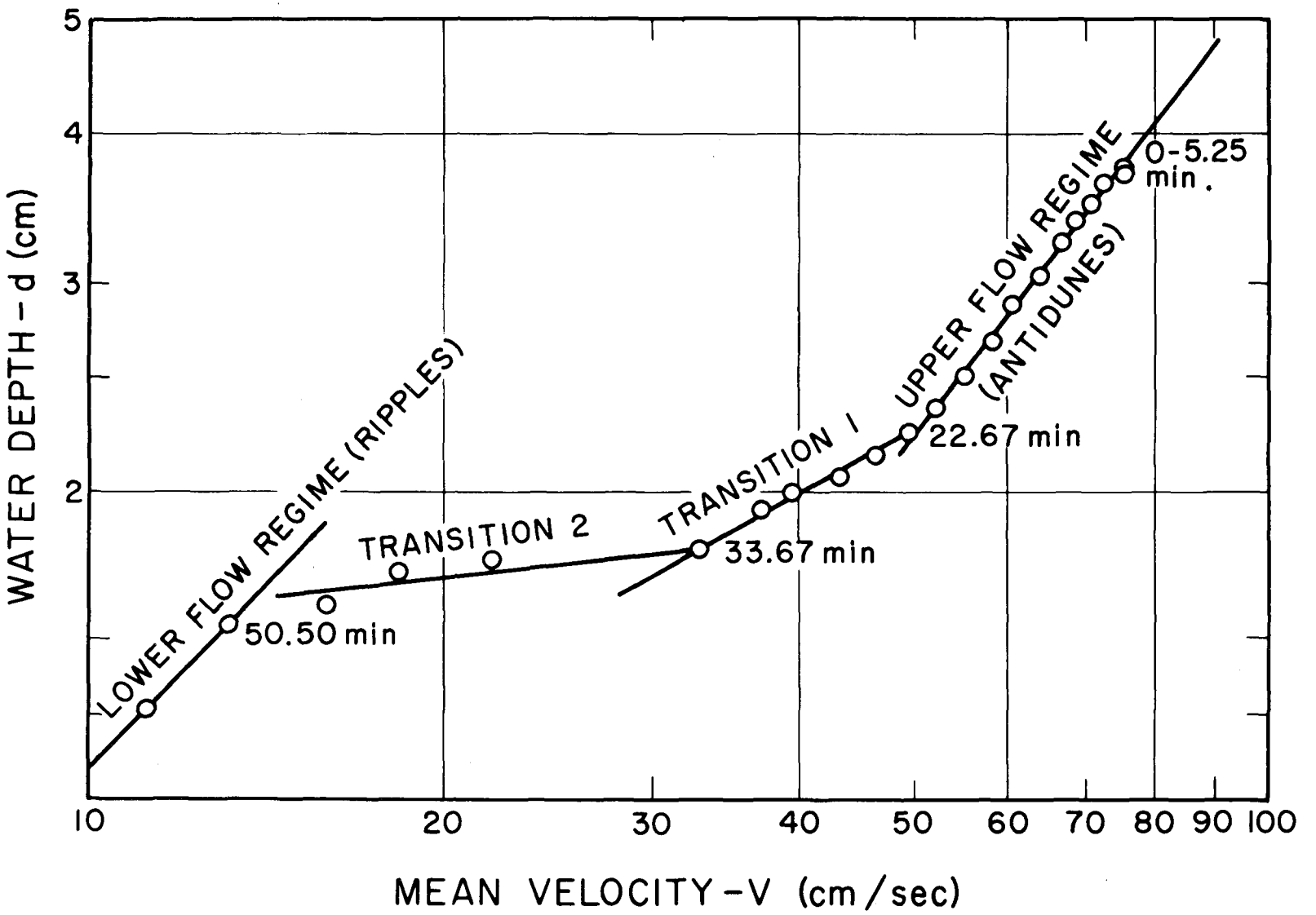

Figure 7-2. Depth-velocity curve for run F-1-11.

the field by Colby (1960). In those instances, transition from flow over antidunes or flat bed to flow over ripples or dunes caused the discontinuity. In the experiments reported here, data suggest that transition is first from normal antidunes to antidunes which migrate downstream, then to ripples. Table 7-1 is an extended data summary for run F-1-11. Figure 7-3 shows plots versus time of data from Table 7-1 for F, f_b, f_b/f_b', and minimum bedform trough depression below initial mean-bed elevation.

In Figure 7-2, break in slope for the F-1-11 depth-velocity curve occurs slightly after 20.67 minutes, and before the next sample point at 22.67 minutes. The bedform trough elevation (Figure 7-3) shows that bedform amplitude reaches a minimum in this same time interval. Less than two minutes later, f_b/f_b' exceeds 2 and signals the end of true antidune flow as defined by Taylor and Brooks (1961). The time difference between break in slope of the depth-velocity curve and f_b/f_b' exceeding 2 is probably not significant, since the slope of f_b/f_b' versus time in this area is so gentle that a very small error in f_b/f_b' produces a time error of several minutes. The region labeled Transition 1 in Figures 7-2 and 7-3 is a flow regime where the bedform is small "antidunes" moving downstream. These bedforms may be more like ripples, but have in-phase stationary waves. Sufficient for the moment is identification of the Transition 1 region as a flow regime with downstream-migrating antidunes.

At 33.67 minutes is a sharp slope break in the F, f_b, f_b/f_b', and bedform trough depth curves (Figure 7-3) which indicates the onset of

TABLE 7-1. EXTENDED DATA SUMMARY FOR RUN F-1-11.

t min	d cm	V cm/sec	Q cm^3/sec	F	r cm	f	f_b	$f_b/f_{b'}$	d/d_g
1.25	3.77	75.09	7550	1.23	2.94	.0358	.0381	1.45	135
2.25	3.77	75.09	7550	1.23	2.94	.0358	.0381	1.45	135
3.25	3.77	75.09	7550	1.23	2.94	.0358	.0381	1.45	135
4.25	3.77	75.09	7550	1.23	2.94	.0358	.0381	1.45	135
5.25	3.77	75.09	7550	1.23	2.94	.0358	.0381	1.45	135
6.25	3.71	75.29	7450	1.25	2.90	.0352	.0373	1.47	133
7.25	3.64	72.62	7050	1.22	2.86	.0373	.0400	1.50	130
8.25	3.50	70.92	6620	1.21	2.77	.0379	.0406	1.51	125
9.25	3.39	68.69	6210	1.19	2.70	.0393	.0423	1.56	121
10.67	3.25	66.68	5780	1.18	2.61	.0404	.0435	1.60	116
12.67	3.05	63.93	5200	1.17	2.48	.0417	.0449	1.60	109
14.67	2.88	60.67	4660	1.14	2.37	.0443	.0479	1.71	103
16.67	2.68	58.06	4150	1.13	2.23	.0455	.0491	1.73	96
18.67	2.51	55.27	3700	1.11	2.11	.0475	.0513	1.77	90
20.67	2.37	52.21	3300	1.08	2.01	.0507	.0548	1.84	85
22.67	2.25	49.49	2970	1.05	1.93	.0542	.0587	1.94	80
24.67	2.15	46.39	2660	1.01	1.85	.0591	.0642	2.14	77
26.67	2.07	43.11	2380	.96	1.79	.0662	.0722	2.27	74
28.67	2.00	39.37	2100	.89	1.74	.0772	.0847	2.65	71
30.67	1.94	37.11	1920	.85	1.69	.0844	.0927	2.88	69
33.67	1.79	32.99	1575	.79	1.58	.0998	.1095	3.27	64
37.67	1.76	21.94	1030	.53	1.55	.2214	.2470	7.48	63
41.75	1.72	18.31	840	.45	1.52	.3117	.3484	9.54	61
46.25	1.61	15.88	682	.40	1.44	.3926	.4367	11.49	57
50.50	1.55	13.18	545	.34	1.39	.5501	.6108	15.66	55
55.50	1.31	11.22	392	.31	1.19	.6498	.7109	16.73	47

$S = .00876$ ($S_{rel} = +.00020$)

$T = 21.4°C$

$d_g = .028$ cm

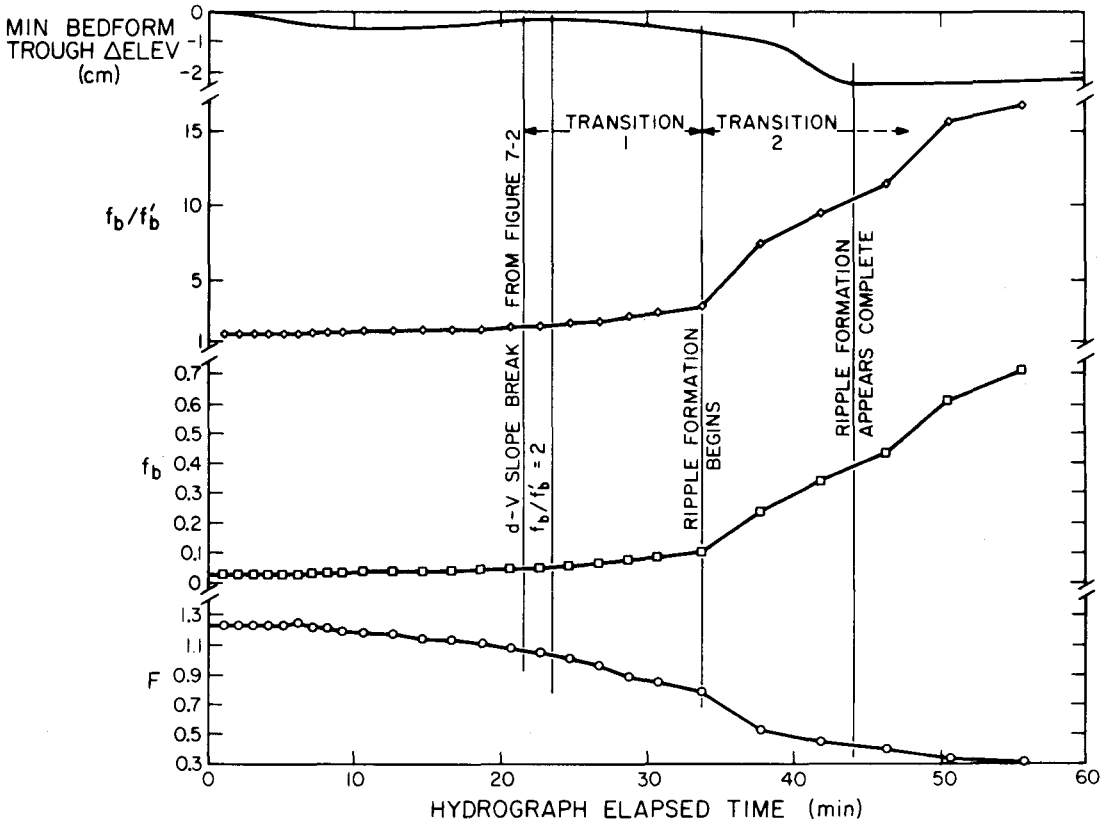

Figure 7-3. Extended data summary plot for run F-1-11.

ripple formation. The region of ripple formation is labeled Transition 2 in Figures 7-2 and 7-3. Ripple formation appears complete by 44 minutes, although Figure 7-2 suggests that it actually continues until 48 minutes. After ripple formation is completed, f_b continues to increase because the depth is decreasing.

The effect of Transitions 1 and 2 on mean-bed fill and scour is that increase in f_b and f_b/f_b' requires a finite amount of time owing to the amount of sediment that has to be moved to increase bed roughness. Thus, whenever a decrease in discharge requires an increase in bed roughness to achieve equilibrium flow conditions, the increase does not occur instantaneously, and a time lag may exist between discharge change and equilibrium flow. The same instantaneous decrease in low discharges should have a longer time lag than at higher discharges because sediment transport rate is lower and more time is required to increase bed roughness. Since discharge is steadily decreasing on the waning flood, the time lag in roughness development should increase through both transition regions, although it eventually should disappear as ripples reach maximum development. This lag between bed roughness required for equilibrium flow and actual bed roughness means that flow velocities and sediment transport rates will be higher than equilibrium values during the transition part of the flood. Water-surface slope relative to the flume (Figure 7-4) supports this interpretation. Comparison between water-surface slope and a linear interpolation between initial and final mean bed slope shows a peak positive relative slope at 25 minutes in Transition 1, and from 40 to 50 minutes in Transition 2.

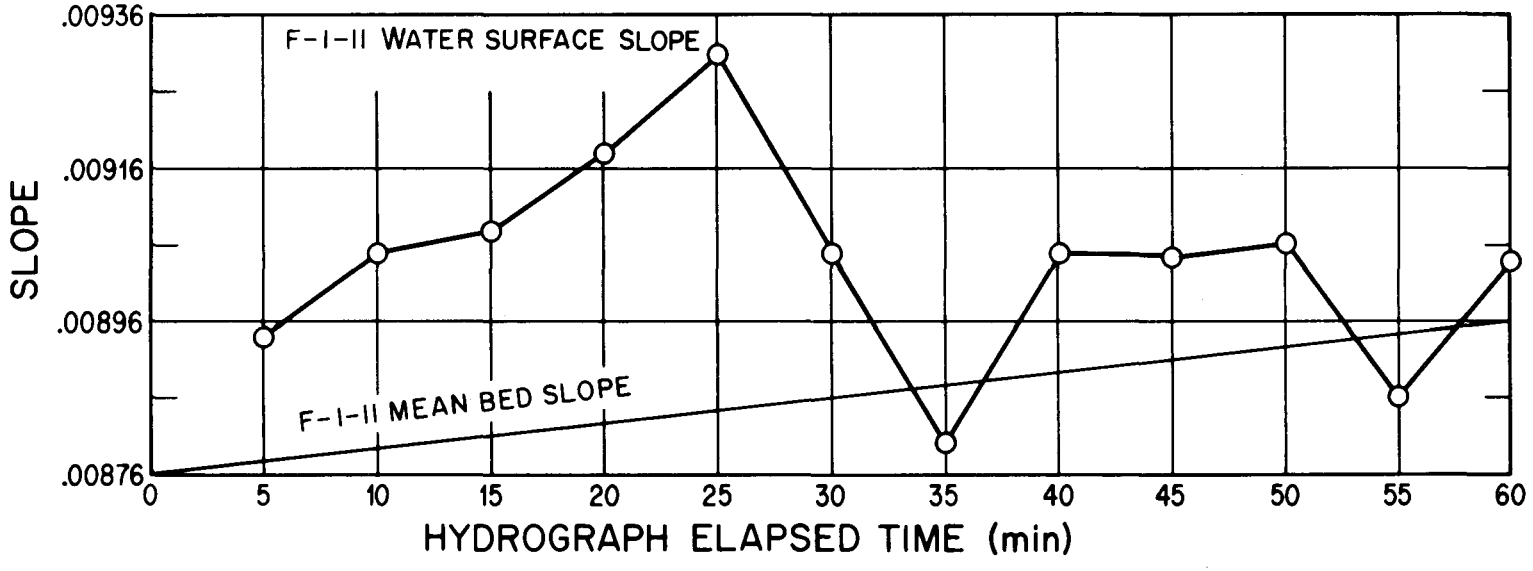

Figure 7-4. Water surface and mean bed slope for run F-1-11.

These positive values suggest that bed roughness is at less than equilibrium value. The dip in relative slope at 35 minutes suggests that flow equilibrium is achieved temporarily between Transition 1 and Transition 2.

This dynamic time-lag effect means that, even if the sediment input-rate is adjusted to steady-state equilibrium transport, mean-bed scour will still occur on the waning flood used in these experiments. This requires an excess of sediment input at the beginning of the flood to balance the scour and achieve overall equilibrium. This sequence of events produces mean-bed fill and scour. Sediment transport rate at the very end of the flood is too low to allow equilibrium to be achieved by a sediment-input excess, so mean-bed scour and fill is not possible unless a power-law sediment input relation with an exponent less than 1.5 is used. Considering the actual magnitude of mean bed elevation fluctuations (Figure 6-7 and 7-1), the question of mean-bed fill and scour versus scour and fill is academic and the important problem in bed reworking is bedform amplitude.

Downstream-migrating antidunes. The Transition I region of the depth-velocity curve for the simulated floods may reflect a scale effect in the small laboratory stream, and may thus not be valid for deeper flows. Kennedy (1961, p.148) states:

> ...dunes which are strongly coupled are, by [Kennedy's] definition, also antidunes...No instances of this phenomenon occurring in natural streams have been reported and dunes strongly coupled with the water surface may be a laboratory curiosity.

Vanoni's (1974) work on bedforms of alluvial streams provides a framework

within which to classify downstream-migrating antidunes. Figure 7-5 is an adaptation of Vanoni's Figure 3 (1974, p.366), a plot of Froude number versus relative roughness (depth-to-grain size ratio) for sand in the mean size range 0.15 to 0.32 mm. Vanoni's plot has been extended to lower d/d_{50} by adding data from run F-1-11, equilibrium steady-state runs A-3-1, A-6-6, and A-7-2, and two of Kennedy's (1961) runs with downstream-migrating antidunes. These data define a trapezoidal field of occurrence of downstream-migrating antidunes with maximum relative roughness of 240 to 380 for Froude numbers of .84 to .47, respectively. For sand with d_g = .028 cm, maximum water depth for occurrence of downstream-migrating antidunes is thus 6.7 to 10.6 cm, depending on Froude number. At greater depths, to be expected in all but the smallest field streams, transition on the waning flood would be from antidunes-to-flat-bed-to-dunes-to-ripples, with no downstream-migrating antidunes forming. Thus, the results of run F-1-11 are quantitatively applicable to flows over the same sand at depths no greater than 6.7 to 10.6 cm.

Estimation of Antidune Amplitude in a Steep Alluvial Channel

Kennedy's (1961) antidune flow relations appear valid for depths of 2 to 120 cm. Thus, behavior of laboratory flows should be analogous to behavior of natural streams in the antidune flow regime, even though details of transition to lower flow regime are inapplicable. Data from runs I-2-2 and I-2-3 allow direct comparison between measured flow and stationary wave parameters and calculated values (Chapter 4), and between measured total scour and fill and that caused by observed bedform migration.

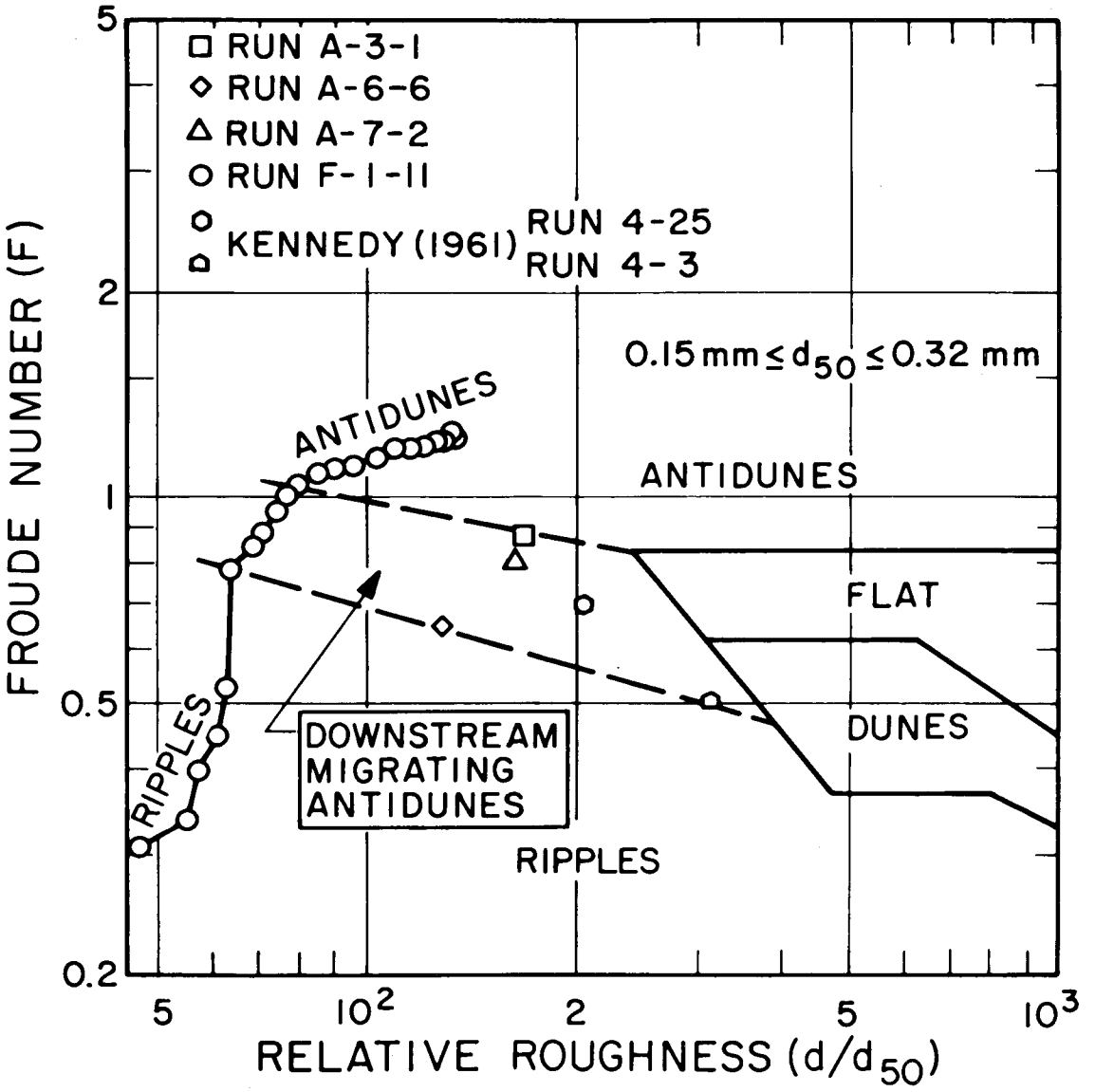

Figure 7-5. Bedform chart showing occurrence of downstream migrating antidunes (adapted from Vanoni, 1974, Fig. 3).

Flow parameter estimation. Channel geometry and bed material constrain maximum flow velocity within about plus or minus 25 percent for the antidune regime if the flow depth is known (Chapter 4). Equations 4-1 through 4-6 applied to runs I-2-2 and I-2-3 give predicted flow parameters shown in Table 7-2. Bed roughness friction factor f_b' is independent of Reynolds number for fully-rough flow, the assumed condition for the first calculation of mean velocity in Table 7-2. The Reynolds numbers derived from this assumption are not in the fully-rough region of Figure 4-1, requiring a total of three iterations before assumed f_b' and Reynolds number values converge.

Comparison of Tables 7-2 and 6-11 show excellent agreement between predicted friction factors and velocities and those calculated from antidune relations in runs I-2-2 and I-2-3. However, actual average friction factors and velocities for these runs are not within the predicted limits. Since overall friction factor ratios for these experiments are between 2 and 3, the overall flow is in the downstream-migrating antidune flow regime. Thus, the flow predictions are only valid for the higher-velocity zone near the center of the channel. Downstream-migrating antidunes are not likely to be a problem for flow depths greater than 11 cm, indicating that the flow estimation technique is probably valid for all but the smallest steep streams in the field.

Antidune amplitude estimation. Stationary wave along-stream and cross-stream wavelengths, and flow parameters from runs I-2-2 and I-2-3 permit calculation of maximum antidune amplitudes (Chapter 4). Table 7-3 shows details of these calculations for maximum measured stationary wave

TABLE 7-2. THEORETICALLY ESTIMATED FLOW PARAMETERS FOR RUNS I-2-2 AND I-2-3.

Run		I-2-2	I-2-3
d	Flow depth (known) cm	1.44	1.24
r	Hydraulic radius (known) cm	1.37	1.20
FIRST ITERATION			
f'_b	Bed roughness friction factor assumed fully rough flow	.0302	.0318
f	Friction factor	.0604-.0272	.0636-.0286
V	Mean velocity $\left(\sqrt{\frac{8grS}{f}}\right)$ cm/sec	49.12-73.23	45.74-68.19
Re	Equivalent pipe friction Reynolds number $\left(\frac{4rV}{\nu}\right)$	$2.75\text{-}4.09\times10^4$	$2.24\text{-}3.34\times10^4$
SECOND ITERATION			
f'_b	Bed roughness friction factor at Reynolds no. of first iteration	.0335-.0325	.0350-.0338
f	Friction factor	.0670-0293	.0700-.0304
V	Mean velocity cm/sec	46.64-70.59	42.89-65.07
Re	Reynolds number	$2.61\text{-}3.95\times10^4$	$2.10\text{-}3.19\times10^4$
THIRD ITERATION			
f'_b	Bed roughness friction factor at Reynolds no. of second iteration	.0336-.0326	.0353-.0341
f	Friction factor	.0672-.0293	.0706-.0307
V	Mean velocity cm/sec	46.57-70.48	42.71-64.78
Re	Reynolds number	$2.60\text{-}3.94\times10^4$	$2.09\text{-}3.17\times10^4$

TABLE 7-3. FLOW AND BEDFORM PARAMETERS FOR I-2-2,3

SCOUR-CHAIN RUN			I-2-2	I-2-3
d	= Mean flow depth	cm	1.44	1.24
L	= Stationary wave wavelength	cm	16	12
B	= Stationary wave transverse wavelength	cm	∿16	∿12
V	$= \sqrt{\frac{gL}{2\pi}} \sqrt[4]{1+\left(\frac{L}{B}\right)^2}$	cm/sec	59.43	51.47
k	$= \frac{2\pi}{L}$ = wave number	cm^{-1}	0.393	0.524
H_{max}	$= \frac{L}{7}$ = Max stationary wave height	cm	2.28	1.72
$\frac{A}{\frac{1}{2}H}$	$= (1- \frac{g}{V^2k} \tanh kd) \cosh kd$		0.743	0.726
A_{max}	= Max antidune amplitude	cm	0.85	0.62
Measured maximum scour		cm	1.16	0.64

wavelengths and inferred flow velocities of runs I-2-2 and I-2-3. Calculated maximum antidune amplitude for run I-2-2 is 3 mm less than the maximum measured scour and fill shown in Figure 6-14. Maximum antidune amplitude calculated for run I-2-3 is not significantly different from scour-chain measurements.

It is tempting to discount the significance of the 3 mm difference between scour prediction and observation in run I-2-2 since observations showed that scour-chains were only exposed in the troughs of antidunes and scour data and predictions for run I-2-3 show such excellent agreement. However, it is probable that the difference is real if small, and related to the nonuniform transverse velocity distribution. This nonuniform flow configuration might well have resulted in mean bed scour in the center of the channel, with the scoured material shifted toward the channel banks downstream. This situation is analogous to that proposed in Chapter 4 for the December 1974 flow in Quatal Creek.

Flume Demonstration of Bedload-Dropout "Armoring"

The 0.7 to 1 cm gravel used as riprap armor in the alluvial-bank channel inlet (Chapter 5) was easily transported by maximum simulated-flood flows unless well-packed in an armor layer. Experiments were conducted in which this gravel was added to an antidune flow at conditions of the D-1 series experiments (Chapter 6). Antidunes had little effect on gravel transport until the stationary waves approached maximum amplitude. As the stationary waves approached maximum amplitude, transported gravel hesitated on the upstream side of each antidune, with an occasional fragment stopped momentarily. When the stationary waves

began breaking, gravel was trapped on the upstream side of the antidunes (Figure 7-6) and rapidly buried. The small patches of bedload-dropout "armor" so formed were usually scoured away on the downstream side of the next antidune to form. Occasionally, a patch of "armor" would be missed by subsequent scour, and survive several cycles of stationary wave buildup and breaking. These patches appear analogous to those observed in scour-cord exploratory pits in Quatal Creek.

If the cobble lenses in Quatal Creek were bedload-dropout "armor" as hypothesized in Chapter 4 and demonstrated in the laboratory flume, two judgments about the January and December 1974 flows are more strongly supported. First, the flow competence calculations are likely based on maximum bedload particle size. Thus, correlation between observed cobble sizes and calculated bankfull competence suggests that the flows were bankfull, an assumption used in the calculations in Tables 4-1 and 4-2. Second, bedload-dropout "armor" only formed in the laboratory when stationary waves were near maximum amplitude or actually breaking. Thus, the calculations of Tables 4-1 and 4-2, which assumed maximum-amplitude or breaking stationary waves, show the probable ranges of antidune amplitude for the two runoff events.

Flume experiments showed that flat gravel was more resistant to erosion than round gravel subsequent to development of a patch of "armor", but no imbrication was apparent in "armor" patches. Pebbles and cobbles in the Quatal Creek "armor" lenses were roughly equant, with no preference for flat clasts and apparently no imbrication developed.

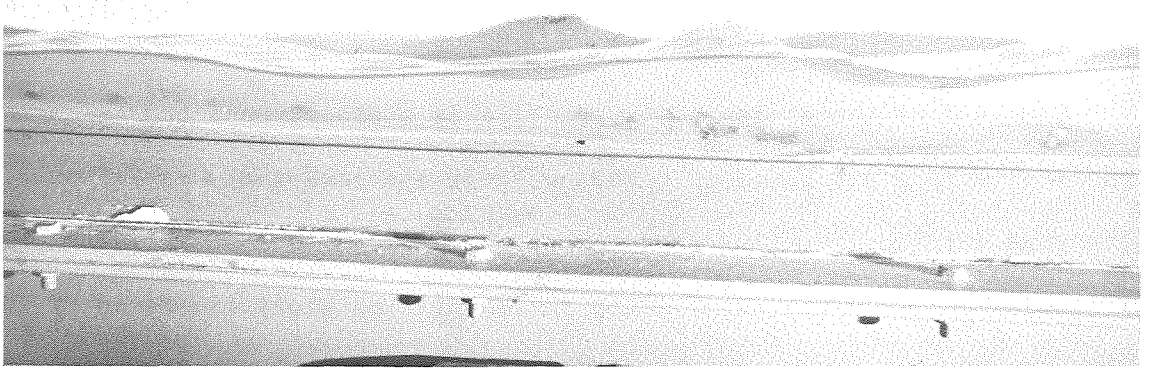

(a) Side view, flow from right to left.

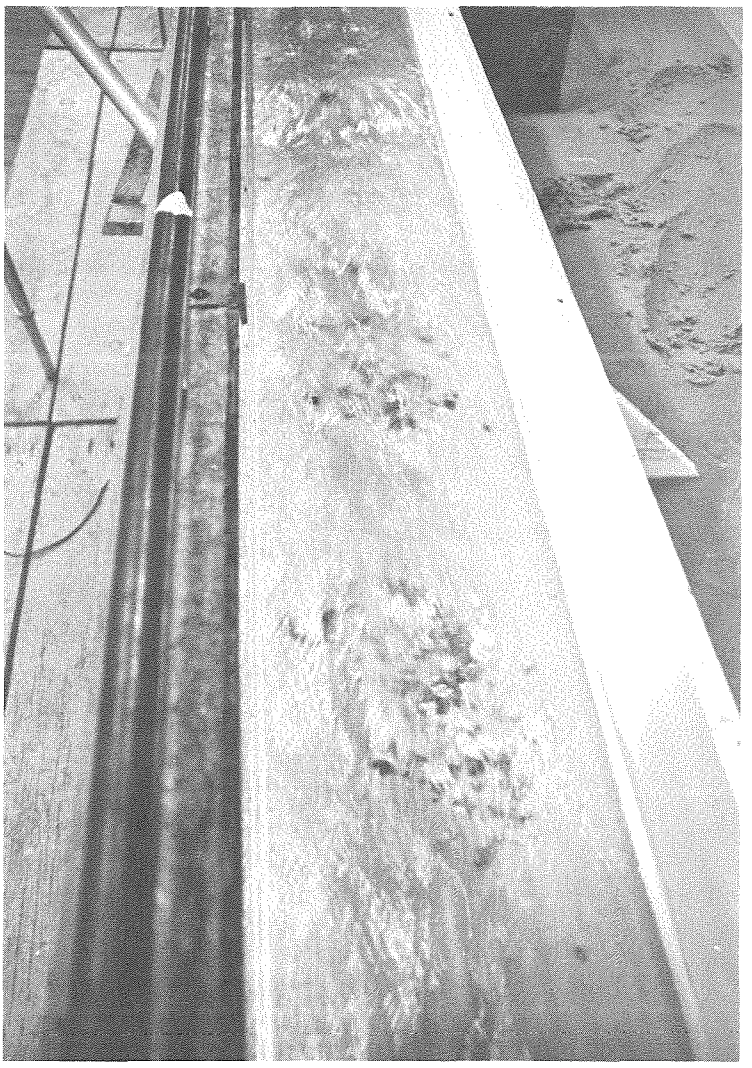

(b) Top view, looking obliquely downstream.

Figure 7-6. Bedload-dropout "armor" forming under breaking stationary waves.

CHAPTER 8. SUMMARY OF CONCLUSIONS

Conclusions concerning scour and fill in a steep, sand-bed ephemeral stream are based on combined field and laboratory experiments. Data were derived from floods of moderate discharge in a natural channel in January and December 1974, and a series of laboratory floods in rigid-wall and alluvial-bank channels.

1. Scour and fill for moderate floods in a uniform sand-bed channel at grade results predominantly from bedform development and migration.

2. Flood flow in the field stream was judged to be entirely in the antidune regime because of steep gradient and lack of evidence for residual lower-flow regime bedforms. For antidunes, maximum theoretical amplitude A_{max} is given by the equation (Kennedy, 1961):

$$A_{max} = \frac{H_{max}}{2}\left(1 - \frac{g}{V^2 k}\tanh kd\right)\cosh kd; \quad [k = \text{wave number}]$$

where flow velocity $V = \left(\frac{8gdS}{f}\right)^{1/2}$; d = bankfull depth

S = bed slope

f = friction factor

$.9 \leq f/f' \leq 2$; f' = equivalent pipe friction factor for bed sediment grain roughness

$$V = \left(\frac{gL}{2\pi}\right)^{1/2}\left[1+\left(\frac{L}{B}\right)^2\right]^{1/4}$$; L = stationary wave longitudinal wavelength

B = stationary wave transverse wavelength

and maximum stationary wave height H_{max} = .142 L. Scour and fill measured by scour-cords was equal to bankfull water depth in the January 1974 flood and twice bankfull water depth in the December 1974 flood. In both instances it was less than the upper limit of A_{max}. Thus, scour and fill measured by scour-cords for the two floods can be explained theoretically by bedform migration, but this is a qualified conclusion since the floods were not directly observed or gaged.

3. Laboratory scour-chain experiments confirmed the flow parameter estimation procedure used in evaluating the natural floods, confirmed that scour-chains were exposed only in bedform troughs, and that scour and fill as measured by scour-chains is predominantly attributable to bedform migration.

4. Laboratory scour-chain experiments showed that chains fall straight downstream when exposed by antidunes; but are contorted and inclined in any direction when exposed by ripples or dunes. Scour-cords in field experiments were pointed straight downstream, confirming the judgment of antidune flow regime.

5. Laboratory gravel-transport experiments demonstrate that during antidune-regime flow, breaking stationary waves reduce stream competence causing coarse material in transport as bedload to be deposited under the breaking stationary waves on the upstream sides of antidunes. The debris so laid down forms a lens of dropout "armor" within stream-bed material if it survives the scour of later bedforms. The grain size in such dropout "armors" observed in Quatal Creek deposits supports the assumption of bankfull flow in the January and December 1974 floods.

The dropout "armor" further suggests that stationary waves were breaking at peak flow, and, hence, that the antidunes were at their maximum amplitudes, A_{max}.

6. Reasoning based on bed and bank sediment and channel geometry suggests that the field stream is at grade. This judgment is supported by the fact that net bed elevation change in the study area was only .033 meters as a result of at least four floods in 17 months. Bank erosion has been minor, and motorcycle races may have been responsible for some of the bank deterioration that occurred.

7. For laboratory floods of the form:

$$0 \leq t \leq t_o: \quad Q = Q_{max} \qquad Q = \text{water discharge}$$

$$t_o \leq t \leq t_{max}: \quad Q = Q_{max} \exp\left[-\frac{3(t-t_o)}{(t_{max}-t_o)}\right]$$

where $t_o = 0.1\ t_{max}$, $t_{max} = 1$ hour

and a sediment input relation of the form:

$$G_s \propto Q^2 \qquad G_s = \text{sediment input rate (sediment } d_g = 0.28 \text{ mm)}$$

maximum mean-bed elevation change resulting from mean-bed scour and fill was only 0.06 cm for a rigid-wall channel at grade. For these floods, bedform-trough depth was 2.2 cm, so mean bed fill and scour was negligible (3 percent) compared to maximum scour and fill. Maximum ripple development occurred near the end of the flood, at minimum discharge.

8. In the laboratory, mean-bed fill and scour was strongly influenced by; 1) the ad hoc sediment input rate; and 2) the dynamic effect of discontinuous depth-velocity relations. Sediment input rate decayed faster than sediment transport rate, so the maintenance of channel grade required a surplus of sediment input during the waxing phase of a flood to compensate sediment input deficiency on the waning phase. The time required for development of finite bed-roughness during transition from upper-to lower-flow regime was the cause of a greater-than-equilibrium velocity and greater sediment transport as the flood waned. Both the ad hoc sediment input rate and the bed-roughness time lag resulted in a small amount of mean-bed fill and scour. Transition from upper-to lower-flow regimes could produce the same effect in a natural stream with a discontinuous depth-velocity relationship, provided the rate of change of discharge is of the same order or greater than rate of change of bed roughness. Since flow at the field site was seemingly all in the upper flow regime, this presumably did not occur.

9. Observations in a laboratory alluvial-bank channel show that flow velocities in trains of "roostertail" stationary waves in an approximately rectangular cross-section can be over 50 percent higher than mean velocity for the cross-section. Bed sediment apparently migrates to the sides away from the axes of such trains, resulting in development of narrow troughs of high-velocity flow and net scour and thus localizing mean bed scour and fill. The scoured sediment is transported obliquely downstream. The December 1974 flood produced a net effect of this type in the field streambed (Figure 3-6).

10. During channel-widening in the laboratory alluvial-bank stream course, breaking trains of large roostertails disrupted streamflow, diverting it into and over the banks. Cutting by this diversion and sapping by returning overbank flow caused rapid bank erosion. Local overbank flow which occurred in the December 1974 flood at the field site may have had a similar cause.

11. Downstream-migrating antidunes which caused a two-stage transition from upper-to lower-flow regime in laboratory floods may be a laboratory curiosity limited to flow depths of less than 11 cm for 0.28 mm sand.

APPENDIX 1. SUMMARY OF NOTATION

$\overline{a}$	Coriolis coefficient
A	Amplitude of antidunes
B	Transverse wavelength of "roostertails"
c	Speed of flood wave
d	Channel depth, channel water depth
d_g	Geometric mean sediment size
Δd	Change from initial value of flume mean bed elevation
e	Elevation of energy grade line above flume bottom
F	Froude number
f	Darcy-Weisbach friction factor for channel
f'	Equivalent pipe friction factor for channel sediment grain roughness
f_b	Friction factor of bed
f_b'	Equivalent pipe friction factor for bed sediment grain roughness
f_w	Friction factor of wall
f/f'	Friction factor ratio of channel
f_b/f_b'	Friction factor ratio of bed
g	Gravitational constant
G_s	Flume total sediment discharge
G_{so}	Flume sediment input rate
$G_{so_{max}}$	Maximum flume sediment-input rate for simulated flood
ΔG_s	Flume sediment accumulation rate
H	Trough-to-crest height of stationary waves

APPENDIX 1. SUMMARY OF NOTATION (Cont'd)

k	Wave number of stationary waves
L	Crest-to-crest wavelength of stationary waves
M	Weighted mean percent silt-clay of channel bed and banks
Q	Water discharge
Q_{max}	Maximum discharge of flume water hydrograph
r	Channel hydraulic radius
Re	Reynolds number
S	Channel slope
S_b	Percentage silt-clay in stream bank material
S_c	Percentage silt-clay in stream bed material
S_r	Relative slope of water surface with respect to flume mean bed elevation profile
T	Water temperature
t	Elapsed time in flume hydrograph
t_o	Length of flattop peak of flume hydrograph
t_{max}	Length of flume hydrograph
Δt	Time lag between flume inlet and outlet hydrographs
V	Mean flow velocity
V_L	Inferred velocity of stationary waves in flume
W	Channel width
y	Elevation of water surface above flume bottom
ε_s	Sand-grain roughness for pipe-friction determination
ν	Kinematic fluid viscosity
ρ	Density of fluid

APPENDIX 1. SUMMARY OF NOTATION (Cont'd)

σ_g	Geometric standard deviation of sediment sizes
τ	Elapsed time between flume sediment discharge samples
τ_c	Critical bed shear-stress for particle motion
τ_o	Flow shear-stress at the bed

APPENDIX 2. CHANNEL BORES IN FLUME.

Introduction

In the simulated flood experiments conducted in an alluvial-bank channel, quasiperiodic bores up to 1 cm amplitude developed during the waning flood (Chapter 6, Figure 6-9). No quantitative measurements were made of these bores in the alluvial-bank channel because channel geometry was changing too rapidly to establish steady-state flow conditions in a fixed channel cross-section. These bores had earlier been observed in the rigid-wall simulated flood experiments, but were thought to be related somehow to the artificiality of the rigid walls. Their development in alluvial-bank experiments indicates that they are a phenomenon related to the sand size, flume slope, and type of inlet used in these experiments. To further evaluate this phenomenon, a series of experiments was conducted on bore development in a rigid-wall channel.

Experimental Setup and Procedure

The experimental arrangement was the same as used in the rigid-wall simulated floods (Chapter 6). Flume slope was set at .00853, as in runs F-1-8 through F-1-13. Two simulated floods were run over a non-erodible bed with the hydrograph shown in Figure 6-5, but no sediment input.

In the first simulated flood, the sand bed was covered with a 1 cm thick plywood false bottom (Figure A2-1). This bottom was mounted with its top surface flush with the inlet and outlet sills so channel geometry was the same as that used in the simulated flood experiments,

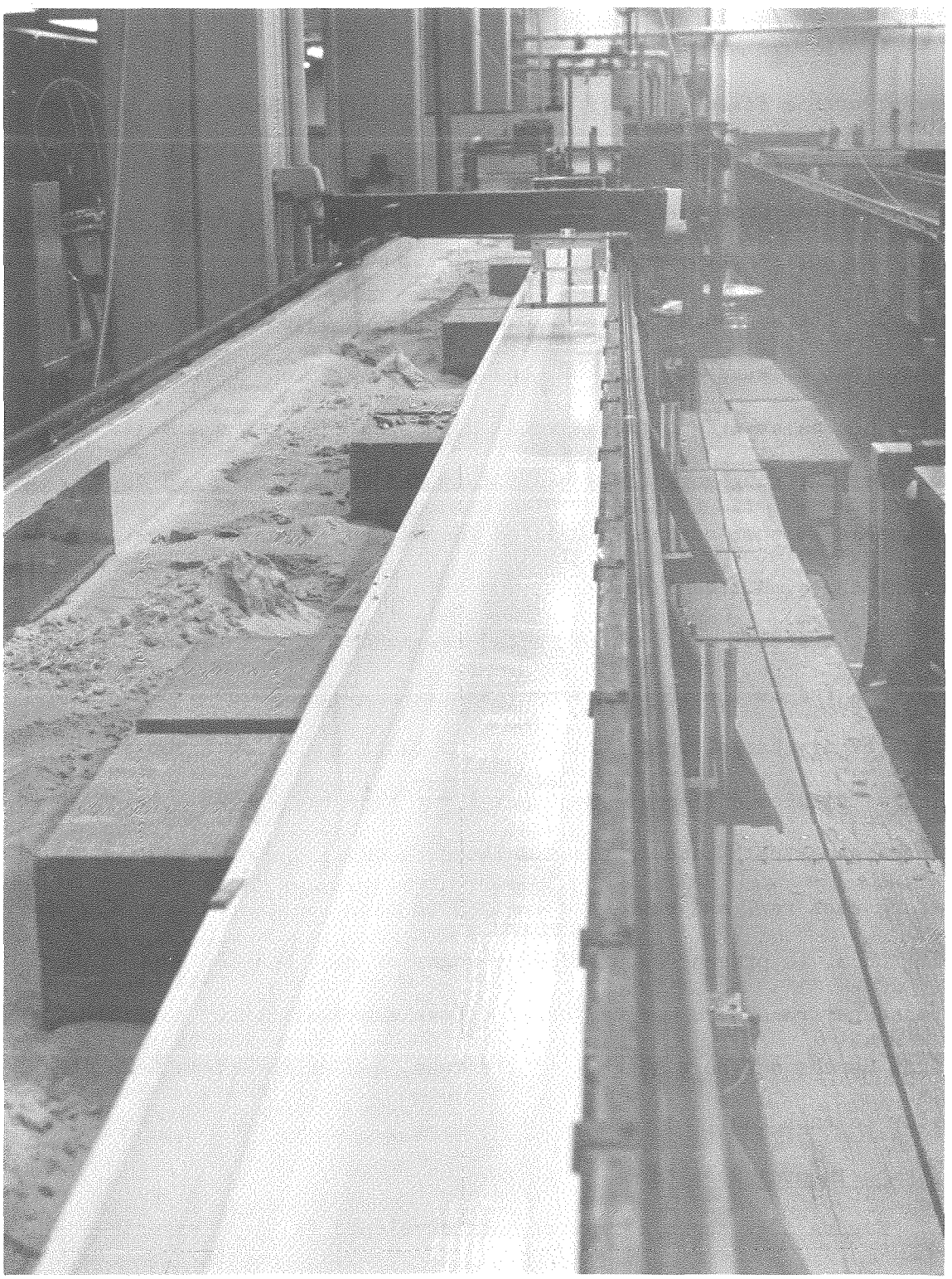

Figure A2-1. Fixed-bed channel.

except with a fixed bed. It was painted with the epoxy resin used on the flume walls, and edges and joints were sealed with vinyl tape. No channel bores developed in the course of the simulated flood run through this channel.

For the second simulated flood in the fixed bed channel, the false bottom was painted and dry bed sand was sprinkled on the wet paint. After the paint dried, excess sand was washed off, and a simulated flood run over the roughened fixed bed. This bed had the same bed sand-grain roughness as that used in simulated floods, but again no bores developed during the simulated flood.

Eight steady-state experiments were conducted with a movable bed and sand fed at the inlet. These experiments were conducted over a range of discharges which bracketed the range producing bores in the earlier simulated floods. Sediment input rate had the same relation to discharge as that used in the simulated floods. The sand bed was leveled before each run, and runs were limited to about 6 minutes duration, except for run 5, to prevent significant changes of mean bed elevation. Pressure transducer recorders were adjusted to maximum sensitivity possible for the water depths and bore heights of the runs, and calibrations were checked prior to each run.

Experimental Results

Figure A2-2 shows a typical bore developed in these experiments. The bore can be seen entering the field of view from the right. Bore height is about .8 cm and water ahead of the bore is about 1.8 cm deep. Small downstream-migrating antidunes can be seen on the bed. Stationary

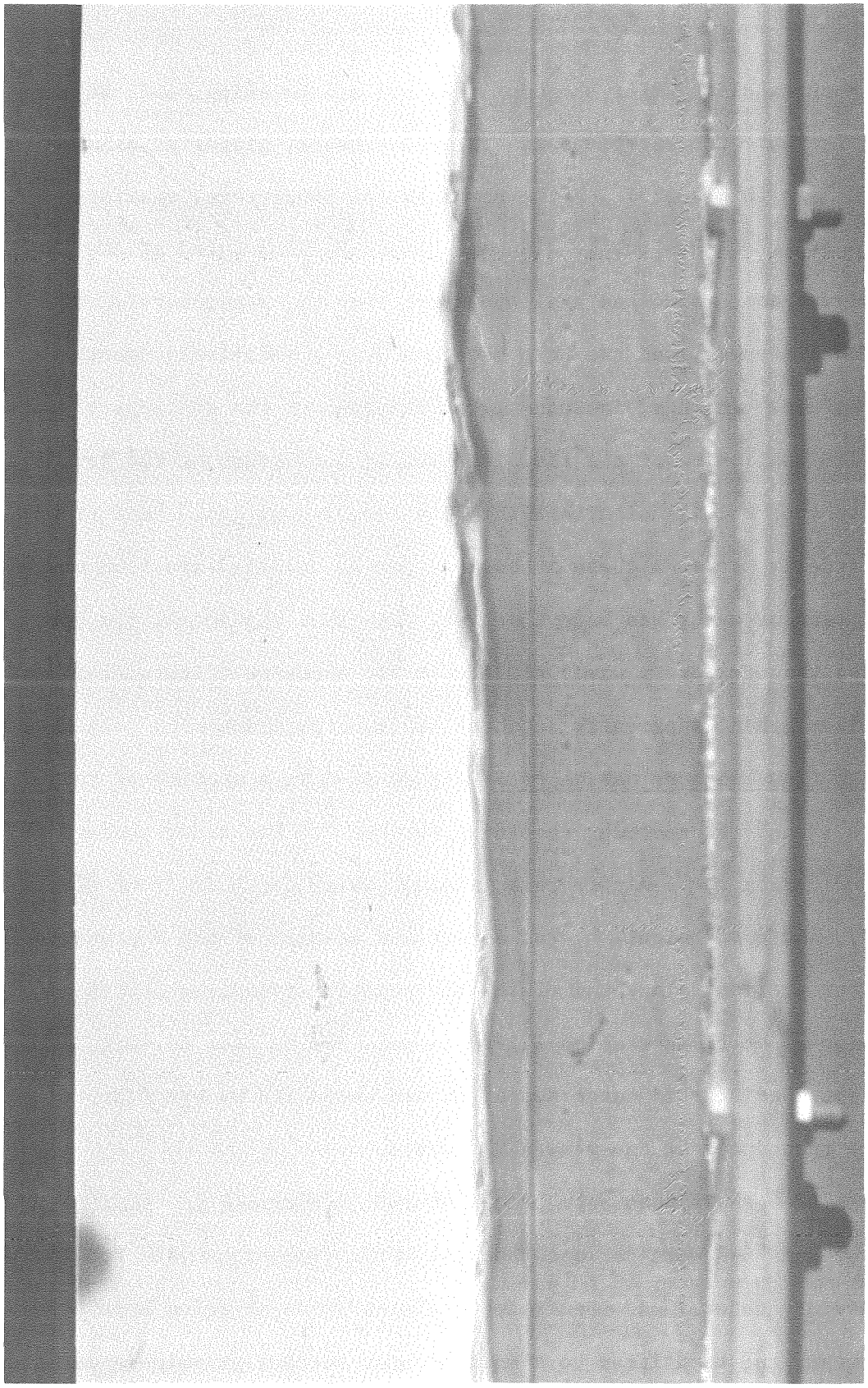

Figure A2-2. Typical bore in rigid-wall channel.

waves in the shallow water ahead of the bore are breaking, and the surface of the bore has superimposed stationary waves, giving it a lumpy appearance in this photo. As the bores travel downstream, stationery waves in front of them break. In some cases the flow ahead of the bores apparently becomes slow and shallow enough that the stationary waves break and disappear, and the bore advances over a relatively smooth water surface. In these instances, the breaking of the stationary waves and sudden shallowing of the flow immediately downstream of the bore gives the apparent illusion that the flow surges upstream. Sand transport virtually stops in these instances, but no verified upstream movement of sand or water has been observed. In other instances, the bore overrides the stationary waves while they are breaking (Figure A2-2) and leaves them behind apparently in about the same position.

Mean flow and bore parameters. Figure A2-3 is a section of the pressure transducer recorder recording for Run 2. For every bore which developed during the 6-minute runs, minimum water depth in front of the bore, d_ℓ, and bore height, h, was determined at each of the 6 pressure transducer stations along the flume (the seventh transducer described in Chapter 5, at flume station 15.25 m, could not be made to work properly). Undisturbed water depth, d, was estimated by eye (Chapter 6) for each transducer at one-minute intervals.

Figure A2-4 shows mean bore height at each transducer for Runs 1-5. Data from Runs 6-8 were not used because water discharges were too low to be accurately determined, feeder input disturbances affected bore development, and transition to a smooth water surface (ripple-regime flow)

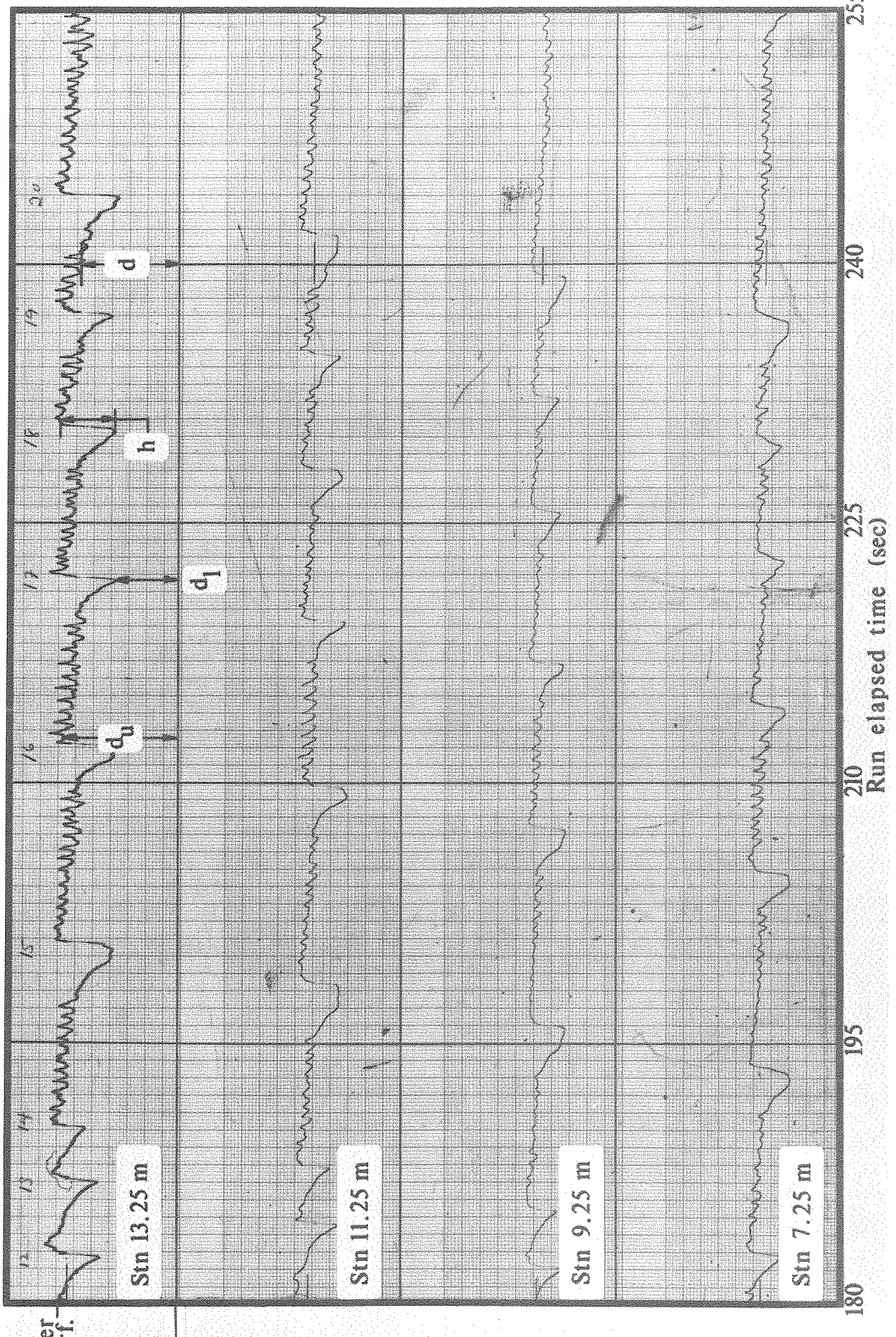

Figure A2-3. Pressure-transducer recorder record for Run 2.

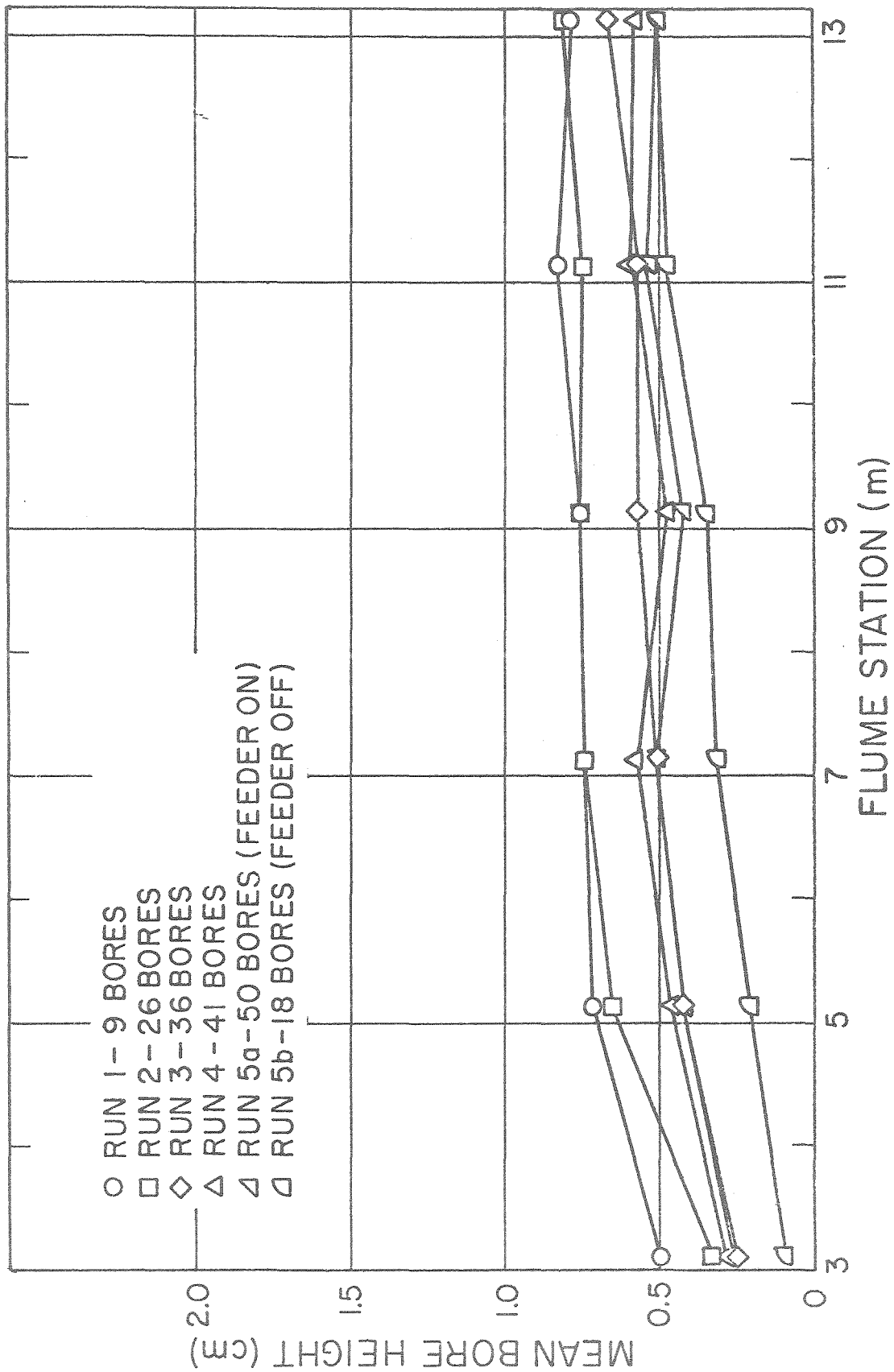

Figure A2-4. Mean bore height along flume for Runs 1-5.

during Runs 7 and 8 apparently ended the development of bores. Figure A2-4 shows that bores in Runs 1-5 were generated upstream of flume station 3.25 m, and observations indicate that they are first visible downstream of station 1.5 m. Bores were observed coming out of the inlet during Run 5. The feeder was shut off after 390 seconds, and Run 5 was separated into Run 5a (feeder on) and Run 5b (feeder off). Figure A2-4 shows that bores in Run 5b form farther downstream than those in Run 5a, but achieve the same height by station 13.25 m. Thus, although the feeder input disturbances had some effect on initial bore generation, final bore size was not affected.

Figure A2-4 shows that mean bore height varies but little downstream of station 7.25 m. Table A2-1 is a summary of mean flow parameters and mean bore parameters for stations 7.25 m to 13.25 m. The quantities in Table A2-1 are as follows:

Q = water discharge in cm^3/sec.

$\overline{d}$ = mean undisturbed water depth for the run, the average for all transducers for times after 60 seconds into the runs, in cm. Flow reached equilibrium depth after 60 seconds, and no bores developed before 60 seconds.

$\overline{r}$ = hydraulic radius in cm = $\frac{W\overline{d}}{W+2\overline{d}}$ where W is flume width, 26.7 cm.

$\overline{V}$ = mean flow velocity in cm/sec = $\frac{Q}{W\overline{d}}$

No. of bores = total number of bores which occurred during each 6-minute run

$\overline{h}$ = mean bore height in cm for flume stations 7.25 to 13.25 m.

$\overline{V}_w$ = mean bore velocity relative to flume in cm/sec = 6 m/mean travel time from station 7.25 m to station 13.25 m.

c = bore celerity in cm/sec = $\bar{V}_w - \bar{V}$

F = Froude number = $\frac{\bar{V}}{\sqrt{g\bar{d}}}$

f = Darcy-Weisbach friction factor of channel = $\frac{8g\bar{r}S}{\bar{V}^2}$ where S = .00853.

TABLE A2-1. MEAN FLOW AND BORE PARAMETERS FOR RUNS 1-5.

Run	Q	$\bar{d}$	$\bar{r}$	$\bar{V}$	No of	$\bar{h}$	$\bar{V}_w$	c	F	f
	cm^3/sec	cm	cm	cm/sec	Bores	cm	cm/sec	cm/sec		
1	2550	2.03	1.76	47.1	9	.79	86.5	39.4	1.06	.053
2	2070	1.93	1.69	40.2	26	.76	79.7	39.5	.92	.070
3	1649	1.73	1.53	35.7	36	.58	74.9	39.2	.87	.080
4	1380	1.66	1.48	31.2	41	.56	73.7	42.5	.77	.102
5a	1130	1.54	1.38	27.5	50	.50	72.2	44.7	.71	.122
5b	1130	1.50	1.35	28.3	18	.42	69.8	41.5	.74	.113

S = .00853

T = 23°C

d_g = .28 mm

Discussion. Visually the channel bores resemble roll waves in terms of morphology, regularity of spacing, and the impression that larger waves overtake smaller ones. However, Brock's (1967) analysis indicates that roll waves should not form at Froude numbers less than 2; and Koloseus and Davidian (1966, Figure 4) indicate they should not form at Froude

numbers less than about 1.8 for the width-depth ratio and friction factor of these flows (Table A2-1).

Quantitative data from Runs 1 to 5 show that the bores do not behave like roll waves. Although the average bores increase slightly in amplitude after initiation (Figure A2-4), many individual bores decayed after reaching peak height. Also, in the rare instances where one bore overtook another, the overtaking bore was of smaller height. This behavior is typical of surges (Henderson, 1966, p. 77 and 300). Henderson indicates that celerity of surges of finite amplitude should be within the limits $\sqrt{gd_\ell} < c < \sqrt{gd_u}$ where d_ℓ and d_u are water depths downstream and upstream of the bore, respectively (Figure A2-3). Table A2-2 shows that observed experimental bore celerities behave this way except for Run 5, where bore celerities are greater than $\sqrt{gd_u}$. In Table A2-2, $\bar{d}_\ell$ and $\bar{d}_u$ are the mean low and high water depths in front of and behind the bores, respectively, in cm, for flume stations 7.25 to 13.25 m.

TABLE A2-2. COMPUTED AND ACTUAL BORE CELERITIES.

Run	$\bar{d}_\ell$ cm	$\bar{d}_u$ cm	$\sqrt{g\bar{d}_\ell}$ cm/sec	c cm/sec	$\sqrt{g\bar{d}_u}$ cm/sec
1	1.42	2.21	37.3	39.4	46.6
2	1.37	2.13	36.7	39.5	45.7
3	1.33	1.91	36.1	39.2	43.3
4	1.32	1.88	36.0	42.5	42.9
5a	1.21	1.71	34.5	44.7	41.0
5b	1.19	1.61	34.2	41.5	39.7

The greater celerities calculated from transducer data than predicted from hydraulic theory for Run 5 may be artifacts of the instrumentation. Brock (1967) used an alternate method for determining roll wave crest height because pressure transducer response time was slower than wave-front rise time. Transducer response in these experiments is even slower than in Brock's, because water pressure increase must be transmitted through 6 cm of sand before reaching the piezometric taps. Apparent dips in bore height at station 9.25 m for Runs 4 and 5 (Figure A2-4) are probably caused by slower response time for that transducer relative to the others, giving a smaller apparent d_h. All of the transducers should give systematically low readings for d_h, which can account for the failure in Run 5 for $\sqrt{gd_h}$ to be greater than c. This transducer response problem also means that all values of $\overline{h}$ and $\overline{d}_h$ are systematically low, hence no quantitative use of wave-height data in Table A2-1 should be made beyond that in Table A2-2.

Henderson (1966) and Lighthill and Whitham (1955, p. 294) indicate that bores in Runs 1 to 5 should decay in height once initiated. This decay is observed in some bores, but on the average the experimental bores do not decay (Figure A2-4). The mechanism of bore generation must be explained. It was mentioned earlier that in Run 5, bores were observed coming out of the inlet, suggesting that blobs of sand falling from the feeder initiated the bores. Figure A2-4 showed however, that bores form with the feeder off, and Figure A2-5 shows that the frequency of bores does not change appreciably when the feeder is shut off. Data in Figure A2-5 are the number of bores passing station 13.25 m during successive

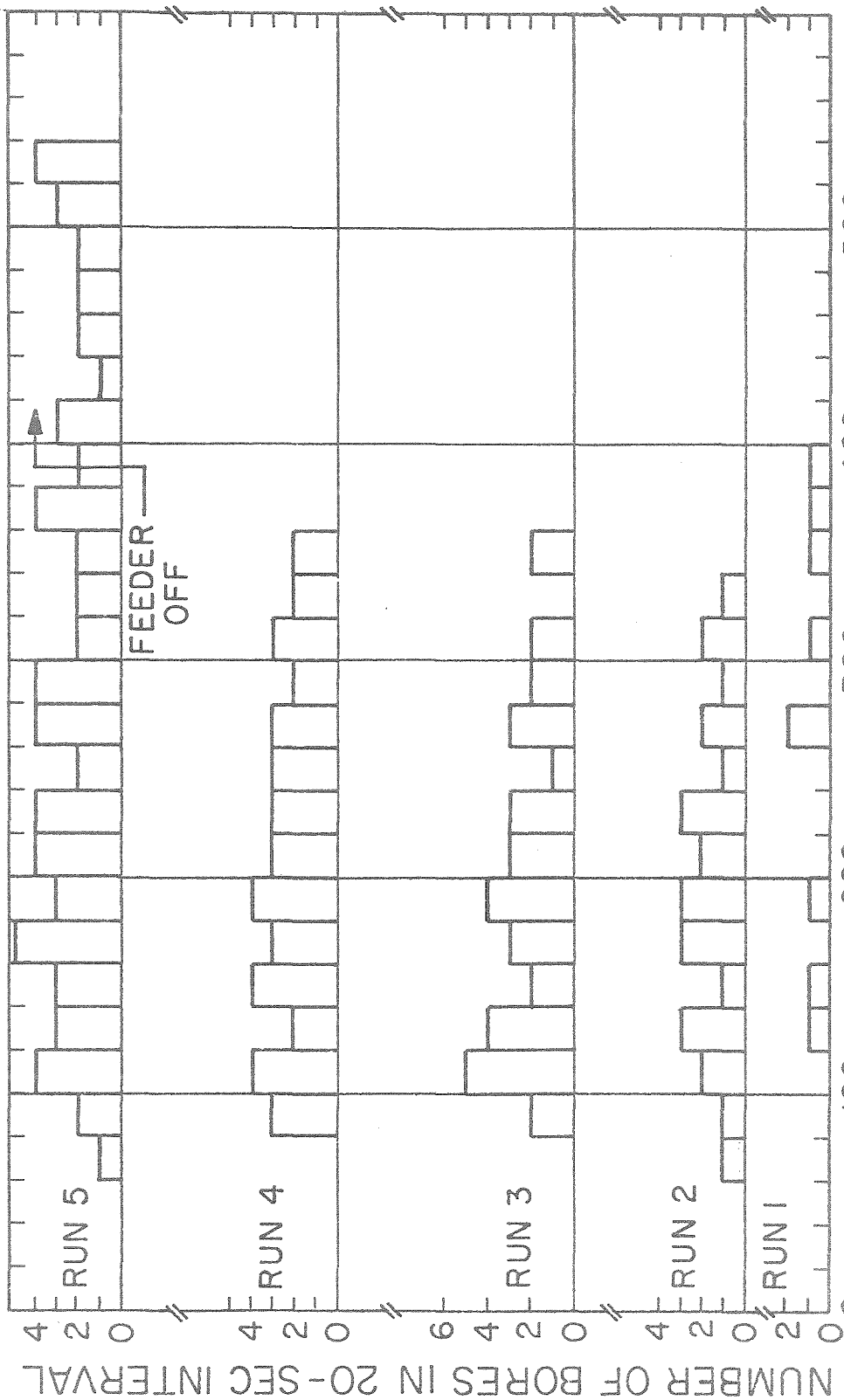

Figure A2-5. Bore frequency for Runs 1-5.

20-second intervals. In all cases there is a slight peak in bore frequency in the middle of the run, but no significant difference in frequency in the 100 sec before and the 100 sec after feeder shutoff in Run 5. Thus, the feeder apparently does not cause the bores.

Since these bores are only observed during flows with downstream-migrating antidunes, the suggestion in Chapter 6 that the bores are initiated by successive breaking of stationary waves starting at the upstream ends of trains of downstream-migrating antidunes is supported. A bore so formed could be reinforced with water stored by breaking stationary waves overriden by the bore as it travels downstream, thus preventing decay of bore height. Bores which travel over the relatively smooth water surface left by completely dissipated stationary waves would presumably decay in the conventional fashion, accounting for the observed decay of many bores.

Field occurrence of bores. In discussion in Chapter 7, downstream-migrating antidunes were deduced to be restricted to flows less than 11 cm deep for bed sand in the .15 to .32 mm size range. Thus, if bores are somehow related to the occurrence of downstream-migrating antidunes, as suggested here, the same restriction must apply. The only field occurrence of such bores known to the writer was reported by Dr. John S. Shelton, who observed them on a flow on the floor of the San Gabriel Reservoir, California, on 14 October 1953. Figure A2-6 is a frame from a motion picture of these bores. Flow, from right to left, is apparently less than 11 cm deep, and the bed material is apparently fine sand. The film shows small-amplitude stationary waves breaking just before passage of

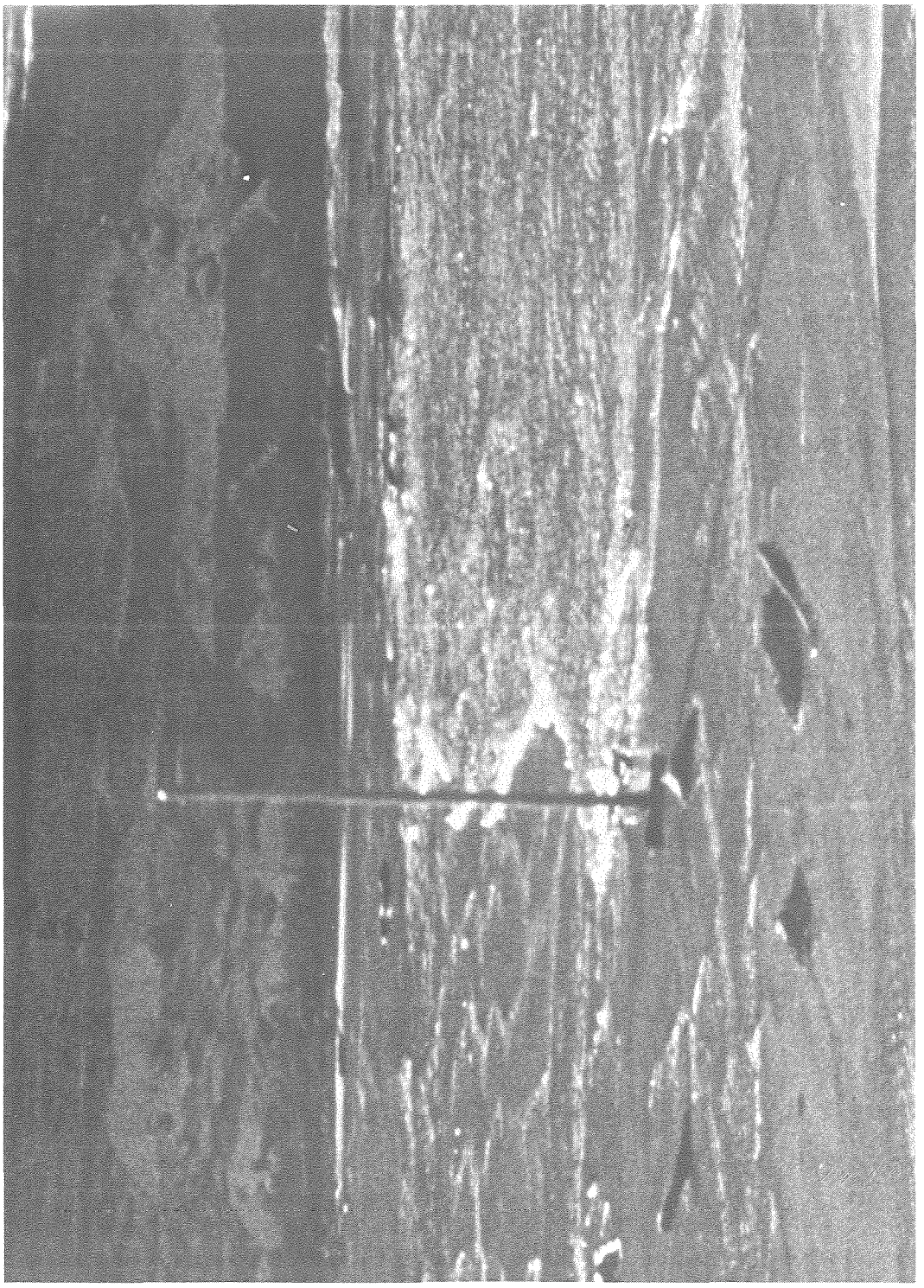

Figure A2-6. Bore in stream on floor of San Gabriel Reservoir, Calif., 14 October 1953. (Photo from film by John S. Shelton).

the bore, but whether their normal migration is upstream or downstream cannot be observed. This field occurrence is possibly within flow parameter limits of downstream-migrating antidunes, and confirms that laboratory production of bores is not an artifact of the apparatus. However, the bores may remain curiosities unless field occurrences in deeper channels are observed.

Conclusion

The channel bores observed in simulated flood experiments in rigid-wall and alluvial-bank channels are apparently related to the existence and quasiperiodic breaking of trains of stationary waves associated with downstream-migrating antidunes. Release of water stored by breaking stationary waves apparently both initiates and nurtures the bores, which otherwise would decay even if independently initiated. Similar bores have been observed in the field under flow conditions similar to those in the laboratory, suggesting that bores are a bona fide natural phenomenon, which these experiments suggest may be associated with downstream migrating antidunes.

REFERENCES

Alvarez, Jose Antonio Maza and Alfaro Francisco J. Echavarria (1973) Contribution to the study of general scour: Proc. Int. Symposium on River Mechanics, IAHR, Bangkok, Thailand, p. 795-803.

Bennett, James P. and Sabol, George V. (1973) Investigation of sediment transport curves constructed using periodic and aperiodic samples: Proc. Int. Symposium on River Mechanics, IAHR, Bangkok, Thailand, p. 49-60.

Blatt, Harvey, Middleton, Gerard, Murray, Raymond (1972) Origin of Sedimentary Rocks, Prentice-Hall, Inc., New Jersey, 634 p.

Brock, Richard R. (1967) Development of roll waves in open channels: Report No. KH-R-16, W. M. Keck Laboratory of Hydraulics and Water Resources, Calif. Inst. of Tech., Pasadena, Calif., 226 p.

Brooks, Norman H. (1954) Laboratory studies of the mechanics of streams flowing over a movable bed of fine sand: Ph.D. Thesis, Calif. Inst. of Tech., Pasadena, Calif., 225 p.

_____(1958) Mechanics of streams with movable beds of fine sand: Trans. ASCE, v. 123, p. 526-549.

Climatological Data: California (Nov 73 - Mar 75) v. 77, nos. 11-12; v. 78, nos. 1-12; v. 79, nos. 1-3; NOAA, Environmental Data Service, Asheville, N. C.

Colby, B. R. (1960) Discontinuous rating curves for Pigeon Roost and Cuffawa Creeks in northern Mississippi: U.S. Dept. Agriculture, Agr. Research Service pub. ARS41-36, 31 p.

REFERENCES (Cont'd)

_____(1964a) Scour and fill in sand-bed streams: U.S. Geol. Survey Prof. Paper 462-D, 32 p.

_____(1964b) Sand discharge and mean-velocity relationships in sandbed streams: U.S. Geol. Survey Prof. Paper 462-A, 47 p.

Culbertson, James K. and Dawdy, David R. (1964) A study of fluvial characteristics and hydraulic variables, Middle Rio Grande, New Mexico: U.S. Geol. Survey Water Supply Paper 1498-F, 73 p.

Emmett, William W. and Leopold, Luna B. (1963) Downstream pattern of river-bed scour and fill: Proc. of the Federal Interagency Sedimentation Conference, USDA, ARS Misc. Pub. No. 170, p. 399-408.

Gessler, Johannes (1973) Behavior of sediment mixtures in rivers: Proc. Int. Symposium on River Mechanics, IAHR, Bangkok, Thailand, p. 395-405.

Gilbert, Grove Karl (1914) The transportation of débris by running water: U.S. Geol. Prof. Paper 86, 263 p.

Gupta, Vulli L. and Moin, Syed A. (1974) Surface runoff hydrograph equation: J. Hyd. Div., ASCE, v. 100, HY10, p. 1353-1368.

Henderson, F. M. (1966) Open Channel Flow: The Macmillan Company, New York, 522 p.

Hooke, Roger LeB. (1968) Laboratory study of the influence of granules on flow over a sand bed: GSA Bull., v. 79, p. 495-500.

Hwang, Li-San (1965) Flow resistance of dunes in alluvial streams: Ph.D. Thesis, Calif. Inst. of Tech., Pasadena, Calif., 144 p.

James, Gideon T. (1963) Paleontology and nonmarine stratigraphy of the Cuyama Badlands, California: Univ. Calif. Pub. Geol. Sci., v. 45, Pt. 1, 170 p.

REFERENCES (Cont'd)

Jayaraman, R. and Sethuraman, V. (1973) Improving the accuracy of point-gauge measurements in high-velocity flows: J. Hyd. Research, v. 11, no. 4, p. 317-323.

Kennedy, John F. (1961) Stationary waves and antidunes in alluvial channels: Report No. KH-R-2, W. M. Keck Laboratory of Hydraulics and Water Resources, Calif. Inst. of Tech., Pasadena, Calif., 146 p.

_____(1971) Sediment transportation mechanics: F. Hydraulic relations for alluvial streams [Task Committee for Preparation of the Sedimentation Manual, Vito A. Vanoni, Chmn.]: J. Hyd. Div., ASCE, v. 97, no. HY1, p. 101-141.

Koloseus, H. J. and Davidian, Jacob (1966) Free-surface instability correlations: U.S.G.S. Water-Supply Paper 1592-C, 72 p.

Krumbein, W. C. and Pettijohn, F. J. (1938) Manual of Sedimentary Petrography, Appleton-Century-Crofts, Inc., New York, 549 p.

Lane, E. W. and Borland, W. M. (1954) River-bed scour during floods: Trans. ASCE, v. 119, p. 1069-1079.

Leopold, L. B. and Maddock, Thomas, Jr. (1952) Relation of suspended-sediment concentration to channel scour and fill: Iowa State Univ., Proc. 5th Hydraulic Conf., Studies in Eng., Bull. 34, p. 159-178 [1953].

Leopold, Luna B. and Wolman, M. Gordon (1956) Floods in relation to the river channel: Proc. of the Darcy Symp., Dijon, IAHR Pub. No. 42, p. 85-98.

REFERENCES (Cont'd)

Leopold, Luna B., Wolman, M. Gordon, and Miller, John P. (1964) Fluvial Processes in Geomorphology, W. H. Freeman and Company, San Francisco and London, 522 p.

Lighthill, M. J. and Whitham, G. B. (1955) On kinematic waves. I. Flood movement in long rivers: Proc. of the Royal Society, Series A, v. 229, no. 1178, p. 281-316.

Mackin, J. Hoover (1948) Concept of the graded river: GSA Bull., v. 59, p. 463-512.

Miller, J. P. and Leopold, L. B. (1963) Simple measurements of morphological changes in river channels and hill slopes: in Changes of Climate, Proc. of the Rome Symposium organized by UNESCO and the World Meteorological Organization, p. 421-427.

Moody, L. F. (1944) Friction factors for pipe flow: Trans. ASCE, v. 66, no. 8, p. 671.

Nordin, Carl F., Jr. (1964) Aspects of flow resistance and sediment transport, Rio Grande near Bernalillo, New Mexico: U.S.G.S. Water-Supply Paper 1498-H, 41 p.

Pierce, Raymond C. (1916) The measurement of silt-laden streams: U.S.G.S. Water-Supply Paper 400, p. 39-59.

Renard, Kenneth G. and Keppel, Robert V. (1966) Hydrographs of ephemeral streams in the Southwest: J. Hyd. Div., ASCE, v. 92, HY2, p. 33-52.

Schumm, S. A. (1960) The shape of alluvial channels in relation to sediment type: U.S.G.S. Prof. Paper 352-B, 30 p.

REFERENCES (Cont'd)

_____(1961) Effect of sediment characteristics on erosion and deposition in ephemeral-stream channels: U.S.G.S. Prof. Paper 352-C, 70 p.

Schwade, I. T. (1954) Geology of the Cuyama Valley and adjacent ranges, San Luis Obispo, Santa Barbara, Kern and Ventura Counties: Calif. Div. Mines, Bull. 170, Map sheet 1.

Taylor, R. Hugh, Jr. and Brooks, Norman H. (1961) Discussion of paper "Resistance to flow in alluvial channels," by D. B. Simons and E. V. Richardson: J. Hyd. Div., ASCE, v. 86, HY1, p. 246-256.

Vanoni, Vito A. (1944) Transportation of suspended sediment by water: Trans. ASCE, v. 109, p. 67-133.

_____ (1974) Factors determining bed forms of alluvial streams: J. Hyd. Div., ASCE, v. 100, HY3, p. 363-377.

Vanoni, Vito A., Chmn. (1966) Sediment transportation mechanics: Initiation of motion, Progress report of the Task Committee on Preparation of the Sedimentation Manual: J. Hyd. Div., ASCE, v. 92, HY2, p. 291-314.

_____(1971) Sedimentation transportation mechanics: G. Fundamentals of sediment transportation, Task Committee on Preparation of Sedimentation Manual, Committee on Sedimentation: J. Hyd. Div., ASCE, v. 97, HY12, p. 1979-2022.